University of Southern Queensland

Faculty of Engineering and Surveying

DEVELOPING PHYSICAL MODEL FOR BEARING CAPACITY AND FLOW NET APPLICATIONS

A dissertation submitted by

Manop Jiankulprasert

in fulfillment of the requirements of

Course ENG4111 and ENG 4112 Research Project

towards the degree of

Bachelor of Engineering (Civil)

Submitted: November, 2006

Abstract

Bearing capacity and flow nets are geotechnical problems that civil engineers will encounter in practice. Small scaled physical models can be used to improve understanding of physical behavior for these two particular problems.

The ultimate load which a foundation can support may be calculated using bearing capacity theory. An experimental study procedure of soil ultimate bearing capacity was developed based on a previous research project student. One dimension consolidation was introduced in order to reduce the moisture content of the clay sample after mixed. Fine sand and coarse sand were also used in this study.

Flow net is a graphical solution of the Laplace equation used to estimated the seepage quantities. Seepage quantities are often required for foundation engineering work to determine the pumping requirements to dewater excavation sites and cofferdams. The double-wall cofferdam model was selected to simulate the flow nets concept. The model was also used for the study of the quicksand failure condition.

University of Southern Queensland

Faculty of Engineering and Surveying

ENG4111 & ENG4112 *Research Project*

Limitations of Use

The Council of the University of Southern Queensland, its Faculty of Engineering and Surveying, and the staff of the University of Southern Queensland, do not accept any responsibility for the truth, accuracy or completeness of material contained within or associated with this dissertation.

Persons using all or any part of this material do so at their own risk, and not at the risk of the Council of the University of Southern Queensland, its Faculty of Engineering and Surveying or the staff of the University of Southern Queensland.

This dissertation reports an educational exercise and has no purpose or validity beyond this exercise. The sole purpose of the course pair entitled "Research Project" is to contributed to the overall education within the student's chosen degree program. This document, the associated hardware, software, drawings, and other material set out in the associated appendices should not be used for any other purpose: if they are so used, it is entirely at the risk of the user.

Prof G Baker
Dean
Faculty of Engineering and Surveying

Certification

I certify that the ideas, designs and experimental work, results, analyses and conclusions set out in this dissertation are entirely my own effort, except where otherwise indicated and acknowledged.

I further certify that the work is original and has not been previously submitted for assessment in any other course or institution, except where specifically stated.

Manop Jiankulprasert
Student Number: D10321702

____
Signature

_____/_____/_____

Acknowledgement

I would like to take this opportunity to thank my supervisor for his proficient help and guidance throughout this research project.

I would like to sincerely appreciate the help in technical support from Mr. Glen Bartkowski in construct the models and Mr. Mohan Trada in model testing.

My appreciation extends to all of my family members, Mr. Tagarajan Perumal, Mr. Samy, Mr. Ngoo Wai Fei for the support and encouragement during the progress of this project.

University of Southern Queensland.
Year 2006

Sincerely,
Mr. Manop Jiankulprasert

Table of Content

Abstract **i**
Acknowledgement **iv**
Table of content **v**
List of Figures **viii**
List of Tables **xii**

Chapter 1: Introduction 1

1.1 Introduction 2
  1.1.1 Principal types of soils 2
  1.1.2 Permeability of soils 5
  1.1.3 Stress and strain in soils 7
1.2 Project Aim and Scope 9

Chapter 2: Part A – Bearing Capacity 11

2.1 Introduction 12
2.2 Mohr's Rupture Diagram and Coulomb's Equation 14
2.3 Types of Failure in Soil at Ultimate Load 18
2.4 Bearing Capacity Equations 23
  2.4.1 The Terzaghi bearing capacity equation 26
  2.4.2 Meyerhof's bearing capacity equation 29
  2.4.3 Hansen's bearing capacity equation 31
  2.4.4 Vesic's bearing capacity equation 35
  2.4.5 Which equations to use 35
2.5 Analysis of the Physical Models 36
  2.5.1 Preparation 36
  2.5.2 Construction 38
  2.5.3 Testing of the models 43
  2.5.4 Results and discussions 44

2.6 Kaolin Clay 48

  2.6.1 Properties of the Kaolin clay 48

  2.6.2 Preparation of the Kaolin clay 48

2.7 Comparison of Results 56

Chapter 3: Part B – Flow Net **59**

3.1 Introduction 60

3.2 Seepage 64

  3.2.1 Flow net 65

  3.2.2 Construction of flow net 67

  3.2.3 Calculation of pore water pressure using flow net 74

  3.2.4 Mechanics of piping due to heave 76

3.3 Analysis of the Physical Model 79

  3.3.1 Preparation 79

  3.3.2 Construction 80

  3.3.3 Results and discussions 83

3.4 Comparison of Results 88

Chapter 4: Open Day Demonstration **90**

4.1 Introduction 91

4.2 Procedure 98

  4.2.1 Bearing capacity models 98

  4.2.2 Cofferdam model 101

Chapter 5: Project Conclusions **105**

5.1 Project Achievements 106

5.2 Conclusions 107

5.3 Recommendations for Further Study 107

References **112**

Appendices **117**

Appendix A: Project Specification 118

Appendix B: Project Working Schedule 120

Appendix C: Quotation for Physical Model Development 122

Appendix D: Bearing Capacity Models Construction Plan 124

Appendix E: Cofferdam Model Construction Plan 128

List of Figures

PAGE

Figure 1.1: Clay structures (a) dispersed, (b) flocculated, (c) bookhouse, (d) turbostratic, (e) example of a natural clay. (*Craig, 1992*) 3

Figure 1.2: Particle size ranges. (*Terzaghi & Peck, 1967)*) 4

Figure 1.3: Coefficient of permeability. (*Terzaghi & Peck, 1967*) 5

Figure 1.4: Schematic for permeability determination. (*a*) Constant-head permeameter; (*b*) falling-head permeameter; t = time for head to change from h_1 to h_2. (*Bowles, 1996*) 7

Figure 1.5: Diagram illustrating principal features of triaxial-test apparatus. (*Terzaghi, 19*48) 8

Figure 2.1: Common types of foundations. (*Das, 1979*) 12

Figure 2.2: Diagram illustrating Mohr's circle of stress and rupture diagrams. (*a*) Principal stresses and inclined plane on which normal and shearing stresses p and t act. (*b*) Circle of stress. (*c*) Rupture line from series of failure circles. (*d*) Relation between angles α and ϕ. (*Terzaghi, 1948*) 15

Figure 2.3: General shear failure in soil. (*Das, 2000*) 18

Figure 2.4: Local shear failure in soil. (*Das, 2000*) 19

Figure 2.5: Punching shear failure in soil. (*Das, 2000*) 20

Figure 2.6: Nature of failure in soil with relative density of sand (D_r) and D_f/R. (*Das, 2000*) 21

Figure 2.7: Definition of conditions for developing the ultimate bearing capacity equation. (*David, 1998*) 24

Figure 2.8: Bearing capacity approximation on a $\phi = 0$ soil. (*Bowles, 1996*) 25

Figure 2.9: Simplified bearing capacity for a ϕ - c soil. (*Bowles, 1996*) 26

Figure 2.10: (*a*) Shallow foundation with rough base defined. Terzaghi and Hansen equations of Table 2.X neglect shear along cd; (*b*) general footing-soil interaction for bearing capacity equations for strip footing; left side for Terzaghi (1943), Hansen (1970), and right side Meyerhof (1951). (*Bowles, 1996*) 27

Figure 2.11: Front view of the one layer sand model. 36

Figure 2.12: Front view of the two layers sand model. 37
Figure 2.13: Front view of the sand on clay model. 37
Figure 2.14: Finished one layer sand model. 39
Figure 2.15: Finished two layers sand model. 39
Figure 2.16: Completed tank, Perspex front cover, screen, and top cover. 41
Figure 2.17: Soil reinforcement of sand on clay model. 41
Figure 2.18: Scaled footing 42
Figure 2.19: Finished sand on clay model. 42
Figure 2.20: The compression machine. 43
Figure 2.21: Failure mechanism of one layer sand model. 45
Figure 2.22: Plot of load vs. deformation of one layer sand model. 45
Figure 2.23: Failure mechanism of two layers sand model. 46
Figure 2.24: Plot of load vs. deformation of two layers sand model. 46
Figure 2.25: Failure mechanism of sand on clay model. 47
Figure 2.26: Plot of load vs. deformation of sand on clay model. 47
Figure 2.27: Mold for casting the concrete block. 50
Figure 2.28: Pure concrete into the mold. 50
Figure 2.29: Flatten and keep in a safe place for one week. 51
Figure 2.30: Concrete block ready to use. 51
Figure 2.31: Applied the first concrete block. 52
Figure 2.32: Water dropping from the bottom drainage holes. 52
Figure 2.33: Applied the second concrete block. 53
Figure 2.34: Settlement after applied the second concrete block. 53
Figure 2.35: Diagram of clay model settlement. 55

Figure 3.1: Principal types of Cofferdam. (*Lee, 1961*) 62
Figure 3.2: Seepage by Underflow. (*Lee, 1961*) 64
Figure 3.3: Flow net. (*Liu & Evett, 1998*) 66
Figure 3.4: Geometry for example flow net construction: excavation for cooling water outfall pipe. (*Powrie, 1997*) 68
Figure 3.5: Construction of flow net for cooling water outfall pipe excavation: (a) identify the sink, the source and the bounding flow lines; (b), (c) start sketch in intermediate flow lines and equipotentials, but keep it simple; (d) the finished flow net. (*Powrie, 1997*) 70

Figure 3.6: Flow channel and equipotential drops. (*Liu & Evett, 1998*) 72
Figure 3.7: Calculating pore water pressure form flow net. (a) Determining the total head h_A; (b) relationship between total head and pore water pressure. (*Powrie, 1997*) 75
Figure 3.8: Use of flow net to determine factor of safety of row of sheet piles in sand with respect to piping. (*a*) Flow net. (*b*) Forces acting on sand within zone of potential heave. (*Terzaghi, 1922*) 78
Figure 3.9: Methods of improving seepage conditions. (a) Cofferdam. (b) Concrete or masonry dam. (*Whitlow, 1996*) 79
Figure 3.10: Expect flow lines. 80
Figure 3.11: Front view drawing of the physical model. 81
Figure 3.12: Physical model under construction. 82
Figure 3.13: Testing the tank for leakage after construction. 83
Figure 3.14: Fill up the water and saturated the sand sample. 83
Figure 3.15: Finished cofferdam model. 84
Figure 3.16: Dewatering the cofferdam. 85
Figure 3.17: Injecting the dye. 86
Figure 3.18: Shortest flow path. 86
Figure 3.19: Flow lines. 87
Figure 3.20: Heave and boiling. 88
Figure 3.21: Collapse. 88

Figure 4.1: Poster for the bearing capacity model. 92
Figure 4.2: Bearing capacity background and applications. 93
Figure 4.3: Failure mode and derivation of equations. 94
Figure 4.4: Poster for the cofferdam model. 95
Figure 4.5: Cofferdam background and applications. 96
Figure 4.6: Seepage and flow net. 96
Figure 4.7: Types of cofferdam. 97
Figure 4.8: Covered physical model. 98
Figure 4.9: Participants listening to the background information. 99
Figure 4.10: Drawing for sketching the failure patterns. 99
Figure 4.11: Revealed failure patterns. 100
Figure 4.12: Setting the cofferdam model. 101

Figure 4.13: Participants listening to the concepts and application. 102

Figure 4.14: Drawing for sketching the flow lines. 102

Figure 4.15: Participants checking the results. 103

Figure 4.16: Revealed flow lines. 103

List of Tables

PAGE

Table 2.1: Bearing capacity equations by the several authors indicated. (*Bowles, 1996*) 28

Table 2.2: Bearing capacity factors for the Terzaghi equations. (*Bowles, 1996*) 29

Table 2.3: Shape, depth, and inclination factors for Meyerhof bearing capacity equation of Table 2.1. (*Bowles, 1996*) 30

Table 2.4: Bearing capacity factors for Meyerhof, Hansen, and Vesic bearing capacity equations. (*Bowles, 1996*) 30

Table 2.5*a*: Shape and depth factors for use in either the Hansen (1970) or Vesic (1973, 1975) bearing capacity equations of Table 2.1. Use s'_c, d'_c when $\phi = 0$ only for Hansen equations. Subscripts *H*, *V* for Hansen, Vesic, respectively. (*Bowles, 1996*) 33

Table 2.5*b*: Table of inclination, ground, and base factors for the Hansen (1970) equations. See Table 2.5*c* for equivalent Vesic equations. (*Bowles, 1996*) 33

Table 2.5*c*: Table of inclination, ground, and base factors for the Vesic (1973, 1975) bearing capacity equations. (*Bowles, 1996*) 34

Chapter 1

INTRODUCTION

1.1 Introduction

1.1.1 Principal Types of Soils

In foundation and earthwork engineering, more than in any other field of civil engineering, success depends on practical experience. The design of ordinary soil-supporting or soil-supported structures is necessarily based on simple empirical rules, but these rules can be used safely only by the engineer who has a background of experience. The properties of the soils on which the distinctions based are known as *index properties*, and the tests required determining the index properties are *classification tests*. (*Terzaghi, 1948*)

Soils may be classified according to the sizes of the particles of which they are composed, by their physical properties, or by their behavior when the moisture content varies. The following list of soil types are commonly used by experienced foremen and practical engineers for field classification.

Gravel is rounded or semi-round particles of rock that will pass a 3-in. and be retained on a 2.0-mm. No. 10 sieve. Sizes larger than 10 in. are usually called boulders.

Sand is disintegrated rock whose particles very in size from the lower limit of gravel 2.0 mm down to 0.074 mm (No. 200 sieve). It may be classified as coarse or fine sand, depending on the sizes of the grains. Sand is a granular noncohesive material.

Silt is a material finer than sand, and thus its particles are smaller than 0.074 mm but larger than 0.005 mm. It is a noncohesive material that has little or no strength. It compacts very poorly.

Clay is a cohesive material whose particles are less than 0.005 mm. The cohesion between the particles gives a clay high strength when air-dried. Clay can be subject to considerable changes in volume with variations in moisture content. They will exhibit plasticity within a range of "water contents."

Organic matter is a partly decomposed vegetable matter. It has a spongy, unstable structure that will continue to decompose and is chemically reactive. If present in soil that is used for construction purposes, organic matter should be removed and replaced with a more suitable soil.

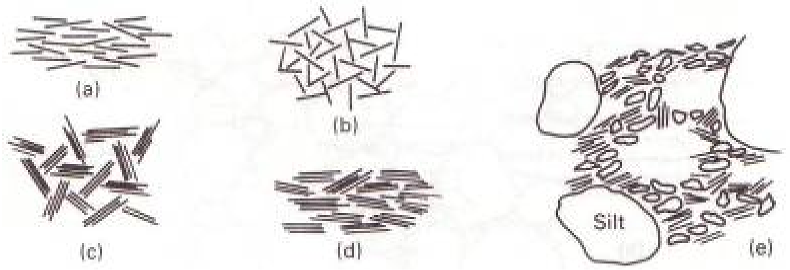

Figure 1.1: Clay structures (a) dispersed, (b) flocculated, (c) bookhouse, (d) turbostratic, (e) example of a natural clay. (*Craig, 1992*)

In the field classification of soils includes a rather great variety of different materials. Furthermore, the choice of terms relating to stiffness and density depends to a considerable extent on the person who examines the soil. Because of these facts, the field classification of soils is usually uncertain and inaccurate. More specific information can be obtained only by physical tests that furnish numerical values representative of the properties of the soil.

The methods of soil exploration, including boring and sampling, are the procedures for determining average numerical values for the soil properties and are part of the design and construction process.

The size of the particles that constitute soils may vary from that of boulders to that of large molecules.

Grains larger than approximately 0.06 mm can be inspected with the naked eye or by means of a hand lens. They constitute the *very coarse* and *coarse* fractions of the soils.

Grains ranging in size from about 0.06 mm to 2μ ($1\mu = 1$ micron $= 0.001$ mm) can be examined only under the microscope. They represent the *fine* fraction.

Grains smaller than 2μ constitute the *very fine* fraction. Grains having a size between 2μ and about 0.1μ can be differentiated under the microscope, but their shape cannot be determined by means of an electron microscope. Their molecular structure can be investigated by means of X-ray analysis.

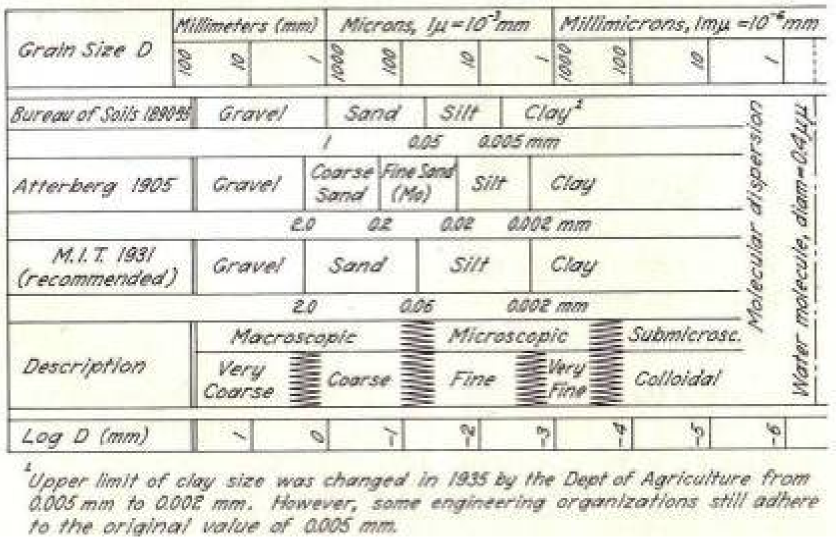
Grain Size D
Millimeters (mm)
Microns, $1\mu = 10^{-3}$mm
Millimicrons, $1m\mu = 10^{-6}$mm
100
10
1
1000
100
10
1
1000
100
10
1
Bureau of Soils 1890-95
Gravel
Sand
Silt
Clay^1
1
0.05
0.005 mm
Atterberg 1905
Gravel
Coarse Sand
Fine Sand (Mo)
Silt
Clay
2.0
0.2
0.02
0.002 mm
M.I.T. 1931 (recommended)
Gravel
Sand
Silt
Clay
2.0
0.06
0.002 mm
Description
Macroscopic
Microscopic
Submicrosc.
Very Coarse
Coarse
Fine
Very Fine
Colloidal
Molecular dispersion
Water molecule, diam=0.4$m\mu$
Log D (mm)
1
0
-1
-2
-3
-4
-5
-6

[1] Upper limit of clay size was changed in 1935 by the Dept of Agriculture from 0.005 mm to 0.002 mm. However, some engineering organizations still adhere to the original value of 0.005 mm.

Figure 1.2: Particle size ranges. (*Terzaghi & Peck, 1967)*)

1.1.2 Permeability of Soils

A material is said to be permeable if it contains continuous voids. Since such voids are contained in all soils including the stiffest clays, and in practically all nonmetallic construction materials including sound granite and neat cement, all these materials are permeable. Furthermore, the flow of water through all of them obeys approximately the same laws. Hence the difference between the flow of water through clean sand and through sound granite is merely one degree. (*Terzaghi, 1948*)

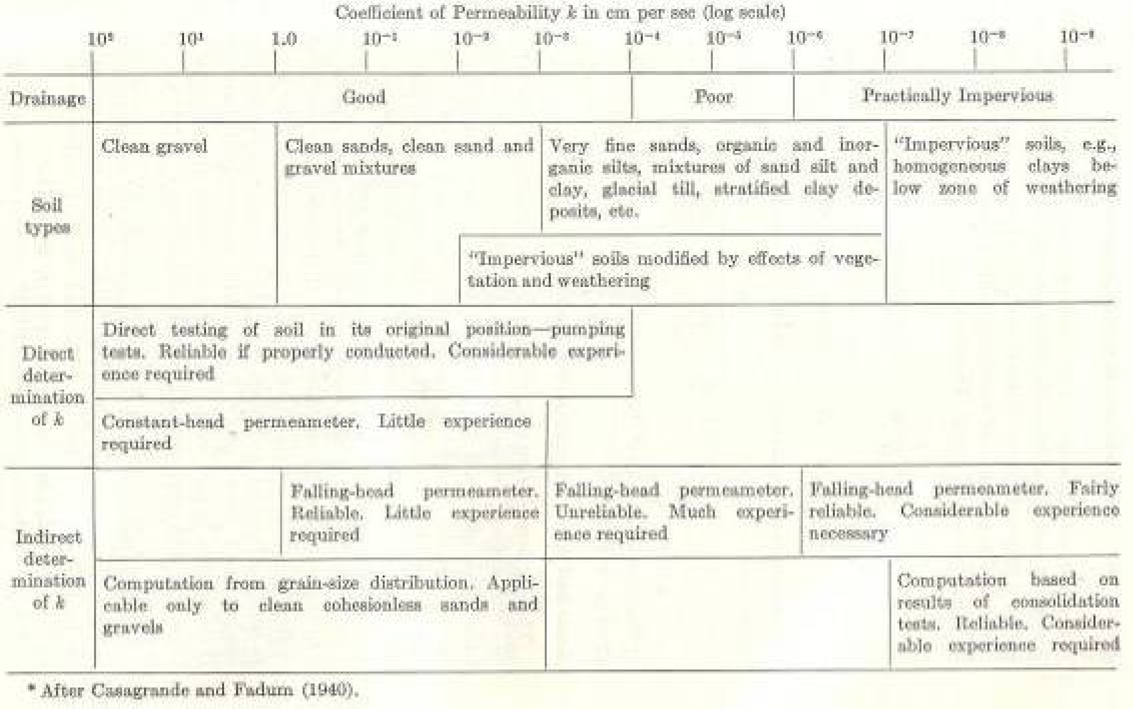

<table>
<tr><th></th><th colspan="12">Coefficient of Permeability k in cm per sec (log scale)</th></tr>
<tr><th></th><th>10^2</th><th>10^1</th><th>1.0</th><th>10^{-1}</th><th>10^{-2}</th><th>10^{-3}</th><th>10^{-4}</th><th>10^{-5}</th><th>10^{-6}</th><th>10^{-7}</th><th>10^{-8}</th><th>10^{-9}</th></tr>
<tr><td>Drainage</td><td colspan="6">Good</td><td colspan="2">Poor</td><td colspan="4">Practically Impervious</td></tr>
<tr><td rowspan="2">Soil types</td><td colspan="2" rowspan="2">Clean gravel</td><td colspan="3">Clean sands, clean sand and gravel mixtures</td><td colspan="4">Very fine sands, organic and inorganic silts, mixtures of sand silt and clay, glacial till, stratified clay deposits, etc.</td><td colspan="3" rowspan="2">"Impervious" soils, e.g., homogeneous clays below zone of weathering</td></tr>
<tr><td colspan="2"></td><td colspan="5">"Impervious" soils modified by effects of vegetation and weathering</td></tr>
<tr><td rowspan="2">Direct determination of k</td><td colspan="6">Direct testing of soil in its original position—pumping tests. Reliable if properly conducted. Considerable experience required</td><td colspan="6"></td></tr>
<tr><td colspan="5">Constant-head permeameter. Little experience required</td><td colspan="7"></td></tr>
<tr><td rowspan="2">Indirect determination of k</td><td colspan="2"></td><td colspan="3">Falling-head permeameter. Reliable. Little experience required</td><td colspan="3">Falling-head permeameter. Unreliable. Much experience required</td><td colspan="4">Falling-head permeameter. Fairly reliable. Considerable experience necessary</td></tr>
<tr><td colspan="5">Computation from grain-size distribution. Applicable only to clean cohesionless sands and gravels</td><td colspan="4"></td><td colspan="3">Computation based on results of consolidation tests. Reliable. Considerable experience required</td></tr>
</table>

* After Casagrande and Fadum (1940).

Figure 1.3: Coefficient of permeability. (*Terzaghi & Peck, 1967*)

The permeability of soils has a decisive effect on the cost and the difficulty of many construction operations, such as the excavation of open cuts in water-bearing sand, or on the rate at which a soft clay stratum consolidates under the influence of the weight of a superimposed fill. Even the permeability of dense concrete or rock may have important practical implications, because water exerts a pressure on the porous material through which it percolates. This pressure, which is known as *seepage pressure*, can be very high.

The erroneous but widespread conception that stiff clay and dense concrete are impermeable is due to the fact that the entire quantity of water that percolates through such materials toward an exposed surface is likely to evaporate, even in a very humid atmosphere. As a consequence, the surface appears to be dry. However, since the mechanical effects of seepage are entirely independent of the rate of percolation, the absence of visible discharge does not indicate the absence of seepage pressures.

Flow of soil water for non turbulent conditions has been expressed by *Darcy's* as

$$\boldsymbol{v = ki} \tag{1.1}$$

where i = hydraulic gradient h/L
k = coefficient of permeability, *length/time*

Figure 1.3 lists typical order-of-magnitude (exponent of 10) for various soils. The quantity of flow q through a cross section A is

$$\boldsymbol{q = kiA} \tag{1.2}$$

Two tests commonly used in the laboratory to determine k are the Constant-Head and Falling-Head methods. Figure 1.4 gives the schematic diagrams and the equations used for computing k. The falling-head test is usually used for $k < 10^{-5}$ m/s (cohesive soils), and the constant-head test is usually used for cohesionless soils.

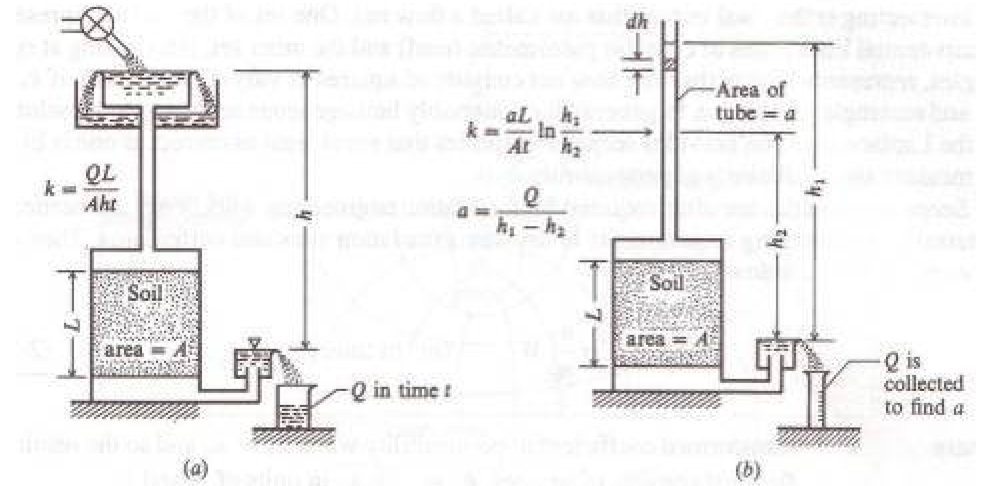
$k = \frac{QL}{Aht}$
Soil
area = A
L
h
Q in time t
(a)
dh
Area of tube = a
$k = \frac{aL}{At} \ln \frac{h_1}{h_2}$
$a = \frac{Q}{h_1 - h_2}$
h_1
h_2
Soil
area = A
L
Q is collected to find a
(b)

Figure 1.4: Schematic for permeability determination. (*a*) Constant-head permeameter; (*b*) falling-head permeameter; t = time for head to change from h_1 to h_2. (*Bowles, 1996*)

1.1.3 Stress and Strain in Soils

The relations between stress and strain in soils determine the settlements of soil-supported foundations. They also determine the change in earth pressure due to small movements of retaining walls or other earth supports. (*Terzaghi, 1948*)

The stress-strain relationships for soils are much more complex than those for manufactured construction materials such as steel. Whereas the stress-strain relationships for steel can be described adequately for many engineering applications by two numerical values expressing the modulus of elasticity and Poisson's ratio, the corresponding values for soils are functions of stress, strain, time, and various other factors.

Furthermore, the experimental determination of these values for soils is much more difficult. The investigations are usually carried out by means of triaxial compression tests. In a triaxial test, a cylindrical specimen of soil is subjected to an equal all-round pressure, known as the *cell pressure,* in addition to an axial pressure that may be varied independently of the cell pressure.

The essential features of the triaxial apparatus are shown diagrammatically in Fig. 1.5. The cylindrical surface of the sample is covered by a rubber membrane sealed to a pedestal at the bottom and to a cap at the top. The assemblage in contained in a chamber into which water may admit under any desired pressure; this pressure acts laterally on the cylindrical surface of the sample through the rubber membrane and vertically through the top cap. The additional axial load is applied by means of a piston passing through the top of the chamber.

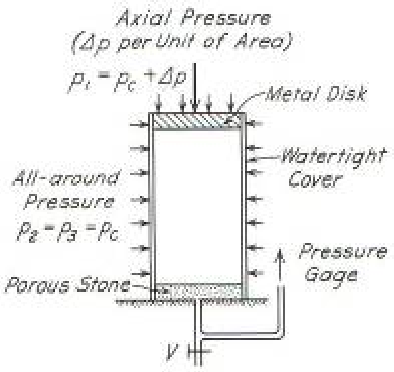

Figure 1.5: Diagram illustrating principal features of triaxial-test apparatus. (*Terzaghi, 19*48)

A porous disk is placed against the bottom of the sample and is connected to the outside of the chamber by tubing. By means of the connection the pressure in the water contained in the pores of the sample can be measured if drainage is not allowed. Alternatively, if flow is permitted through the connection, the quantity of water passing into or out of the sample during the test can be measured. As the loads are altered, the vertical deformation of the specimen is measured by a dial gage. A test is usually conducted in two steps: the application of the cell pressure, followed by the additional axial load.

1.2 Project Aim and Scope

The aim of my project is to design and construct small scaled physical models that will illustrate the overall behavior of ultimate bearing capacity of shallow foundations and flow net under a cofferdam.

This will involve designing and building the physical models using simply available materials. Five models will be used for testing of ultimate bearing capacity of shallow foundations, and one model will be used for demonstration of flow net application.

Thus, this project will be in two parts, and the scopes for each part are outlined below.

Bearing Capacity

- To design and construct small scaled physical models to study the ultimate bearing capacity of shallow foundations.
- To compare the experimental results with the theoretical results.
- To demonstrate the models at the USQ Open Day for the geotechnical demonstration area.

Flow Nets

- To design and construct small scaled physical models to study the flow net under a cofferdam
- To compare the experimental results with the theoretical results.
- To demonstrate the models at the USQ Open Day for the geotechnical demonstration area.

Chapter 2

BEARING CAPACITY

2.1 Introduction

The lowest part of a structure is generally called a foundation and its function is to transfer the load of the structure to the soil on which it is resting. Proper design requires that the load transferred should not overstress the soil. Overstressing of soil might result in excessive settlement or shear failure of soil, which would damage the structure. Thus, for geotechnical and structural engineers engaged in foundation design, it is important to evaluate the safe bearing capacity of soils. (*Das*, *1979*)

Depending on the structure and the soil, various types of foundations are used. The most common types of foundations are shown in Fig. 2.1. A *spread footing* is simply an enlargement of a load-bearing wall or column, which spreads the load of the structure over a large area of the soil. Sometimes the size of the spread footings will be too large for the low load-bearing capacity of soil. Then it becomes more economical to construct the entire structure over a concrete pad, which is called a *mat* foundation.

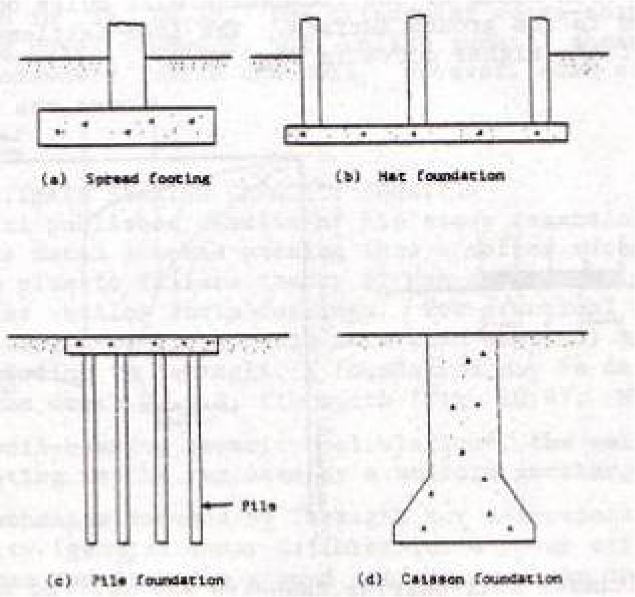
(a) Spread footing
(b) Mat foundation
(c) Pile foundation
(d) Caisson foundation

Figure 2.1: Common types of foundations. (*Das, 1979*)

Pile and *caisson* foundations are used for heavier structures in which the depth required for supporting the load is large.

Piles are structural members made of timber, concrete, or steel that transmits the load of the superstructure into the lower layers of the soil. Depending on the way in which piles transmit the load into the subsoil, they are divided into two categories: (1) friction pile and (2) end-bearing pile. In the case of friction pile, the superstructure load is resisted by the frictional force generated along the surface of the pile. In end-bearing pile, the load carried by the pile is transmitted at its point to a firm stratum.

In a caisson foundation, a shaft is drilled into the subsoil and filled with concrete. During the shaft drilling a metal casing may be used; it may be left in place or may be withdrawn during the pouring of concrete. The basic functions of a pile and caisson are practically the same, but the diameter of a caisson shaft is much larger than that of a pile.

For safe performance the load carried by a foundation must be such that (1) the settlement of soil caused by the load is within the tolerable limit and (2) shear failure of soil supporting the foundation does not occur.

Spread footings and mat foundations are generally classified as shallow; pile and caisson foundations are deep foundations.

This part of the project will discuss the soil-ultimate bearing capacity for shallow foundations.

2.2 Mohr's Rupture Diagram and Coulomb's Equation

Soils, like most solid materials, fail either in tension or in shear. Tensile stresses may cause the opening of cracks that, under some circumstances of practical importance, are undesirable or detrimental. In the majority of engineering problems, however, only the resistance to failure by shear requires consideration. (*Peck, 1967*)

Shear failure starts at a point in a mass of soil when, on some surface passing through the point, a critical combination of shearing and a normal stress is reached. Various types of equipment have been developed to determine and investigate these critical combinations. At present the most widely used is the triaxial apparatus described in Chapter 1. Because only principal stresses can be applied to the boundaries of the specimen in this equipment, the state of stress on any other than principal planes must be determined indirectly.

According to the principles of mechanics, the normal stress and shearing stress on a plane inclined at angle α to the plane of the major principal stress and perpendicular to the plane of the intermediate principal stress (Fig. 2.2*a*) are determined by the following equations

$$p = \frac{1}{2}(p_1 + p_3) + \frac{1}{2}(p_1 - p_3)\cos 2\alpha \tag{2.1}$$

$$t = \frac{1}{2}(p_1 - p_3)\sin 2\alpha \tag{2.2}$$

These equations represent points on a circle in a rectangular system of coordinates (Fig. 2.2*b*) in which the horizontal axis is that of normal stresses and the vertical axis is that of shearing stresses. Similar expressions may be written for the normal and shearing stresses on planes on which the intermediate principal stress acts.

The corresponding components of stress are represented by points on the dash circles plotted on the same axes in Fig. 2.2*b*. Since, in the usual triaxial test, the major principal stress acts in a vertical direction and the cell pressure represents both the intermediate and minor principal stresses which are equal, we are generally concerned only with the outer circle associated with the major and minor principal stresses p_1 and p_3. This is known as the *circle of stress*.

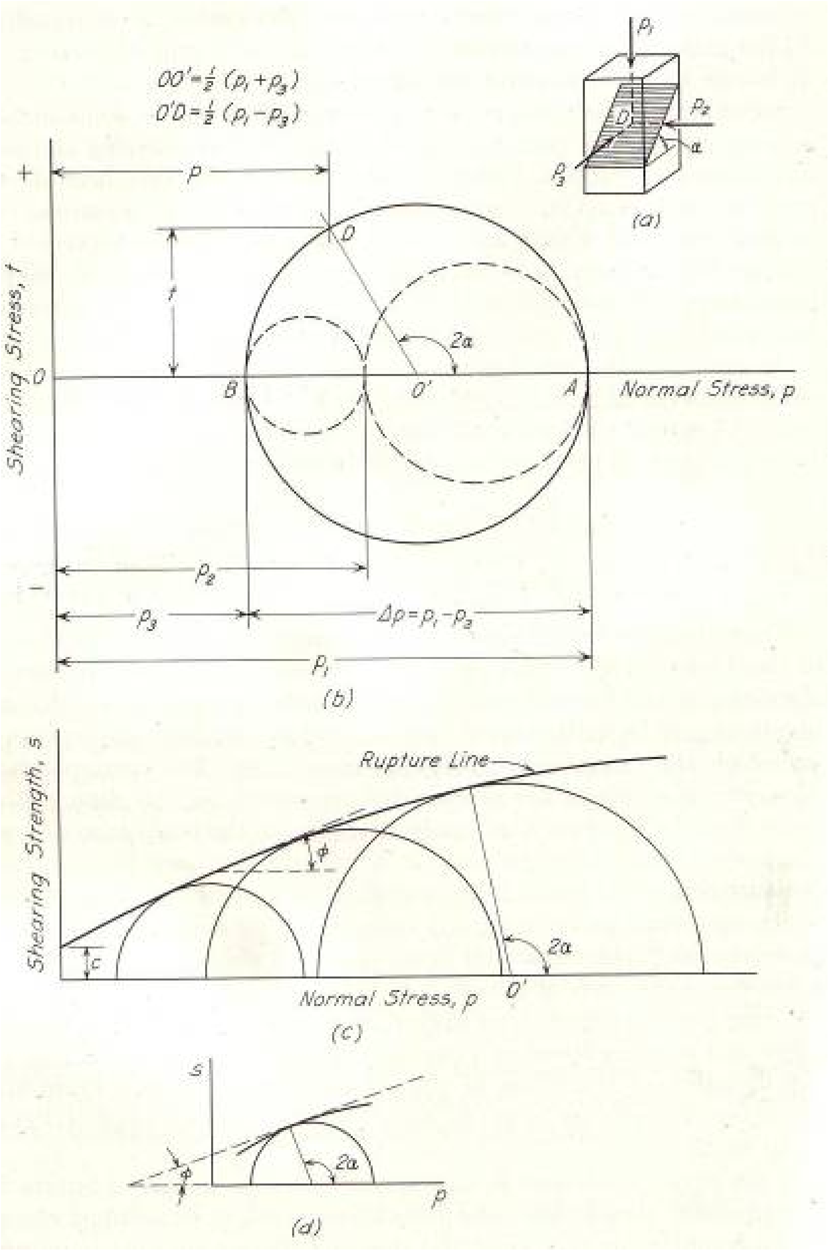
$OO' = \frac{1}{2}(p_1 + p_3)$
$O'D = \frac{1}{2}(p_1 - p_3)$
p_1
p_2
p_3
D
α
(a)
+
p
t
D
2α
0
B
O'
A
Normal Stress, p
Shearing Stress, t
−
p_2
p_3
$\Delta p = p_1 - p_3$
p_1
(b)
Rupture Line
Shearing Strength, s
φ
2α
c
Normal Stress, p
O'
(c)
s
φ
2α
p
(d)

Figure 2.2: Diagram illustrating Mohr's circle of stress and rupture diagrams.
(*a*) Principal stresses and inclined plane on which normal and shearing stresses p and t act. (*b*) Circle of stress. (*c*) Rupture line from series of failure circles. (*d*) Relation between angles α and ϕ. (*Terzaghi, 1948*)

Every point such as *D*, on the circle of stress represents the normal stress and shearing stress on a particular plane inclined at an angle α to the direction of the plane of the major principal stress. From the geometry of the figure it can be shown that the central angle *A O′ D* is equal to 2α.

If the principal stresses p_1 and p_3 correspond to a state of failure in the specimen then at least one point on the circle of stress must represent a combination of normal and shearing stresses that led to failure on some plane through the specimen. Moreover, if the coordinates of that point were known, the inclination of the plane upon which failure took place could be determined from knowledge of the angle α.

If a series of tests is performed and the circle of stress corresponding to failure is plotted for each of the tests, at least one point on each circle must represent the normal and shearing stresses associated with failure. As the number of tests increased indefinitely, and if the material is homogeneous and isotropic, it is apparent that the envelop of the failure circle (Fig. 2.2*c*) represents the locus of points associate with failure of the specimens. The envelop is known as the *rupture line* for the given material under the specific conditions of the series of tests.

From the geometry of Fig. 2.2*d* it may be seen that for any failure circle

$$2\alpha = 90^\circ + \phi \tag{2.3}$$

Therefore the angle between the plane on which failure occurs and the plane of the major principal stress is

$$\alpha = 45^\circ + \frac{\phi}{2} \tag{2.4}$$

In general, the rupture for a series of tests on a soil under a given set of conditions is curved. However, it may often be approximated by a straight line with the equation

$$s = c + p \tan \phi \tag{2.5}$$

This expression is known as *Coulomb's equation*. In this equation symbol *t*, representing shearing stress is replaced by *s*, known as the *shearing resistance* or *shearing strength*, because points on the rupture line refer specifically to states of stress associated with failure.

The triaxial test gives great flexibility with respect to possible stress changes, and pore water drainage conditions, in taking the test specimen to failure. With respect to drainage conditions, one of the following three procedures is usually adopted. (*Parry, 1995)*

1. **Unconsolidated undrained test (UU):** the specimen is taken to failure with no drainage permitted.

2. **Consolidated undrained test (CU):** the drainage valve is initially opened to allow the pore pressure to dissipate to zero, and then closed so that the specimen is taken to failure without permitting any further drainage. It is common to apply a 'back pressure', that is a positive pore pressure, to the specimen initially, balanced by an equal increment in cell pressure to avoid changing the effective stress. This is to ensure that any air in the soil voids or in the ducts connecting to the pore pressure measuring device is driven into solution in the water. It also decreases the possibility of cavitation, that is water vapour forming, or air coming out of solution in the water, if large negative charges in pore pressure take place during a test.

3. **Drained test (CD):** the drainage valve is initially opened to allow the pore pressure to dissipate to zero, and is kept open while the specimen is taken to failure at a sufficiently slow rate to allow excess pore pressure to dissipate.

2.3 Types of Failure in Soil at Ultimate Load

To understand the concept of ultimate soil-bearing capacity and the mode of shear failure in soil, let us consider a long rectangular model footing of width *B* located at the depth D_f below the ground surface and supported by a dense sand layer (or stiff clayey soil) as shown in Fig. 2.3. If this foundation is subjected to a load *Q* which is gradually increased, the load per unit area, $q = Q/A$ (A = area of the foundation), will increase and the foundation will undergo increased settlement. When q becomes equal to q_u at foundation settlement $S = S_u$, the soil supporting the foundation undergoes sudden shear failure. The failure surface in the soil is shown in Fig. 2.3a, and the q versus S plot is shown in Fig2.3b. This type of failure is called *general shear failure*, and q_u is the *ultimate bearing capacity*. Note that, in this type of failure, a peak value $q = q_u$ is clearly defined in the load-settlement curve.

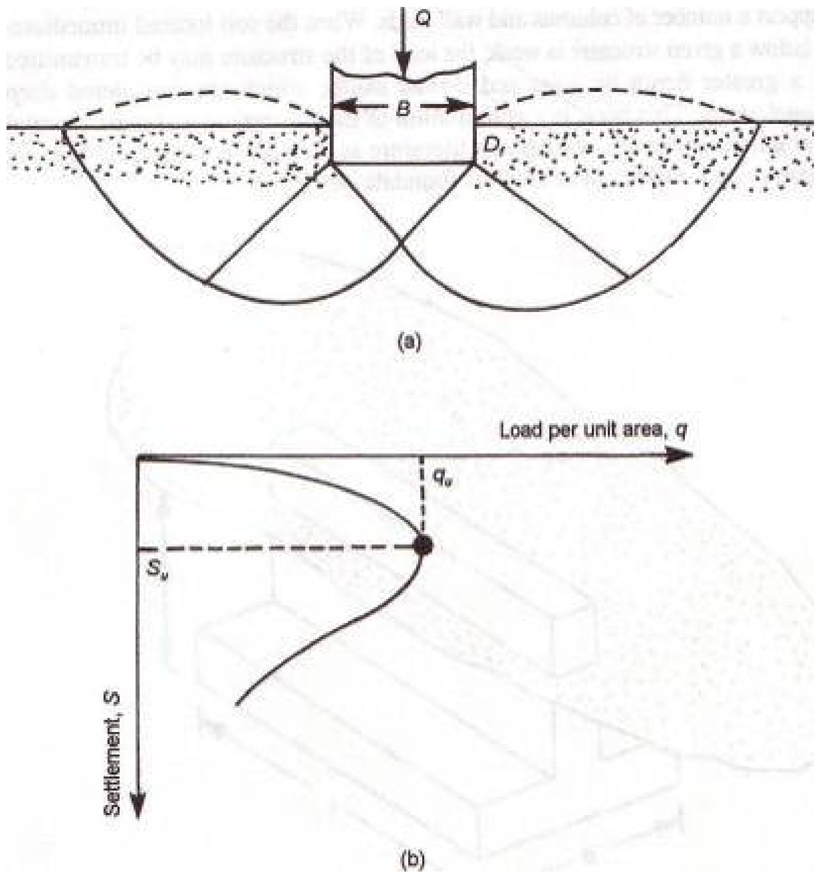

Figure 2.3: General shear failure in soil. (*Das, 2000*)

If the foundation shown in Fig. 2.3a is supported by a medium dense sand or clayey soil of medium consistency (Fig. 2.4a), the plot of q versus S will be as shown in Fig. 2.4b. Note that the magnitude of q increased with settlement up to $q = q'_u$, which is usually referred to as the *first failure load*. At this time, the developed failure surface in the soil will be like that shown by the solid lines in Fig 2.4a.

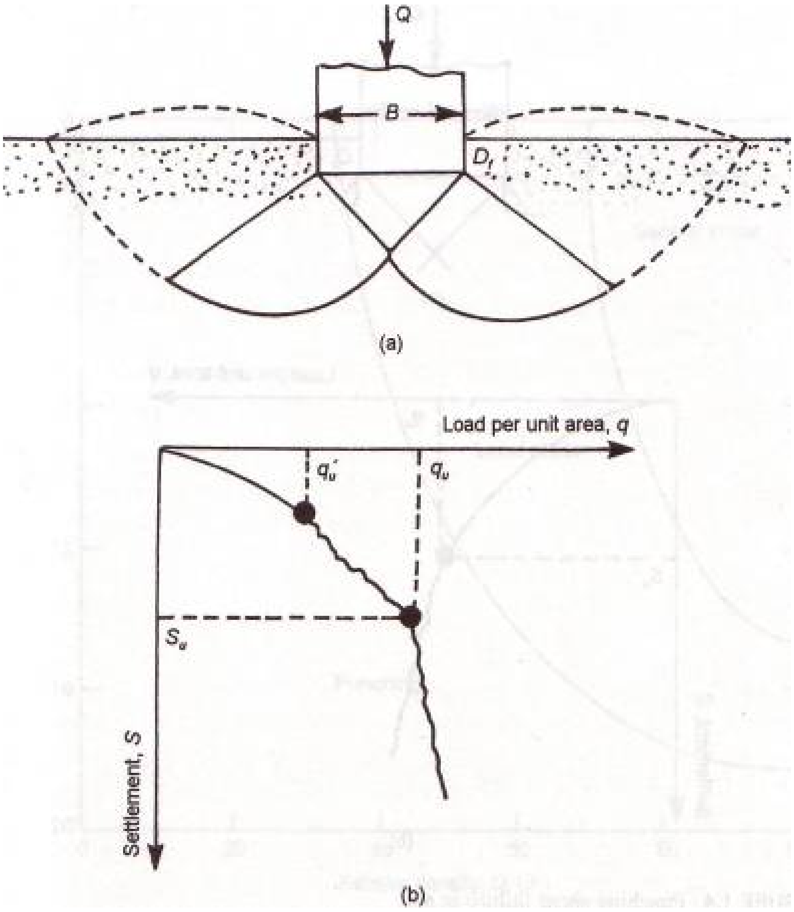

Figure 2.4: Local shear failure in soil. (*Das, 2000*)

If the load on the foundation is further increased, the load-settlement curve becomes steeper and erratic with the gradual outward and upward progress of the failure surface in the soil (shown by the broken line in Fig. 2.4b) under the foundation. When q becomes equal to q_u (ultimate bearing capacity), the failure surface reaches the ground surface. Beyond that, the plot of q versus S takes almost a linear shape, and a peak load is never observed. This type of bearing capacity failure is called *local shear failure*.

Figure 2.5a shows the same foundation located on a loose sand or soft clayey soil. For this case, the load-settlement curve will be like that shown in Fig. 2.5b. A peak value if load per unit area, q, is never observed. The ultimate bearing capacity, q_u, is defined as the point where $\Delta S/\Delta q$ becomes the largest and almost constant thereafter. This type of failure in soil is called *punching shear failure*. In this case, the failure surface never extends up to the ground surface.

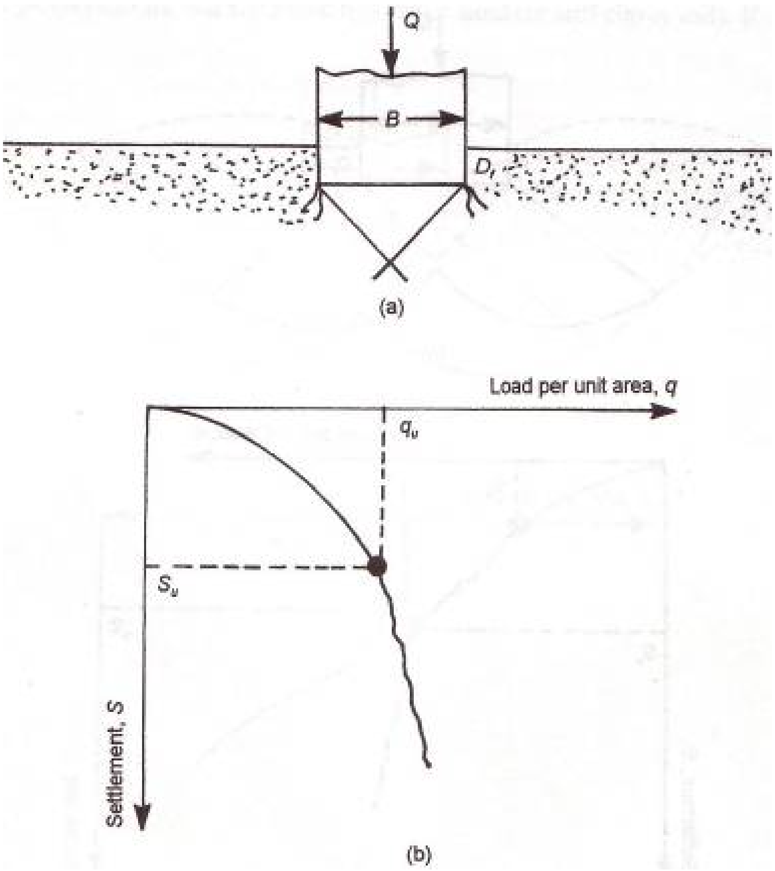

Figure 2.5: Punching shear failure in soil. (*Das, 2000*)

The nature of failure in soil at ultimate load is a function of several factors such as the strength and the relative compressibility of soil, the depth of the foundation (D_f) in relation to the foundation width (B), and the width-to-length ratio (B/L) of the foundation.

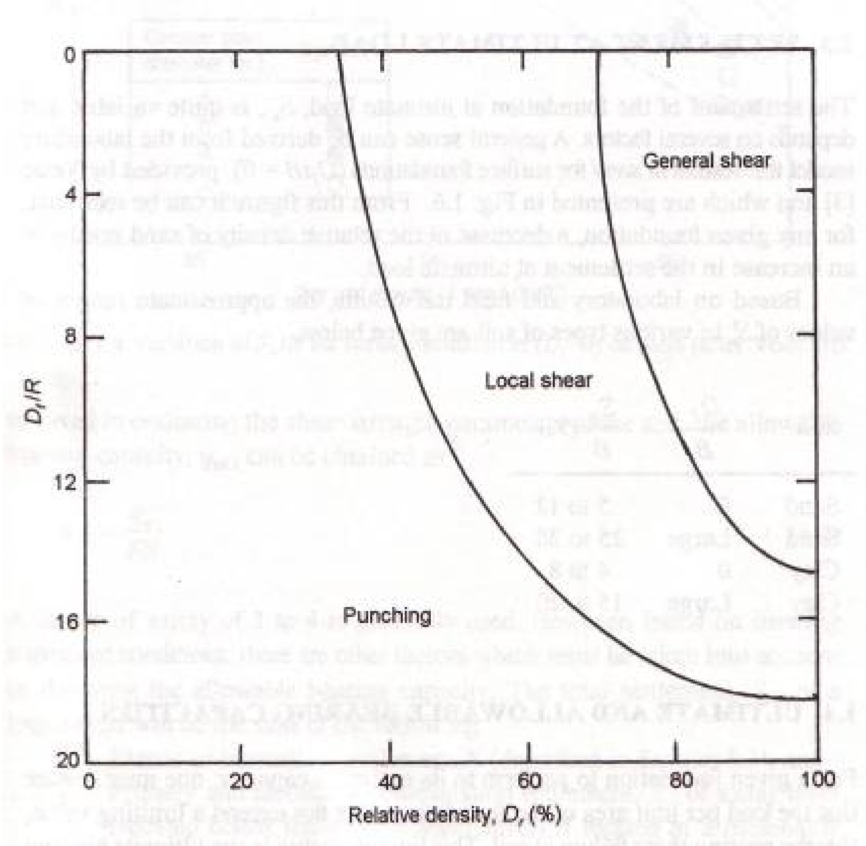

Figure 2.6: Nature of failure in soil with relative density of sand (D_r) and D_f/R. (*Das, 2000*)

This was clearly explained by Vesic (1973) who conducted extensive laboratory model tests in sand. The summary of Vesic's findings is shown in a slightly different form in Fig. 2.6. In this figure, D_r is the relative density of sand, and the hydraulic radius, R, of the foundation is defined as

$$R = \frac{A}{P} \tag{2.6}$$

where A = area of the foundation = $B \times L$

P = perimeter of the foundation = $2(B + L)$

Thus

$$R = \frac{B \times L}{2(B+L)} \tag{2.7}$$

For a square foundation, $B = L$.

So,

$$R = \frac{B}{4}$$

(2.8)

From Fig. 2.6 it can be seen that, when $D_f/R \geq$ about 18, punching shear failure occurs in all cases, irrespective of the relative density of compaction of sand.

2.4 Bearing Capacity Equations

Over the past one hundred years, a number of investigators have undertaken studies relating to foundation bearing capacity, typically applying the classical theories of elasticity and plasticity to soil behavior to develop equations appropriate for foundation design. (*Terzaghi, 1948*)

The original theoretical concepts for analyzing conditions considered applicable to foundation performance using the theory of plasticity are credited to Prandtl (1920) and Reissner (1924). Prandtl studied the effect of a long, narrow metal tool bearing against the surface of a smooth metal mass that possessed cohesion and internal friction but no weight. The results of Prandtl's work were extended by Reissner to include the condition where the bearing area is located below the surface of the resisting material and a surcharge weight acts on a plane that is level with the bearing area. (*Bowls, 1996*)

Terzaghi (1943) applied the developments of Prandtl and Reissner to soil foundation problem, extending the theory to consider rough foundation surfaces bearing on materials that posses weight.

Conditions for relating the classical theory of plasticity to the case of a general shear failure are indicated by Fig. 2.7. The arrangement shown establishes criteria for developing the ultimate bearing capacity for a long strip foundation; because of the infinite foundation length, the analysis proceeds as for a two-dimensional or plane-strain problem. (*David, 1998*)

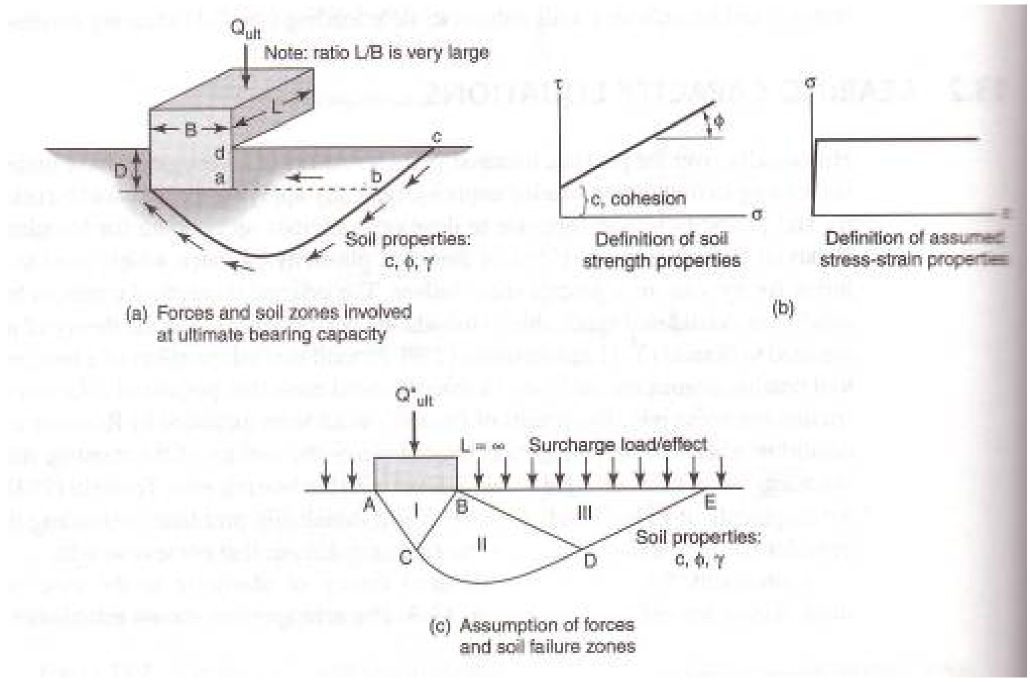
Q_ult
Note: ratio L/B is very large
B
L
d
D
a
b
c
Soil properties:
c, ϕ, γ
(a) Forces and soil zones involved
at ultimate bearing capacity
τ
ϕ
c, cohesion
σ
Definition of soil
strength properties
σ
ε
Definition of assumed
stress-strain properties
(b)
Q'ult
L = ∞
Surcharge load/effect
A
I
B
III
E
II
C
D
Soil properties:
c, ϕ, γ
(c) Assumption of forces
and soil failure zones

Figure 2.7: Definition of conditions for developing the ultimate bearing capacity equation. (*David, 1998*)

The theory assumes that the soil material in zones I, II, and III possesses the stress-strain characteristics of a rigid plastic body (viz., the material shows an infinite initial modulus of elasticity extending to the point of shear failure, followed by a zero modulus; see Fig. 2.7b). Applied to the soil mass providing support for the foundation, the theory assumes that no deformations occur prior to the point of shear failure but that plastic flow occurs at constant stress after shearing failure. It is also assumed that the plastic deformations are small and the geometric shapes of the failure zones remain essentially constant.

The use of an equivalent surcharge to substitute for the soil mass above the level of the foundation, along with some estimation, simplifies the analysis, but the effect is to provide conservative results. When subject to a foundation loading near to the ultimate, zone I behave as an active zone that pushes the radial zone II sideways and the passive zone III laterally upwards. Boundaries AC and DE shown on Fig. 2.7c are essentially straight lines; the shape of section CD varies from circular (when the soil angle of internal friction ϕ is zero degrees) to a curve intermediate between a logarithmic spiral and a circle (when ϕ is greater than zero degrees).

Terzaghi developed a general bearing capacity equation for strip footings that combined the effects of soil cohesion and internal friction, foundation size, soil weight, and surcharge effects in order to simplify the calculations necessary for foundation design. His equation utilized the concept of dimensionless bearing capacity factors whose values are a function of the shear possessed by the supporting soils.

Through ensuing years, the ultimate bearing capacity for shallow and deep foundations has continued to be studied in the quest for refined definition of foundation soil behavior and a generalized bearing capacity equation that agrees well with failure conditions occurring in the model and large-scale foundation tests.

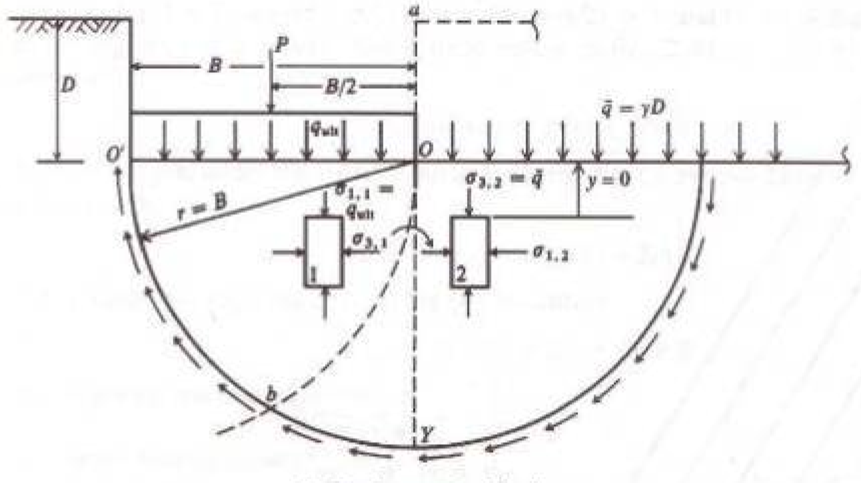
a
P
B
B/2
D
$\bar{q} = \gamma D$
q_{ult}
O'
O
$\sigma_{1,1} = q_{ult}$
$\sigma_{3,2} = \bar{q}$
$y = 0$
$r = B$
$\sigma_{3,1}$
$\sigma_{1,2}$
1
2
b
Y

(a) Footing on $\phi = 0°$ soil.

Note: $\bar{q} = p'_o = \gamma' D$, but use $\bar{q}$, since this is the accepted symbol for bearing capacity computations.

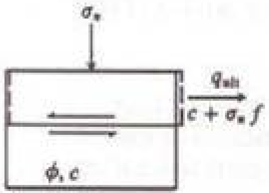
σ_n
q_{ult}
$c + \sigma_n f$
ϕ, c

Area = dA

Friction = $\sigma_n \tan \phi = \sigma_n f$

Cohesion = $\dfrac{c\,dA}{dA}$

(b) Physical meaning of Eq. (2-52) for shear strength.

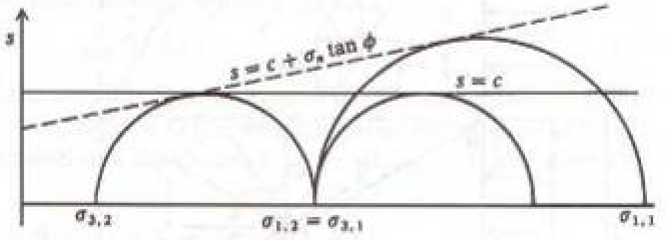
s
$s = c + \sigma_n \tan \phi$
$s = c$
$\sigma_{3,2}$
$\sigma_{1,2} = \sigma_{3,1}$
$\sigma_{1,1}$

(c) Mohr's circle for (a) and for a ϕ–c soil.

Figure 2.8: Bearing capacity approximation on a $\phi = 0$ soil. (*Bowles, 1996*)

Modifications to early concepts have emerged from such studies, but the general form of the Terzaghi bearing capacity equation has been retained because of its practicality. There is currently no method of obtaining the ultimate bearing capacity of a foundation other than as an estimate. Vesic (1973) tabulated 15 theoretical solutions since 1940 and omitted at least one of the more popular methods in current use. There have been several additional proposals since that time.

2.4.1 The Terzaghi Bearing Capacity Equation

One of the early sets of bearing capacity equations was proposed by Terzaghi (1943) as shown in Table 2.1. Terzaghi's equations were produced from a slightly modified bearing capacity theory developed by Prandtl from using the theory of plasticity to analyze the punching of a rigid base into a softer soil material.

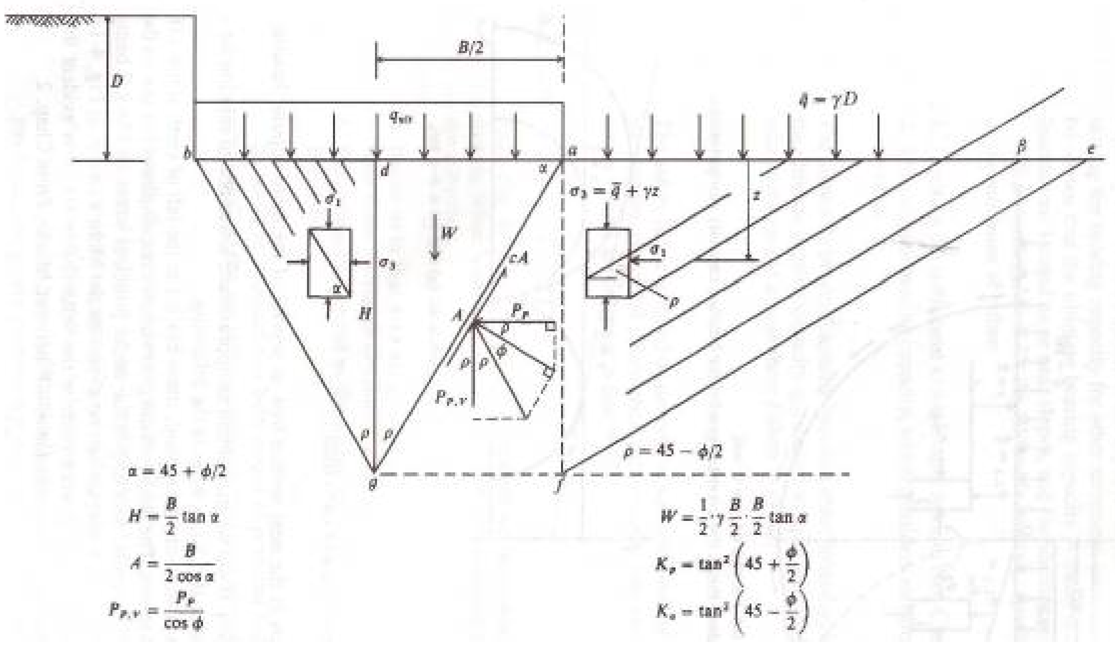

D
B/2
q_{ult}
$\bar{q} = \gamma D$
b
d
a
β
e
α
σ_1
σ_3
$\sigma_3 = \bar{q} + \gamma z$
z
W
cA
H
A
P_p
ρ
ϕ
$P_{p,v}$
$\rho = 45 - \phi/2$
g
f
$\alpha = 45 + \phi/2$
$H = \frac{B}{2} \tan \alpha$
$A = \frac{B}{2 \cos \alpha}$
$P_{p,v} = \frac{P_p}{\cos \phi}$
$W = \frac{1}{2} \cdot \gamma \frac{B}{2} \cdot \frac{B}{2} \tan \alpha$
$K_p = \tan^2 \left(45 + \frac{\phi}{2}\right)$
$K_a = \tan^2 \left(45 - \frac{\phi}{2}\right)$

Figure 2.9: Simplified bearing capacity for a ϕ - c soil. (*Bowles, 1996*)

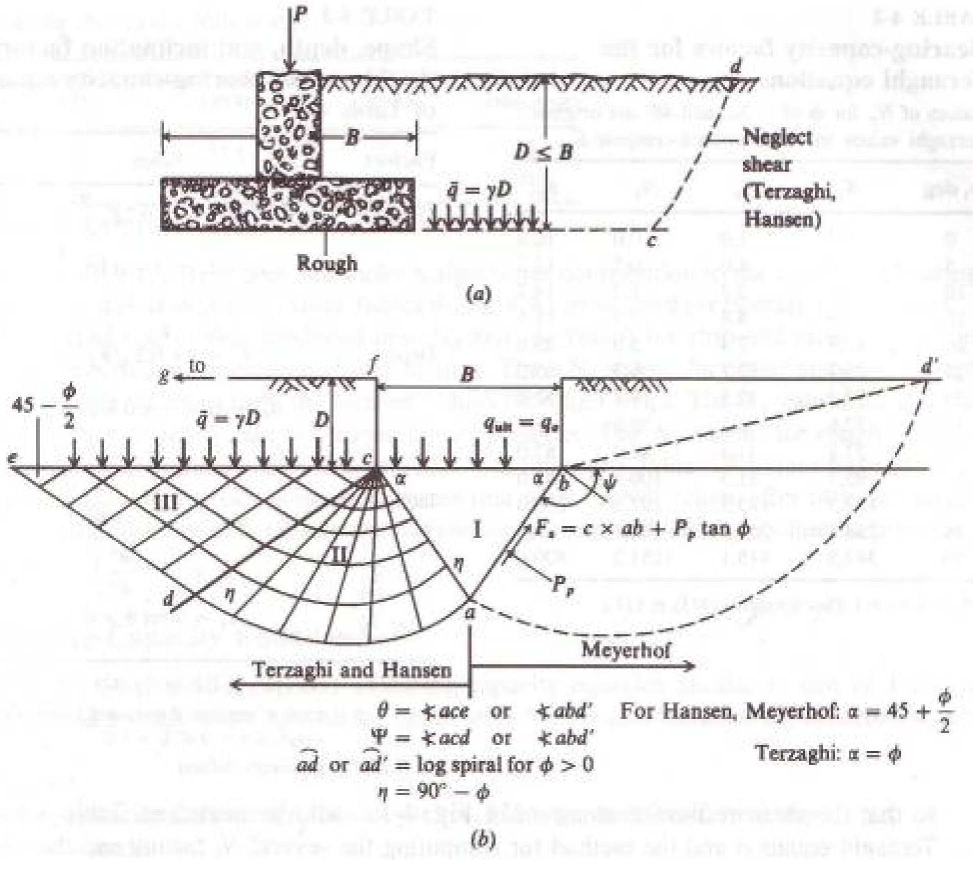
P
d
B
D ≤ B
Neglect shear (Terzaghi, Hansen)
$\bar{q} = \gamma D$
c
Rough
(a)
g
to
f
B
d'
$45 - \frac{\phi}{2}$
$\bar{q} = \gamma D$
D
$q_{ult} = q_o$
e
c
α
α
b
ψ
III
II
I
$F_s = c \times ab + P_p \tan\phi$
η
P_p
d
η
a
Terzaghi and Hansen
Meyerhof
θ = ∢ace or ∢abd'
Ψ = ∢acd or ∢abd'
$\widehat{ad}$ or $\widehat{ad'}$ = log spiral for φ > 0
η = 90° − φ
For Hansen, Meyerhof: $\alpha = 45 + \frac{\phi}{2}$
Terzaghi: α = φ
(b)

Figure 2.10: (*a*) Shallow foundation with rough base defined. Terzaghi and Hansen equations of Table 2.1 neglect shear along cd; (*b*) general footing-soil interaction for bearing capacity equations for strip footing; left side for Terzaghi (1943), Hansen (1970), and right side Meyerhof (1951). (*Bowles, 1996*)

The basic equation was for the case in which a unit width from a long strip produced a plane strain case, all shape factors s_i = 1.00, but the N_i factors were computed differently. Terzaghi used $\alpha = \phi$ in Fig. 2.9 and 2.10 whereas most other theories use the $\alpha = 45 + \phi/2$ shown. We see in Table 2.1 that Terzaghi only used shape factors with the cohesion (s_c) and based (s_γ) terms. The Terzaghi bearing capacity equation is developed, as

$$q_{ult} = cN_c + \bar{q}N_q + \gamma BN_\gamma \qquad (2.9)$$

by summing vertical forces on the wedge *bac* of Fig. 2.10.

Table 2.1: Bearing capacity equations by the several authors indicated. (*Bowles, 1996*)

Terzaghi (1943). See Table 2.2 for typical values and for $K_{p\gamma}$ values.

$$q_{ult} = cN_c s_c + \bar{q}N_q + 0.5\gamma B N_\gamma s_\gamma$$

$$N_q = \frac{a^2}{a\cos^2(45 + \phi/2)}$$

$$a = e^{(0.75\pi - \phi/2)\tan\phi}$$

$$N_c = (N_q - 1)\cot\phi$$

$$N_\gamma = \frac{\tan\phi}{2}\left(\frac{K_{p\gamma}}{\cos^2\phi} - 1\right)$$

For:	strip	round	square
s_c =	1.0	1.3	1.3
s_γ =	1.0	0.6	0.8

Meyerhof (1963). See Table 2.3 for shape, depth, and inclination factors.

Vertical load: $q_{ult} = cN_c s_c d_c + \bar{q}N_q s_q d_q + 0.5\gamma B' N_\gamma s_\gamma d_\gamma$

Inclined load: $q_{ult} = cN_c d_c i_c + \bar{q}N_q d_q i_q + 0.5\gamma B' N_\gamma d_\gamma i_\gamma$

$$N_q = e^{\pi\tan\phi}\tan^2\left(45 + \frac{\phi}{2}\right)$$

$$N_c = (N_q - 1)\cot\phi$$

$$N_\gamma = (N_q - 1)\tan(1.4\phi)$$

Hansen (1970). See Table 2.4 for shape, depth, and other factors.

General: $q_{ult} = cN_c s_c d_c i_c g_c b_c + \bar{q}N_q s_q d_q i_q g_q b_q + 0.5\gamma B' N_\gamma s_\gamma d_\gamma i_\gamma g_\gamma b_\gamma$

when $\phi = 0$

use $q_{ult} = 5.14 s_u(1 + s'_c + d'_c - i'_c - b'_c - g'_c) + \bar{q}$

$N_q =$ same as Meyerhof above

$N_c =$ same as Meyerhof above

$$N_\gamma = 1.5(N_q - 1)\tan\phi$$

Vesic (1973, 1975). See Table 2.4 for shape, depth, and other factors.

Use Hansen's equations above.

$N_q =$ same as Meyerhof above

$N_c =$ same as Meyerhof above

$$N_\gamma = 2\left(N_q + 1\right)\tan\phi$$

The difference in N factors results from the assumption of the log spiral arc *ad* and exit wedge *cde* of Fig. 2.10. This makes a very substantial difference in how P_p is computed, which in turn gives the different N_i values. The shear slip lines shown on Fig. 2.10 qualitatively illustrate stress trajectories in the plastic zone beneath the footing as the ultimate bearing pressure is developed.

Terzaghi's bearing capacity equations were intended for "shallow" foundations where $D \leq B$ so that the shear resistance along *cd* of Fig. 2.10*a* could be neglected. Table 2.1 lists the Terzaghi equation and the method for computing the several N_i factors and the two shape factors s_i. Table 2.2 is shown a short table of N factors.

Table 2.2: Bearing capacity factors for the Terzaghi equations. (*Bowles, 1996*)

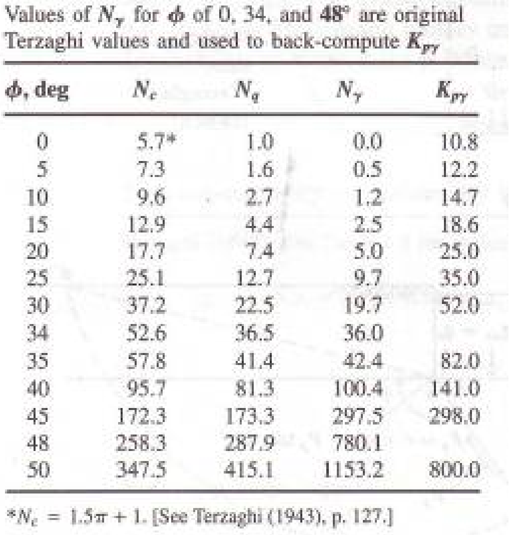

Values of N_γ for ϕ of 0, 34, and **48°** are original Terzaghi values and used to back-compute $K_{p\gamma}$

ϕ, deg	N_c	N_q	N_γ	$K_{p\gamma}$
0	5.7*	1.0	0.0	10.8
5	7.3	1.6	0.5	12.2
10	9.6	2.7	1.2	14.7
15	12.9	4.4	2.5	18.6
20	17.7	7.4	5.0	25.0
25	25.1	12.7	9.7	35.0
30	37.2	22.5	19.7	52.0
34	52.6	36.5	36.0	
35	57.8	41.4	42.4	82.0
40	95.7	81.3	100.4	141.0
45	172.3	173.3	297.5	298.0
48	258.3	287.9	780.1	
50	347.5	415.1	1153.2	800.0

*$N_c = 1.5\pi + 1$. [See Terzaghi (1943), p. 127.]

2.4.2 Meyerhof's Bearing Capacity Equation

Meyerhof (1951, 1963) proposed a bearing capacity equation similar to that of Terzaghi but included a shape factor s_q with the depth term N_q. He also included depth factors d_i and inclination factors i_i for case where the footing load is inclined from the vertical.

These additions produce equations of the general form shown in Table 2.1, with select *N* factor computed in Table 2.4.

Table 2.3: Shape, depth, and inclination factors for Meyerhof bearing capacity equation of Table 2.1. (*Bowles, 1996*)

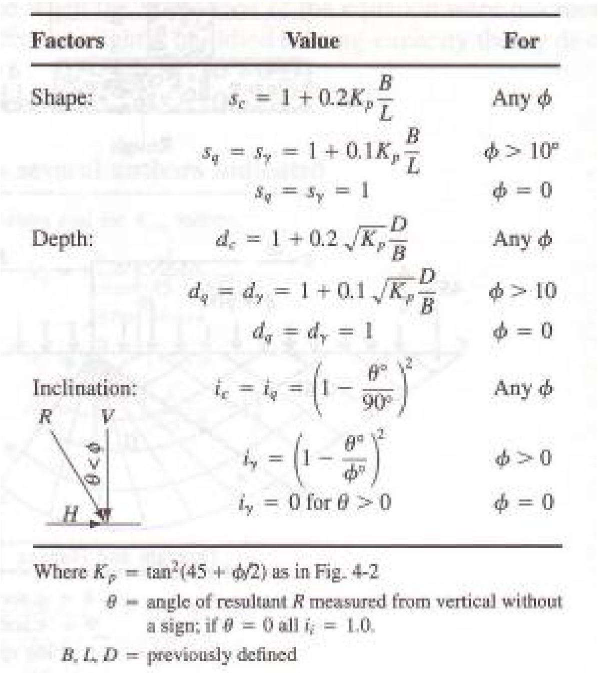

Factors	Value	For
Shape:	$s_c = 1 + 0.2K_p\frac{B}{L}$	Any ϕ
	$s_q = s_\gamma = 1 + 0.1K_p\frac{B}{L}$	$\phi > 10^\circ$
	$s_q = s_\gamma = 1$	$\phi = 0$
Depth:	$d_c = 1 + 0.2\sqrt{K_p}\frac{D}{B}$	Any ϕ
	$d_q = d_\gamma = 1 + 0.1\sqrt{K_p}\frac{D}{B}$	$\phi > 10$
	$d_q = d_\gamma = 1$	$\phi = 0$
Inclination:	$i_c = i_q = \left(1 - \frac{\theta^\circ}{90^\circ}\right)^2$	Any ϕ
	$i_\gamma = \left(1 - \frac{\theta^\circ}{\phi^\circ}\right)^2$	$\phi > 0$
	$i_\gamma = 0$ for $\theta > 0$	$\phi = 0$

R
V
$\theta < \phi$
H

Where $K_p = \tan^2(45 + \phi/2)$ as in Fig. 4-2

θ = angle of resultant R measured from vertical without a sign; if $\theta = 0$ all $i_i = 1.0$.

B, L, D = previously defined

Table 2.4: Bearing capacity factors for Meyerhof, Hansen, and Vesic bearing capacity equations. (*Bowles, 1996*)

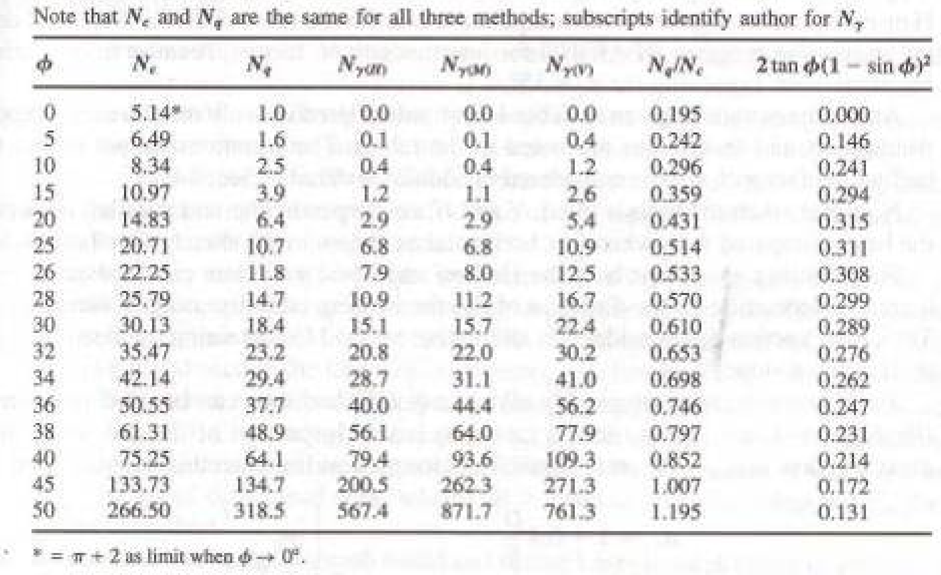

Note that N_c and N_q are the same for all three methods; subscripts identify author for N_γ

ϕ	N_c	N_q	$N_{\gamma(H)}$	$N_{\gamma(M)}$	$N_{\gamma(V)}$	N_q/N_c	$2\tan\phi(1 - \sin\phi)^2$
0	5.14*	1.0	0.0	0.0	0.0	0.195	0.000
5	6.49	1.6	0.1	0.1	0.4	0.242	0.146
10	8.34	2.5	0.4	0.4	1.2	0.296	0.241
15	10.97	3.9	1.2	1.1	2.6	0.359	0.294
20	14.83	6.4	2.9	2.9	5.4	0.431	0.315
25	20.71	10.7	6.8	6.8	10.9	0.514	0.311
26	22.25	11.8	7.9	8.0	12.5	0.533	0.308
28	25.79	14.7	10.9	11.2	16.7	0.570	0.299
30	30.13	18.4	15.1	15.7	22.4	0.610	0.289
32	35.47	23.2	20.8	22.0	30.2	0.653	0.276
34	42.14	29.4	28.7	31.1	41.0	0.698	0.262
36	50.55	37.7	40.0	44.4	56.2	0.746	0.247
38	61.31	48.9	56.1	64.0	77.9	0.797	0.231
40	75.25	64.1	79.4	93.6	109.3	0.852	0.214
45	133.73	134.7	200.5	262.3	271.3	1.007	0.172
50	266.50	318.5	567.4	871.7	761.3	1.195	0.131

* = $\pi + 2$ as limit when $\phi \to 0^\circ$.

Meyerhof obtained his N factors by making trials of the zone *abd'* with arc *ad'* of Fig. 2.10*b*, which include an approximation for shear along line *cd* of Fig. 2.10*a*. The shape, depth, and inclination factors in Table 2.3 are from Meyerhof (1963) *abd* are somewhat different from his 1951 values. The shape factors do not greatly differ from those given by Terzaghi except for addition of s_q. Observing that the shear effect along line *cd* of Fig. 2.10*a* was still being somewhat ignored, Meyerhof proposed depth factors d_i.

He also proposed using the inclination factors of Table 2.3 to reduced the bearing capacity when the load resultant was inclined from the vertical by the angle θ. When the i_γ factor is used, it should be self-evident that it does not apply when $\phi = 0°$, since base slip would occur with this term, even if there is base cohesion for the i_c term. Also, the i_i factors all = 1.0 if the angle $\theta = 0$.

Up to a depth of $D \approx B$ in Fig. 2.10*a*, the Meyerhof q_{ult} is not greatly different from the Terzaghi value. The difference becomes more pronounced at larger D/B ratios.

2.4.3 Hansen's Bearing Capacity Equation

Hansen (1970) proposed the general bearing capacity case and N factor equations shown in Table 2.1. This equation is readily seen to be a further extension of the earlier Meyerhof (1951) work. Hansen's shape, depth, and other factors making up the general bearing capacity equation are given in Table 2.5. These represent revision and extensions in which the footing is tilted from the horizontal b_i and for the possibility of a slope β of the ground supporting the footing to give ground factors g_i. Table 2.4 gives selected N values for the Hansen equations together with computation aids for the more difficult shape and depth factor terms.

Note that when the base is tilted, V and H are perpendicular and parallel, respectively, to the base, compared with when it is horizontal as shown in sketch with Table 4.5.

The Hansen equation implicitly allows any *D*/*B* and thus can be used for both shallow and deep foundations. Inspection of the $\bar{q}N_q$ term suggests a great increase in q_{ult} with great depth. To place modest limits on this, Hansen used

$$\left.\begin{aligned} d_c &= 1 + 0.4\frac{D}{B} \\ d_q &= 1 + 2\tan\phi(1-\sin\phi)^2\frac{D}{B} \end{aligned}\right\} \frac{D}{B} \le 1$$

$$\left.\begin{aligned} d_c &= 1 + 0.4\tan^{-1}\frac{D}{B} \\ d_q &= 1 + 2\tan\phi(1-\sin\phi)^2\tan^{-1}\frac{D}{B} \end{aligned}\right\} \frac{D}{B} > 1$$

Theses expressions give a discontinuity at $D/B = 1$; however, note the use of ≤ and >. For $\phi = 0$ (giving d'_c) we have

$D/B =$	0	1	1.5	2	5	10	20	100
$d'_c =$	0	0.40	0.42	0.44	0.55	0.59	0.61	0.62

We can see that use of tan-1 *D*/*B* for $D/B > 1$ controls the increase in d_c and d_q that are in line with observations that q_{ult} appear to approach a limiting values at some depth ration *D*/*B*, where this value of *D* is often terms the critical depth.

Table 2.5*a*: Shape and depth factors for use in either the Hansen (1970) or Vesic (1973, 1975) bearing capacity equations of Table 2.1. Use s'_c, d'_c when $\phi = 0$ only for Hansen equations. Subscripts *H*, *V* for Hansen, Vesic, respectively. (*Bowles, 1996*)

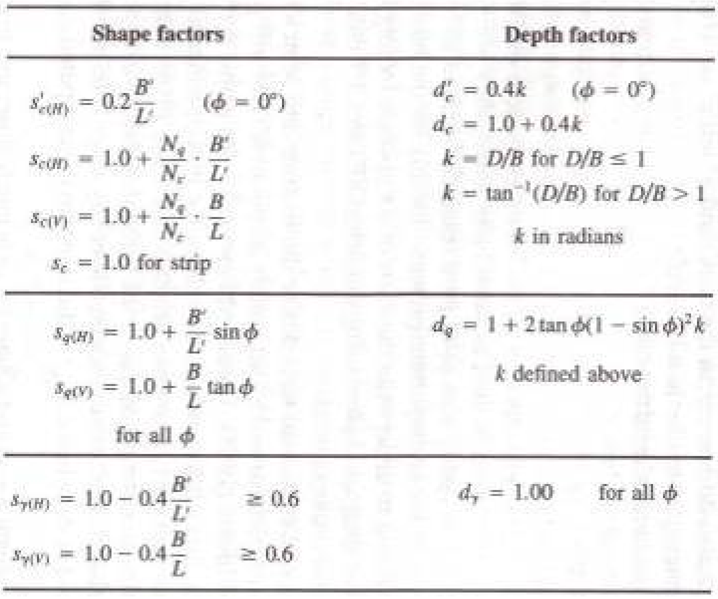

Shape factors	Depth factors
$s'_{c(H)} = 0.2\frac{B'}{L'} \quad (\phi = 0°)$ $s_{c(H)} = 1.0 + \frac{N_q}{N_c}\cdot\frac{B'}{L'}$ $s_{c(V)} = 1.0 + \frac{N_q}{N_c}\cdot\frac{B}{L}$ $s_c = 1.0$ for strip	$d'_c = 0.4k \quad (\phi = 0°)$ $d_c = 1.0 + 0.4k$ $k = D/B$ for $D/B \le 1$ $k = \tan^{-1}(D/B)$ for $D/B > 1$ k in radians
$s_{q(H)} = 1.0 + \frac{B'}{L'}\sin\phi$ $s_{q(V)} = 1.0 + \frac{B}{L}\tan\phi$ for all ϕ	$d_q = 1 + 2\tan\phi(1 - \sin\phi)^2 k$ k defined above
$s_{\gamma(H)} = 1.0 - 0.4\frac{B'}{L'} \ge 0.6$ $s_{\gamma(V)} = 1.0 - 0.4\frac{B}{L} \ge 0.6$	$d_\gamma = 1.00$ for all ϕ

Table 2.5*b*: Table of inclination, ground, and base factors for the Hansen (1970) equations. See Table 2.5*c* for equivalent Vesic equations. (*Bowles, 1996*)

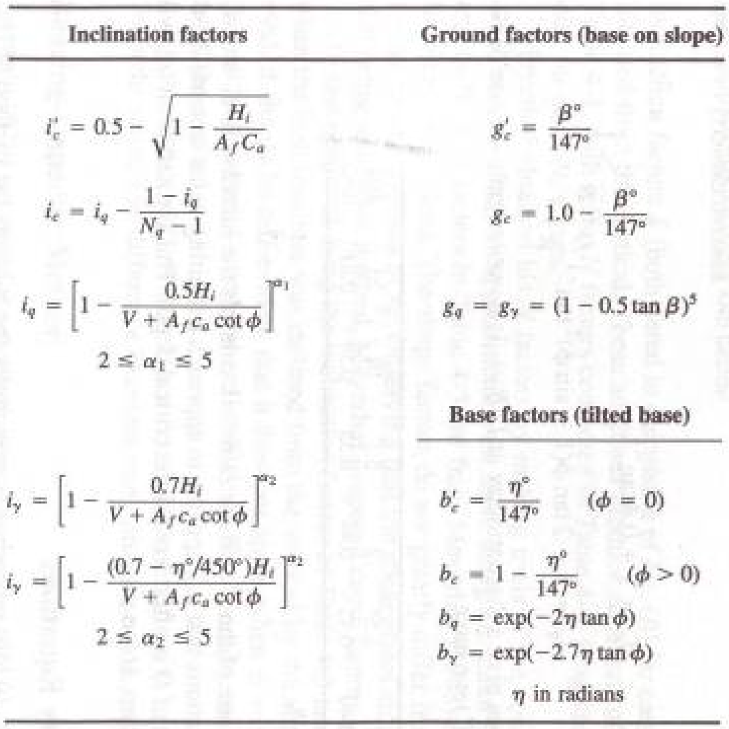

Inclination factors	Ground factors (base on slope)
$i'_c = 0.5 - \sqrt{1 - \frac{H_i}{A_f C_a}}$	$g'_c = \frac{\beta°}{147°}$
$i_c = i_q - \frac{1 - i_q}{N_q - 1}$	$g_c = 1.0 - \frac{\beta°}{147°}$
$i_q = \left[1 - \frac{0.5H_i}{V + A_f c_a \cot\phi}\right]^{\alpha_1}$ $2 \le \alpha_1 \le 5$	$g_q = g_\gamma = (1 - 0.5\tan\beta)^5$
	Base factors (tilted base)
$i_\gamma = \left[1 - \frac{0.7H_i}{V + A_f c_a \cot\phi}\right]^{\alpha_2}$	$b'_c = \frac{\eta°}{147°} \quad (\phi = 0)$
$i_\gamma = \left[1 - \frac{(0.7 - \eta°/450°)H_i}{V + A_f c_a \cot\phi}\right]^{\alpha_2}$ $2 \le \alpha_2 \le 5$	$b_c = 1 - \frac{\eta°}{147°} \quad (\phi > 0)$ $b_q = \exp(-2\eta\tan\phi)$ $b_\gamma = \exp(-2.7\eta\tan\phi)$ η in radians

Table 2.5*c*: Table of inclination, ground, and base factors for the Vesic (1973, 1975) bearing capacity equations. (*Bowles*, *1996*)

Inclination factors	Ground factors (base on slope)
$i'_c = 1 - \dfrac{mH_i}{A_f c_a N_c} \quad (\phi = 0)$	$g'_c = \dfrac{\beta}{5.14} \quad \beta$ in radians
$i_c = i_q - \dfrac{1 - i_q}{N_q - 1} \quad (\phi > 0)$	$g_c = i_q - \dfrac{1 - i_q}{5.14 \tan\phi} \quad \phi > 0$
i_q, and m defined below	i_q defined with i_c
$i_q = \left[1.0 - \dfrac{H_i}{V + A_f c_a \cot\phi}\right]^m$	$g_q = g_\gamma = (1.0 - \tan\beta)^2$
	Base factors (tilted base)
$i_\gamma = \left[1.0 - \dfrac{H_i}{V + A_f c_a \cot\phi}\right]^{m+1}$	$b'_c = g'_c \quad (\phi = 0)$
$m = m_B = \dfrac{2 + B/L}{1 + B/L}$	$b_c = 1 - \dfrac{2\beta}{5.14 \tan\phi}$
$m = m_L = \dfrac{2 + L/B}{1 + L/B}$	$b_q = b_\gamma = (1.0 - \eta \tan\phi)^2$

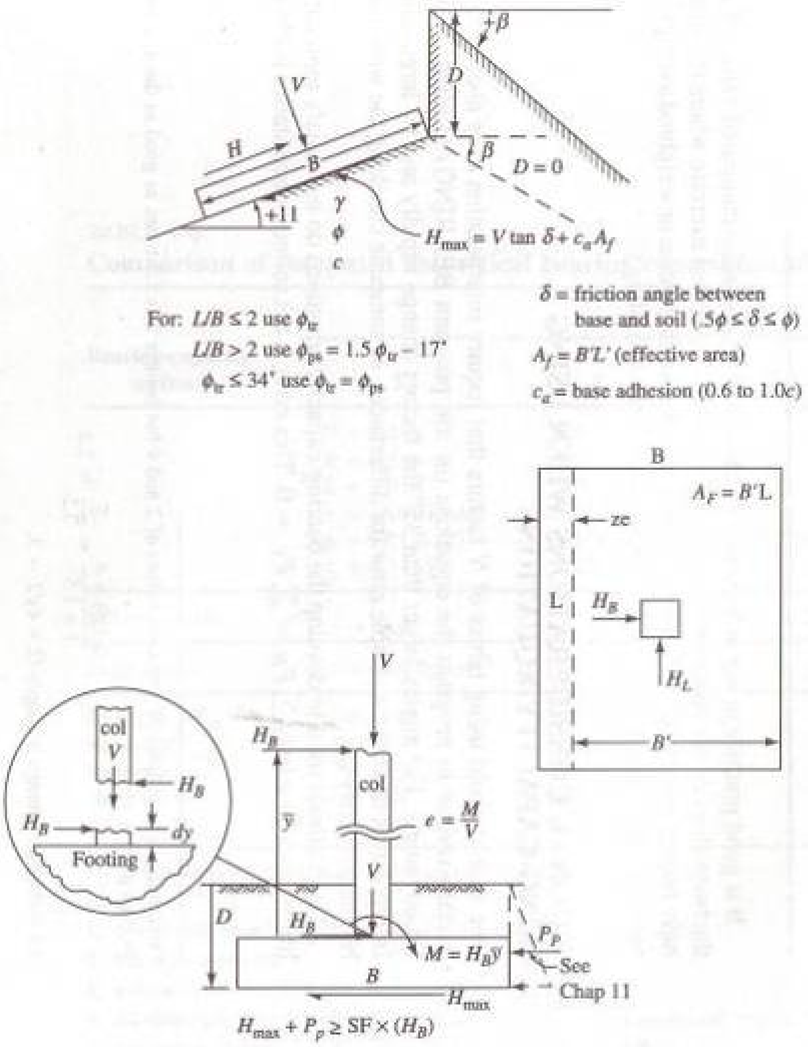
+β
D
V
H
B
D = 0
β
+η
γ
φ
c
$H_{\max} = V \tan\delta + c_a A_f$
B
$A_F = B'L$
ze
L
H_B
H_L
B'
V
H_B
col
V
H_B
H_B
dy
Footing
col
$\bar{y}$
$e = \dfrac{M}{V}$
V
D
H_B
$M = H_B\bar{y}$
P_P
See Chap 11
B
$H_{\max}$

For: $L/B \le 2$ use ϕ_{tr}

$L/B > 2$ use $\phi_{ps} = 1.5\,\phi_{tr} - 17°$

$\phi_{tr} \le 34°$ use $\phi_{tr} = \phi_{ps}$

δ = friction angle between base and soil ($.5\phi \le \delta \le \phi$)

$A_f = B'L'$ (effective area)

c_a = base adhesion (0.6 to 1.0c)

$H_{\max} + P_p \ge \mathrm{SF} \times (H_B)$

2.4.4 Vesic's Bearing Capacity Equations

The Vesic (1973, 1975) procedure is essentially the same as the method of Hansen (1961) with select changes. The N_c and N_q terms are those of Hansen but N_γ is slightly different (see Table 2.4). There are also differences in the i_i, b_i, and g_i terms as in Table 2.5*c*. The Vesic equation is somewhat easier to use than Hansen's because Hansen uses the *i* terms in computing shape factors s_i whereas Versic does not.

2.4.5 Which Equations to Use

There are few full scaled footing tests reported in the past. The reason is that they are very expensive to do and the cost is difficult to justify except as pure research or for a precise determination for an important project, usually on the basis of settlement control. Few clients are willing to underwrite the costs of a full scaled footing load test when the bearing capacity can be obtained, often using empirical Standard Penetration Test (SPT) or Cone Penetration Test (CPT) data directly.

The Terzaghi equations, being the first proposed, have been very widely used. Because of their greater ease of use (does not need to compute all the extra shape, depth, and other factors). They are only suitable for a concentrically loaded footing on horizontal ground. They are not applicable for footings carrying a horizontal shear and/or a moment or for tilted bases.

Use	**Best for**
Terzaghi	Very cohesive soils where $D/B \leq 1$ or for a quick estimate of q_{ult} to compare with other methods. *Do not use* for footings with moments and/or horizontal forces or tilted bases and/or sloping ground.
Hansen, Meyerhof, Vesic	Any situation that applies, depending on user preference or familiarity with a particular method.
Hansen, Vesic	Where base is tilted; when footing is on a slope or when $D/B > 1$.

2.5 Analysis of the Physical Models

In this part of the paper three physical models will be used to illustrate the ultimate bearing capacity of shallow foundations on one layer sand, two layers sand, and sand on clay. The models will be constructed and tested to represent the failure patterns of different soil types.

2.5.1 Preparation

Initially, the design documents were prepared for this physical model. The drawings were achieved using AutoCAD 2005. The front view of the sand model is shown in Fig. 2.11 and 2.12. The front view of the sand on clay model is shown in Fig. 2.13. The complete drawing of the model is in Appendix X.

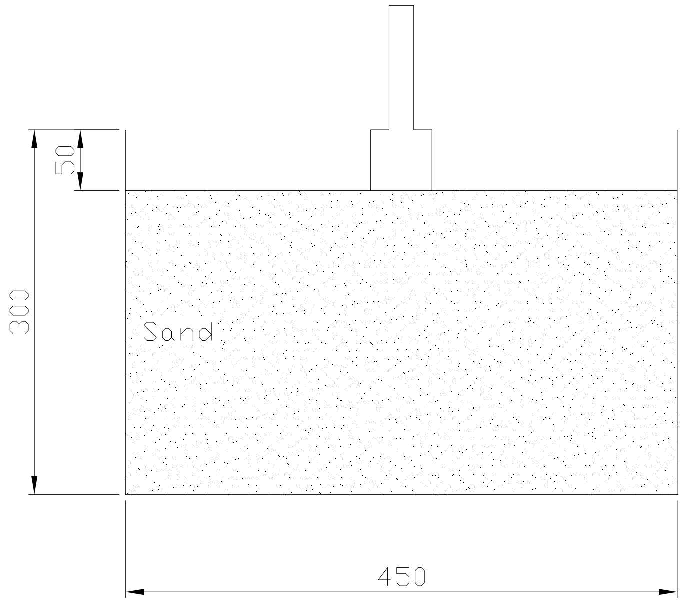

Figure 2.11: Front view of the one layer sand model.

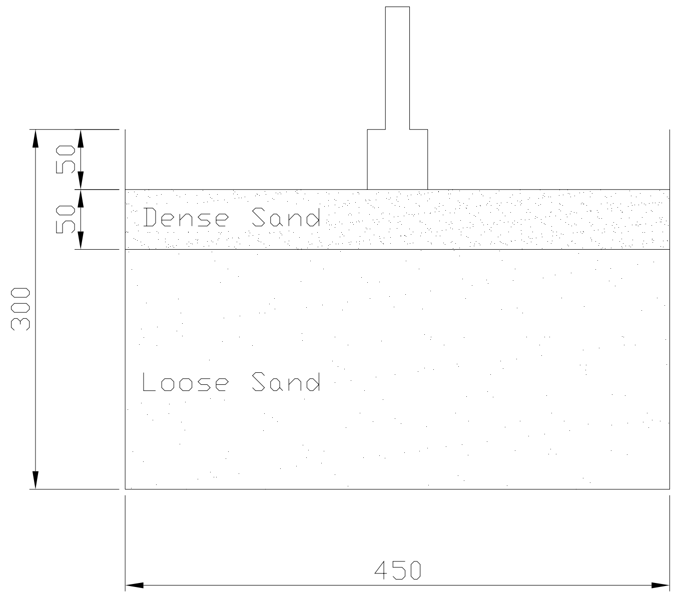
50
50
300
Dense Sand
Loose Sand
450

Figure 2.12: Front view of the two layers sand model.

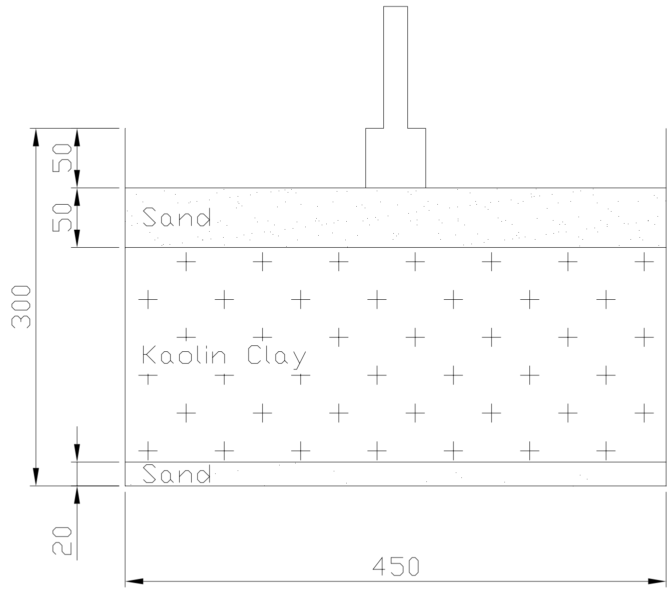
50
50
300
Sand
Kaolin Clay
Sand
20
450

Figure 2.13: Front view of the sand on clay model.

2.5.2 Construction

The materials required to construct the physical models are

- Clear Perspex
- Coated Form Plywood
- Kaolin Clay
- Fine Sand and Coarse Sand
- Small Scaled Footings

The construction involved cutting the Clear Perspex and Coated Form Plywood into the required sizes. The models are then assembled using silicone adhesive and screws. The front cover will be Clear Perspex to allow viewing of the shear failure pattern.

Fine sand was selected to use in one layer sand case. The sand was placed into the tank in layers (50 mm) and compacted well (20 blows each layer). The front cover was then removed and the grid lines were sprayed on top of the grid plate. Then the front cover was fitted and the model was ready for testing.

For the two layer sand case, the procedure is similar to the one layer sand case except that the method of compaction is different because this model aims to demonstrate the ultimate bearing capacity of dense sand over looses sand. Fine sand was placed on the top of coarse sand. Coarse sand was compacted at the rate of 10 blows on each layer and 20 blows on each layer for the fine sand. The grid line was then sprayed with the same process as the one layer sand case.

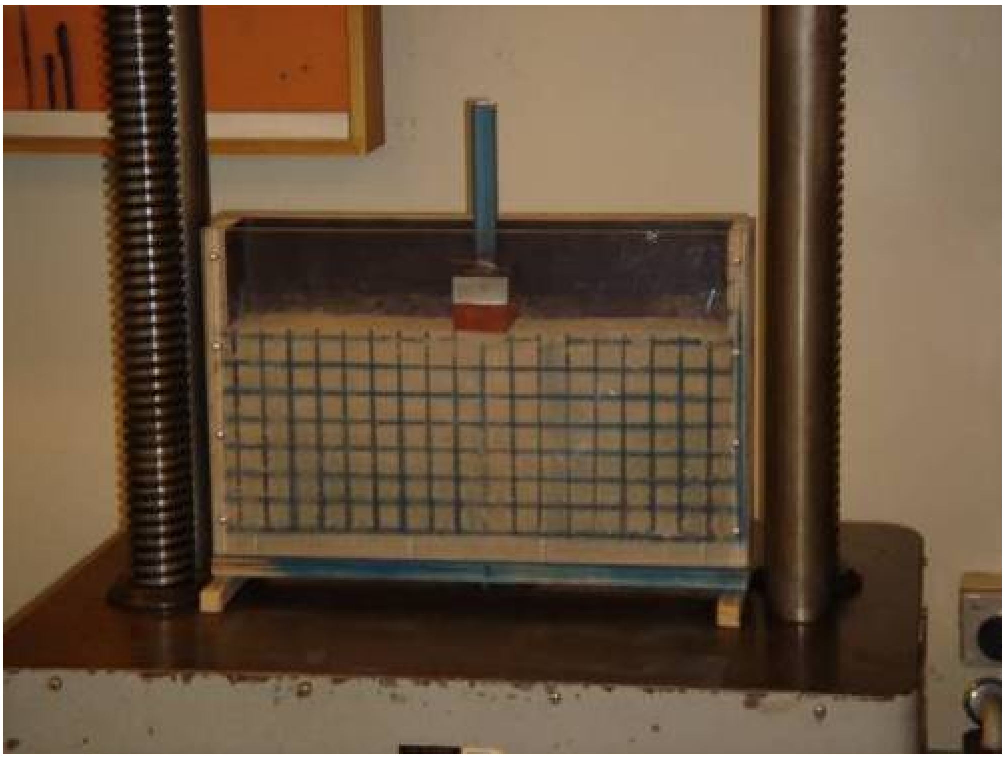

Figure 2.14: Finished one layer sand model.

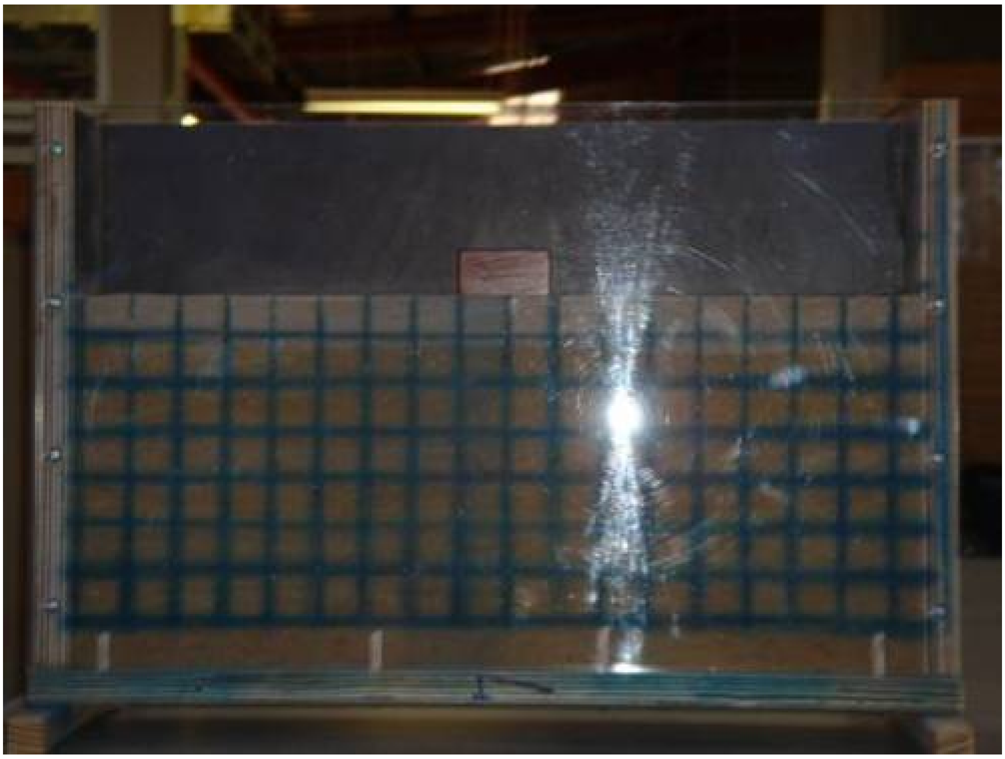

Figure 2.15: Finished two layers sand model.

In preparing the clay model, the model is required to have bottom drainage for reducing the moisture contents. The preparation of the Kaolin clay and its properties will be discussed in detail in Section 2.6.

Steps for preparing the clay model:

1. Place a screen at the bottom of the tank. (to cover the bottom drainage holes and to keep the sand in place)

2. Fill the dry sand on top of the screen for 20 mm. (to drain water from mixed Kaolin clay)

3. Fill the fresh mixed Kaolin clay in layer and compact well.

4. The model will then undergoes the one-dimensional consolidation process until the moisture content reach 40-45%.

5. Remove the front cover and used a red marker to draw a grid line.

6. Put the front cover back and place the footing to the desire location.

7. The model is ready for testing

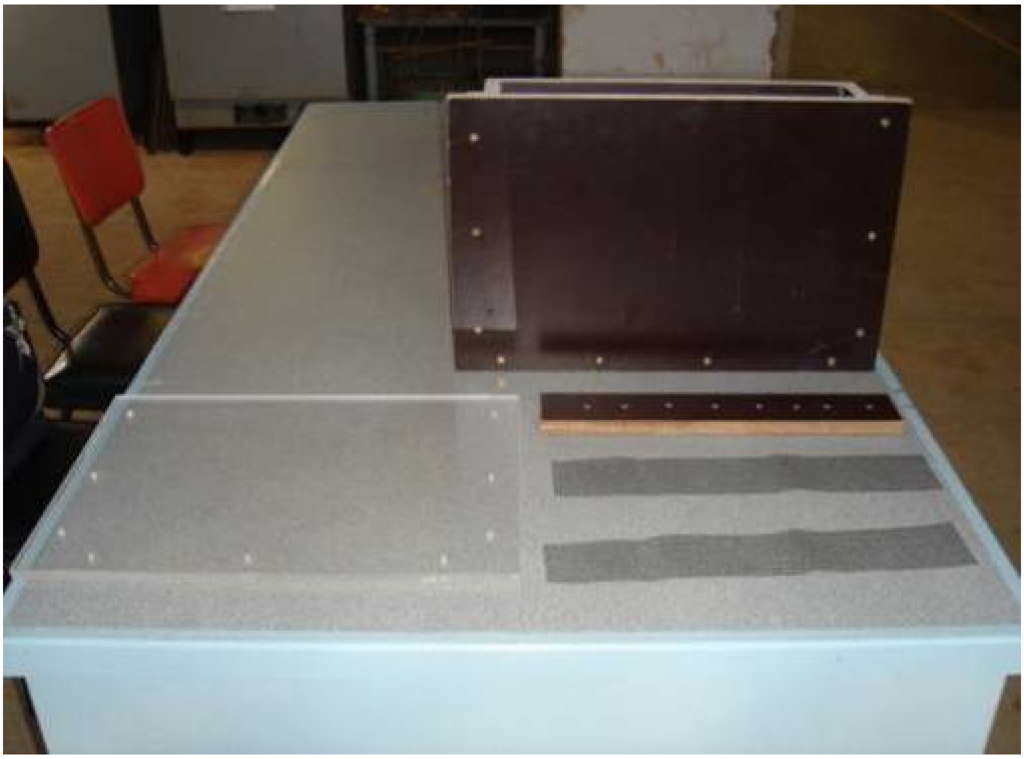

Figure 2.16: Completed tank, Perspex front cover, screen, and top cover.

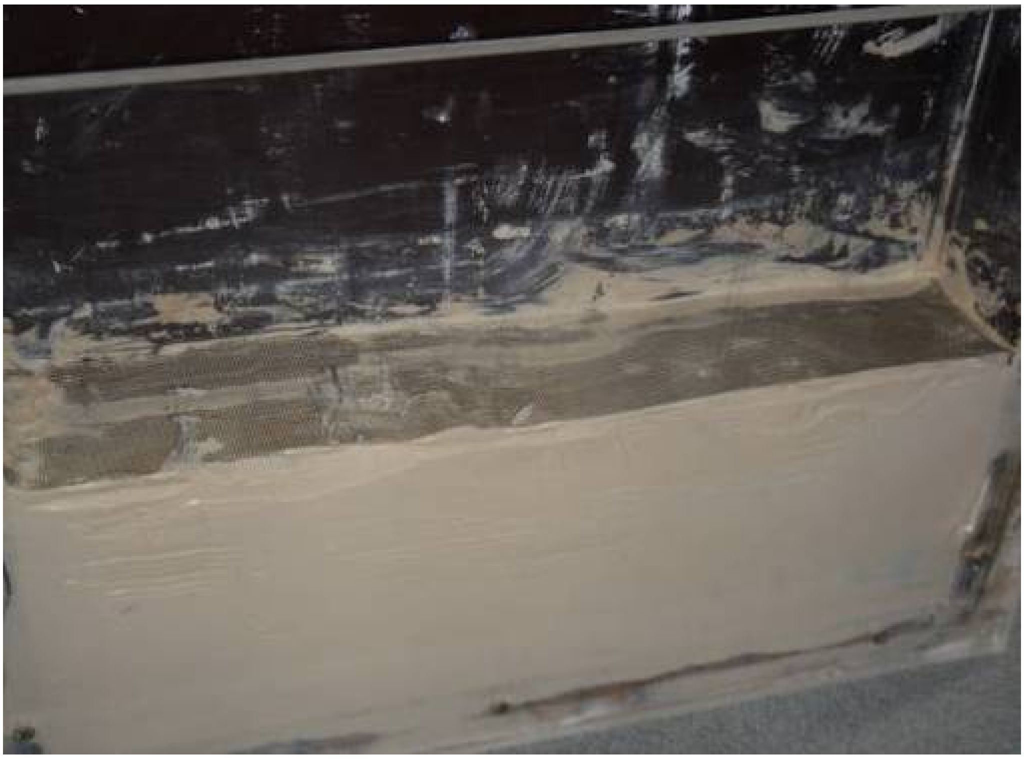

Figure 2.17: Soil reinforcement of sand on clay model.

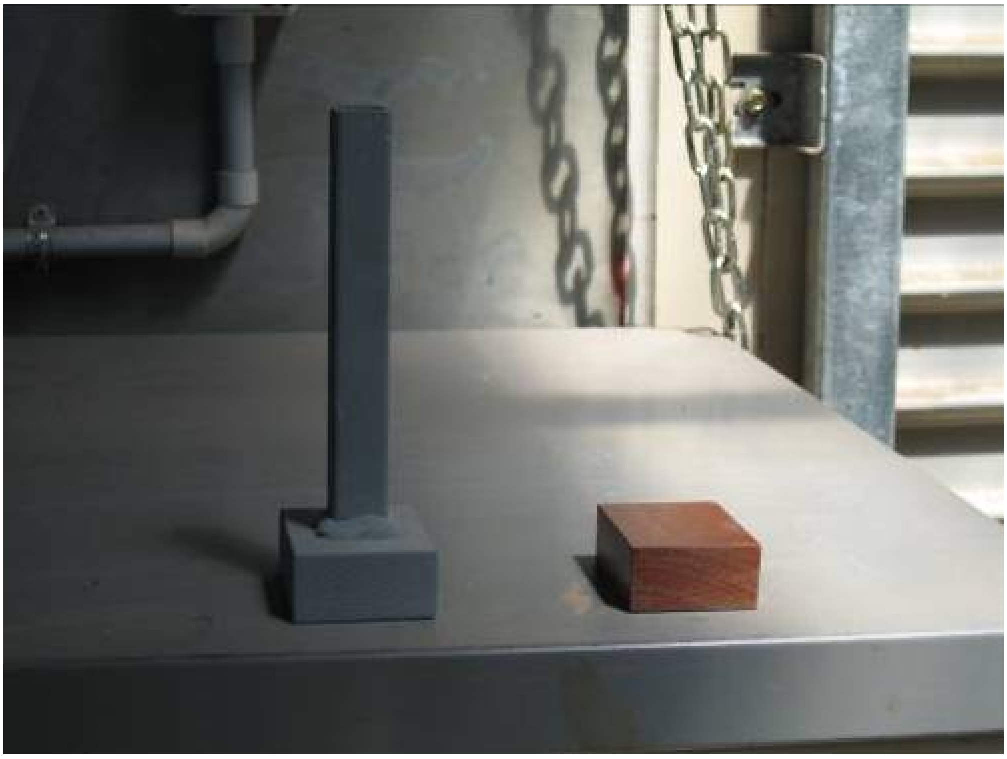

Figure 2.18: Scaled footing

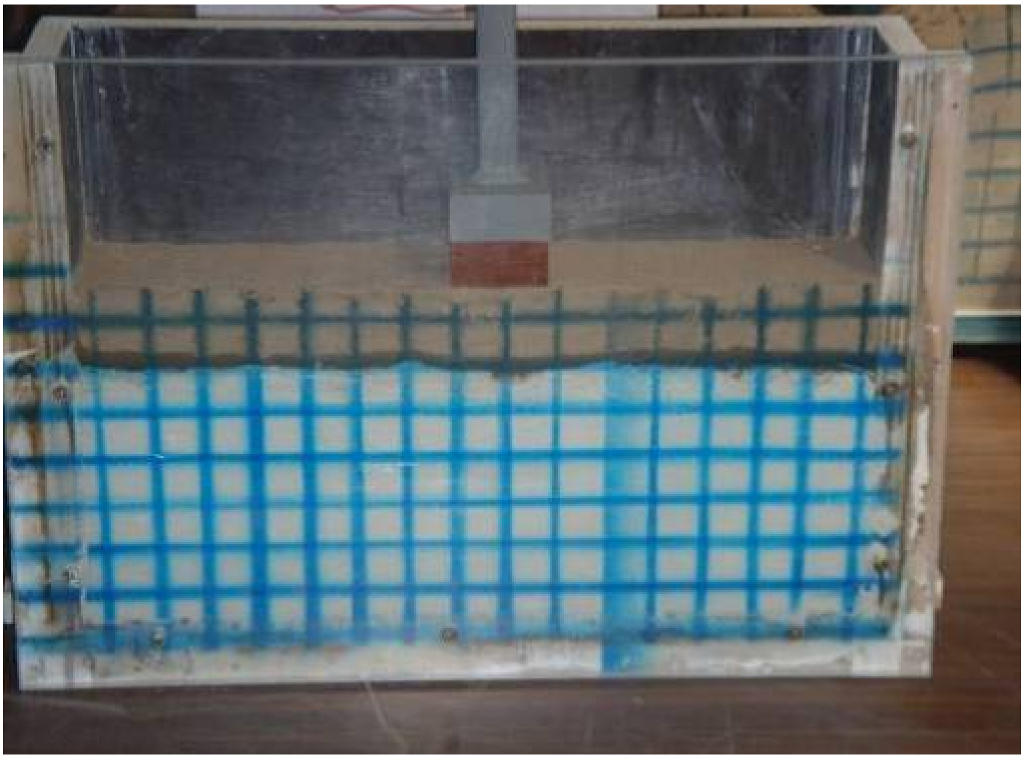

Figure 2.19: Finished sand on clay model.

2.5.3 Testing of the Models

The physical models are tested using a simple compression machine similar to the machine used in concrete testing. Results obtained from this machine can be used to develop a load versus deformation curve.

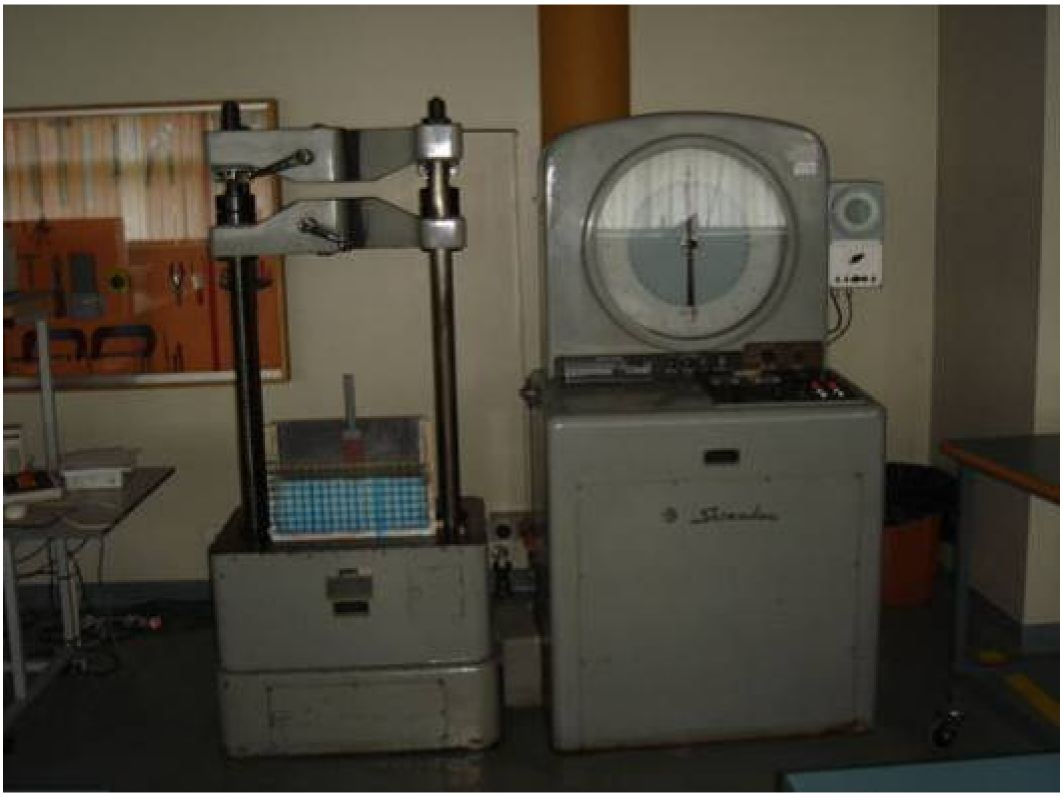

Figure 2.20: The compression machine.

2.5.4 Results and Discussions

The compression machine was started and accelerated at 1 mm per minute until the failure. After failure was occurred, the machine was stopped and taken out of the machine. The model was then placed in a safe place to avoid any disturbance from altering the failure mechanisms. The results for the load and deformation were recorded.

Figure 2.21 and 2.22 shows the failure mechanisms and load versus deformation curve for one layer sand model. The failure mechanism of this model can be compare with the local shear failure mechanism shown in Section 2.2. During the test, the load rate was adjusted to fasten the process.

Figure 2.23 and 2.24 shows the failure mechanisms and load versus deformation curve for two layers sand model. The failure mechanism of this model cannot be compared to any of the failure mechanisms shown in the text book because of the second layer contains too many air voids due to the compaction. When the load applied, the air voids between sand particles was remove but cannot create the particle interlocking (no friction angle, ϕ). Therefore, there is no shear failure plane developed for this model.

Figure 2.25 and 2.26 shows the failure mechanisms and load versus deformation curve for sand on clay model. This model is a special case. A geo-membrane was installed to study the effect of soil reinforcement. However, without any anchorage on both sides of the membrane, the tensile force on the membrane could not gain the full strength. The footing was also tilted to the left which created an unsymmetrical shear failure plane. Only left side of the soils sample was push and fail. Plot off the load-deformation curve shown that the geo-membrane can be used to improve the soil bearing capacity.

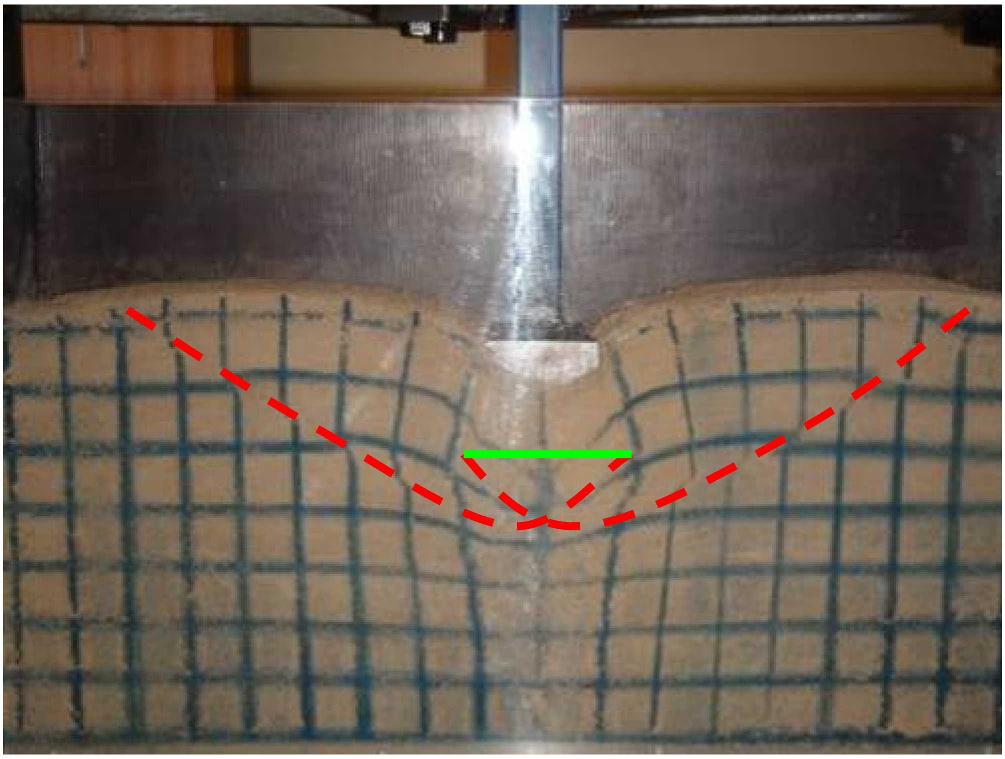

Figure 2.21: Failure mechanism of one layer sand model.

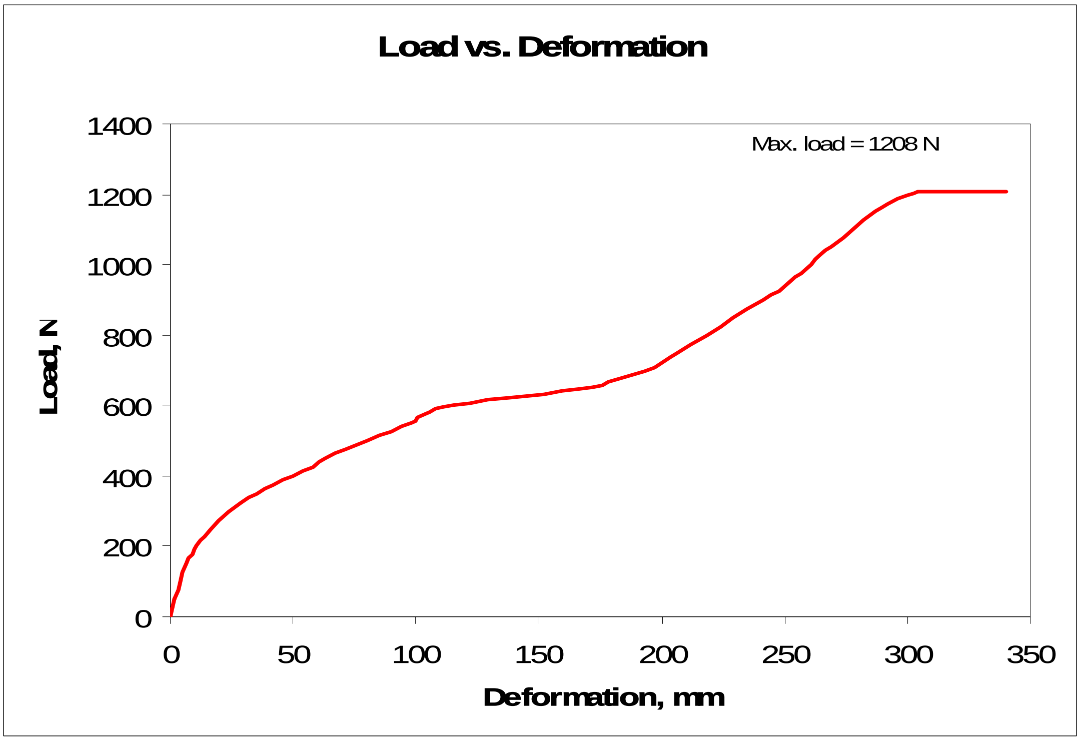

Figure 2.22: Plot of load vs. deformation of one layer sand model.

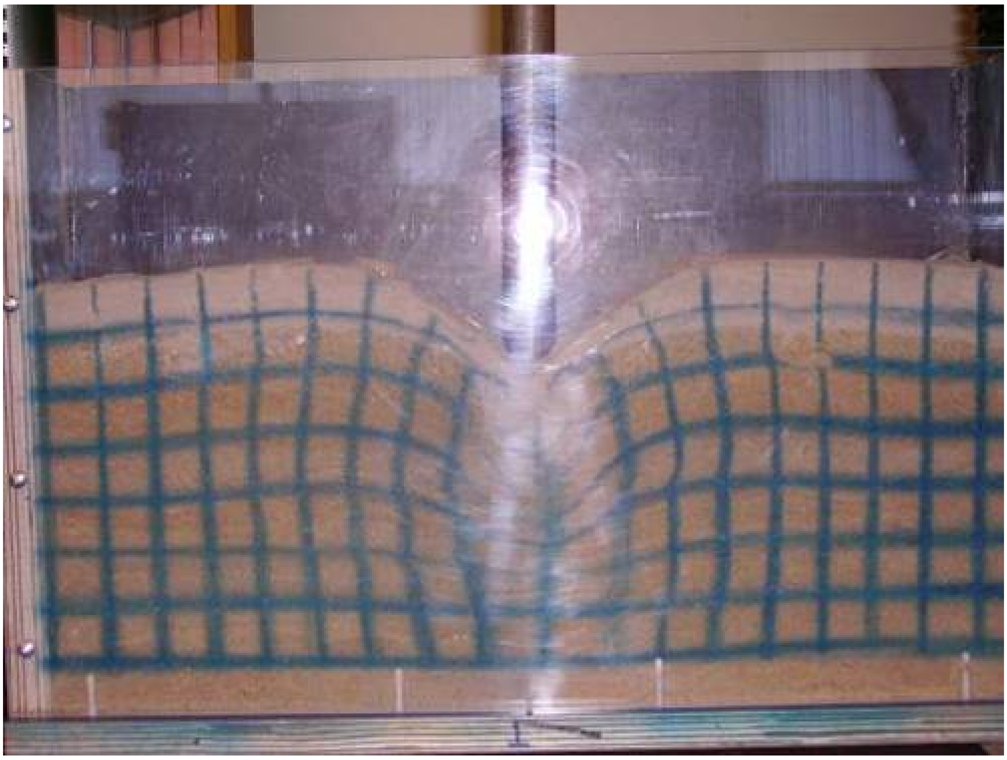

Figure 2.23: Failure after tested of two layers sand model.

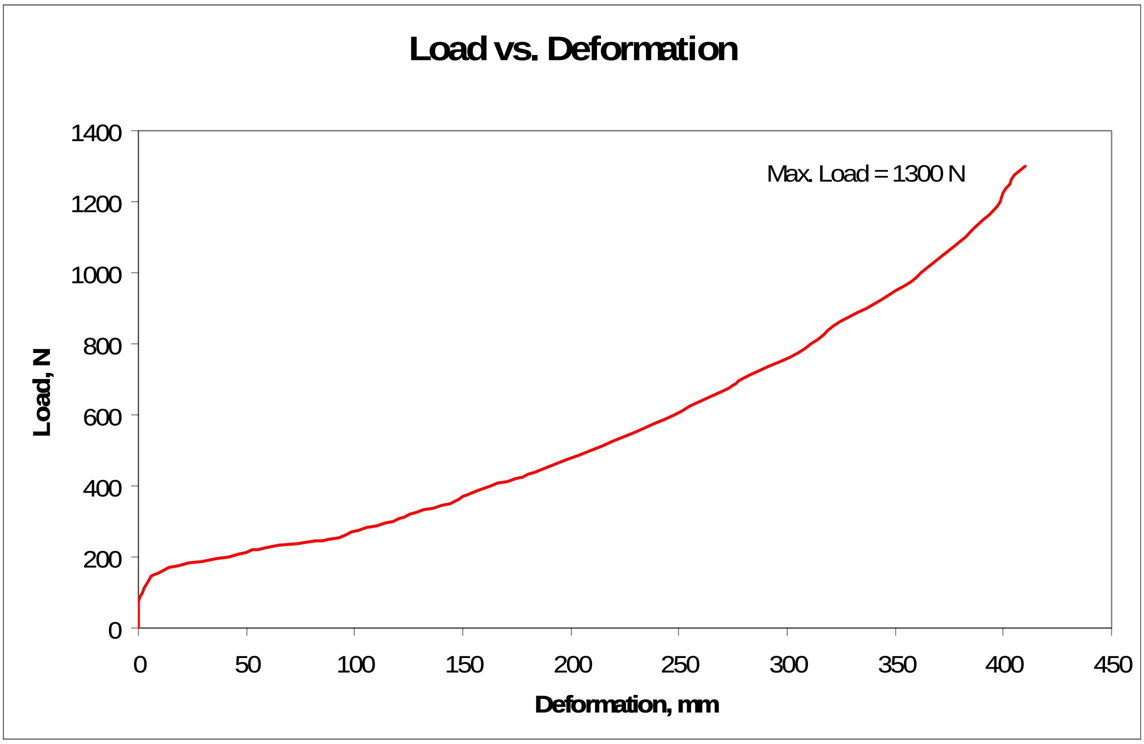

Figure 2.24: Plot of load vs. deformation of two layers sand model.

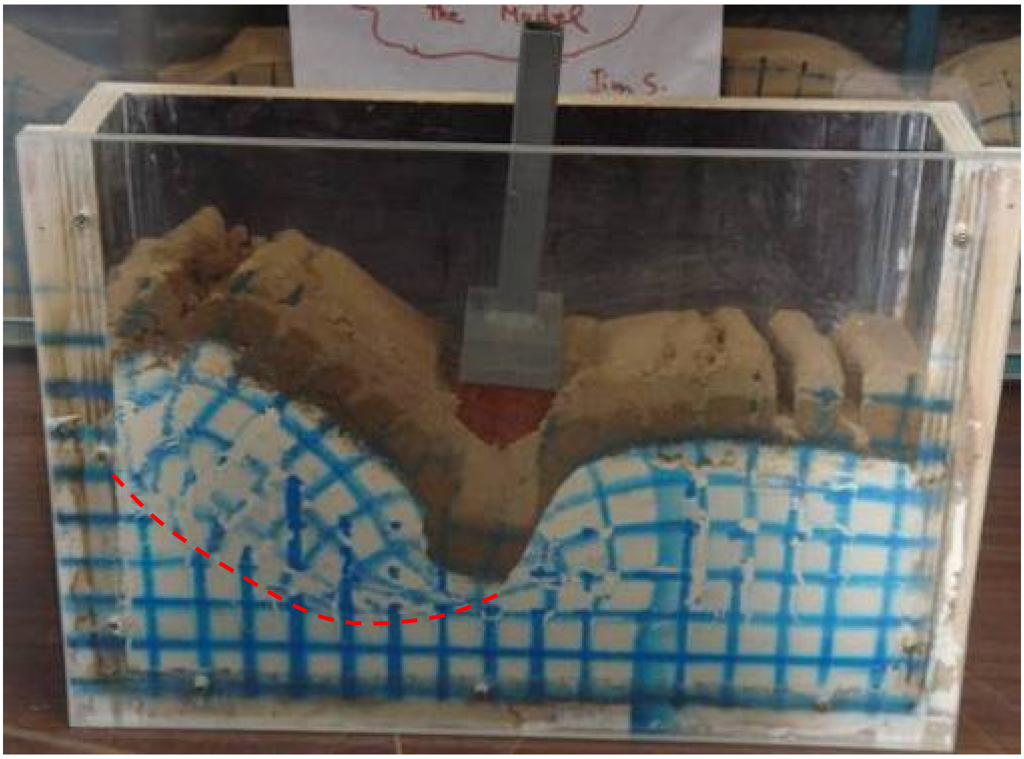

Figure 2.25: Failure mechanism of sand on clay model.

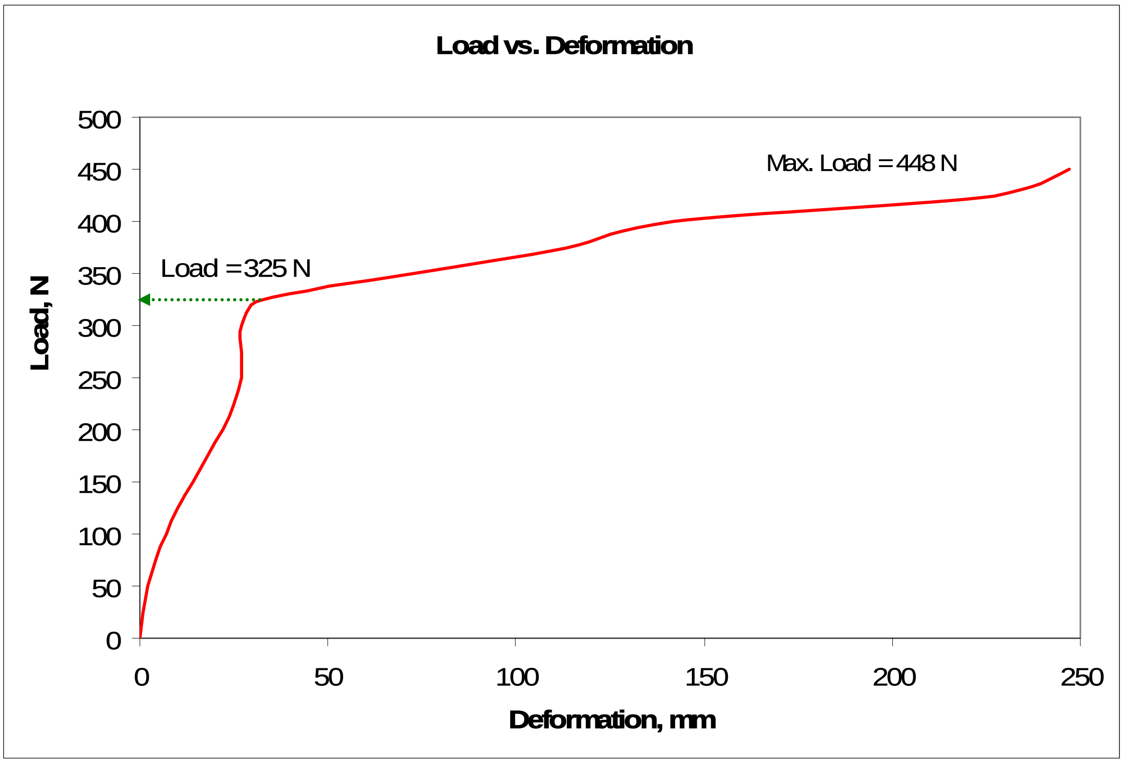

Figure 2.26: Plot of load vs. deformation of sand on clay model.

2.6 Kaolin Clay

2.6.1 Properties of the Kaolin Clay

The properties of Kaolin clay were defined by previous year students.

Unit Weight: $\gamma_d = 12\ kPa$
$\gamma_w = 20\ kPa$

Specific Weight: $G_s = 2.67$

Atterberg Limits: Liquid limit = 43%
Plastic limit = 22%
Plasticity index = 21%

Cohesion Strength: Moisture content = 41%
Cohesive strength = 12 kPa

2.6.2 Preparation of Kaolin Clay

To obtain good homogenous soil from the model, the Kaolin clay had to be prepared in such a way that all air voids is removed without overstressing or overheating the clay sample.

Steps for preparing the Kaolin clay:

1. Mix Kaolin clay powder with water to achieve approximately 120% moisture contents.

2. Place mixed Kaolin clay into the prepared tank in layer and compact well using a rod to remove any air voids.

3. Fill the tank until full, flatten the top surface, and clean any unwanted clay.

4. Incrementally, one-dimensionally consolidated by placing a concrete block on top of the tank.

5. Record the initial settlement.

6. Double the weight every week and record the settlement.

7. Remove the concrete block until the moisture content reached 45-50%. The moisture content can be calculated from the change in volume of the tank. Figure 2.33 shows the diagram of clay model settlement.

8. Take off the front cover and draw the grid line.

9. Screw the front cover back and place the footing to the desire location.

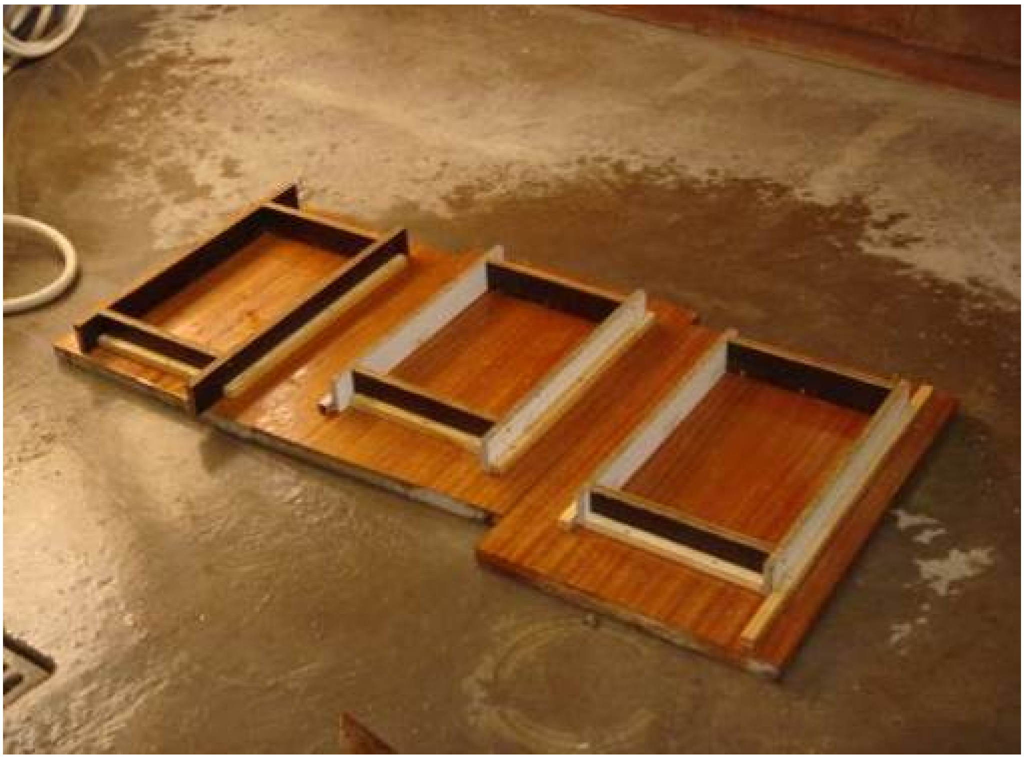

Figure 2.27: Mold for casting the concrete block.

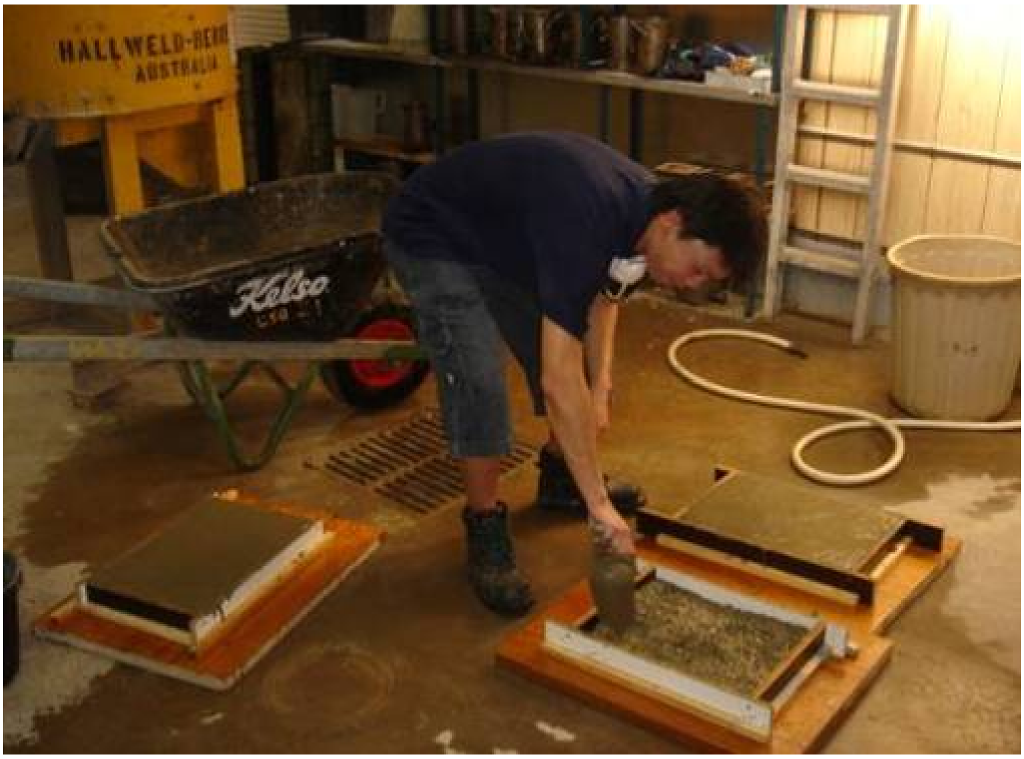
HALLWELD-HERE
AUSTRALIA
Kelso

Figure 2.28: Pure concrete into the mold.

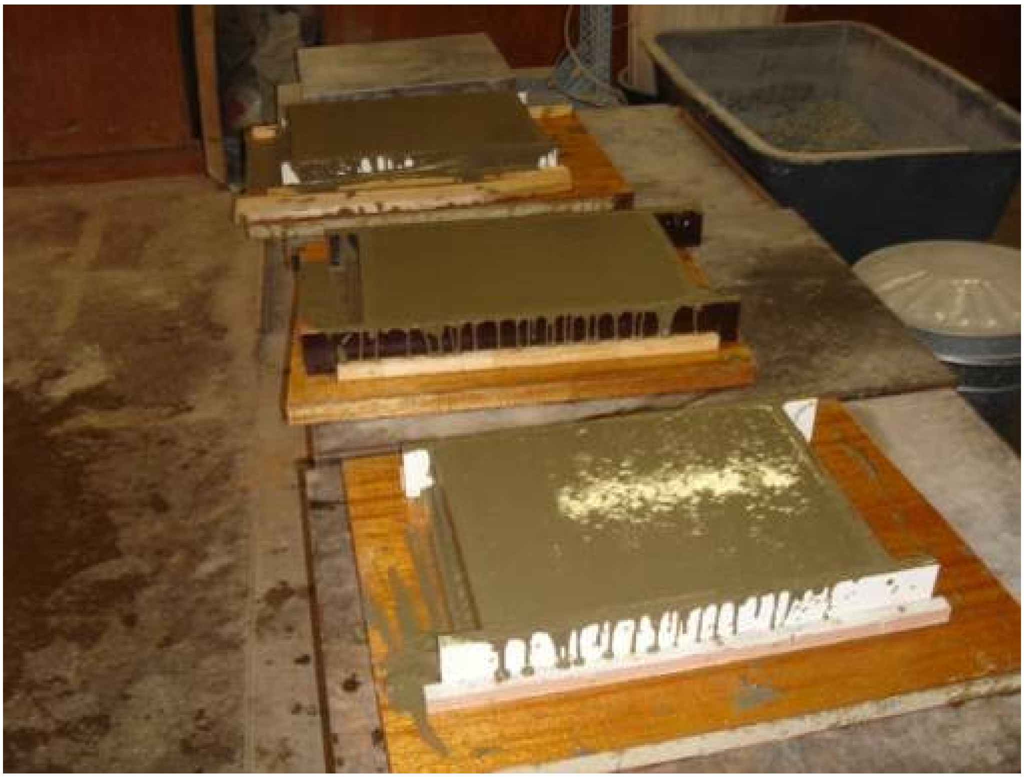

Figure 2.29: Flatten and keep in a safe place for one week.

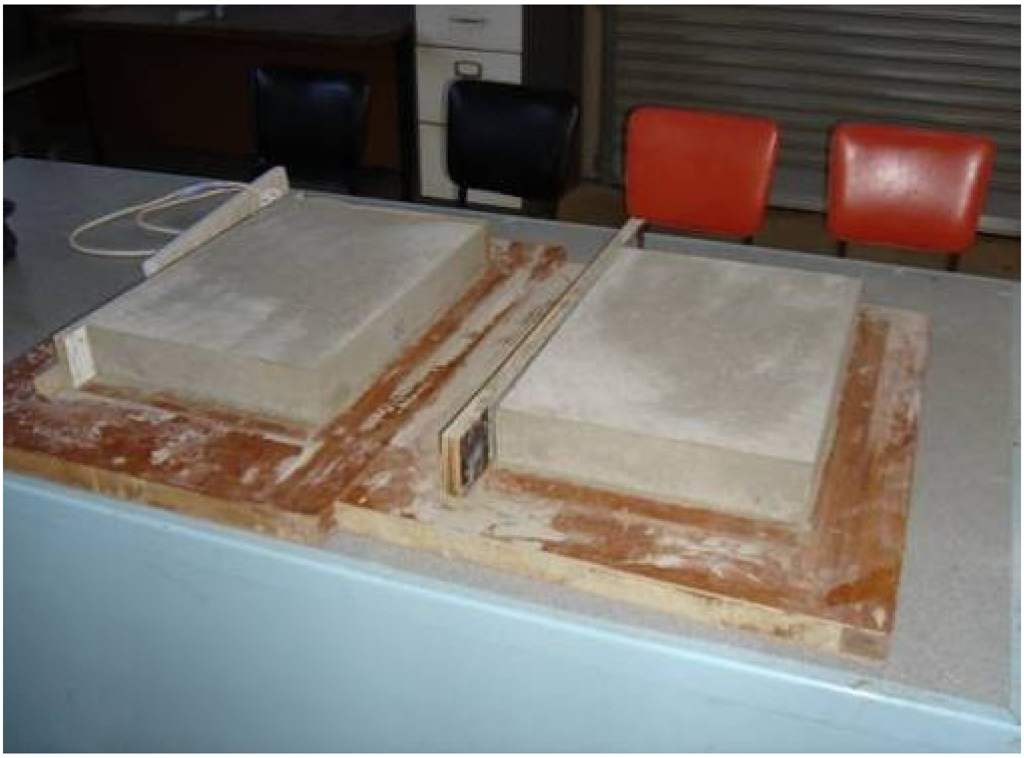

Figure 2.30: Concrete block ready to use.

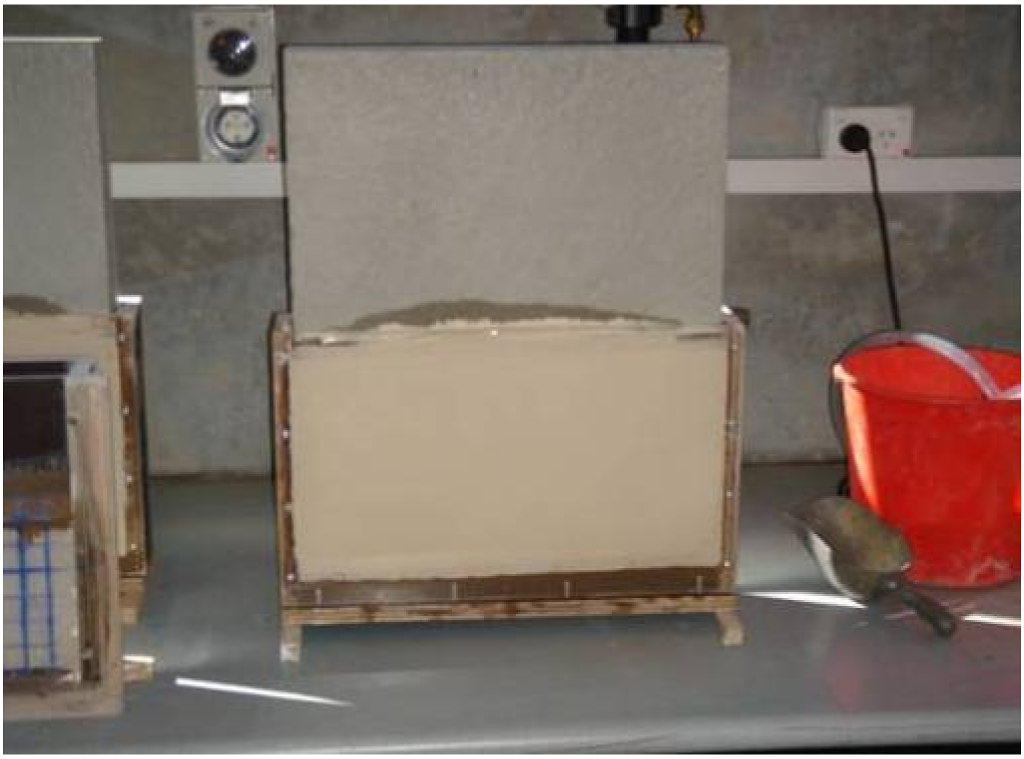

Figure 2.31: Applied the first concrete block.

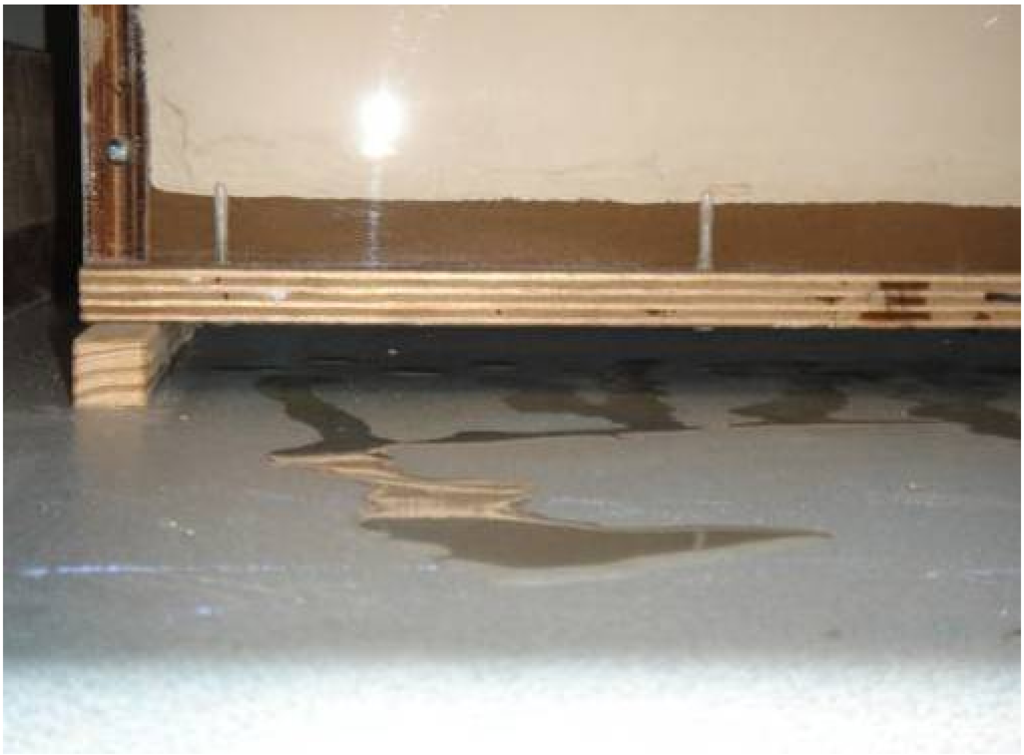

Figure 2.32: Water dropping from the bottom drainage holes.

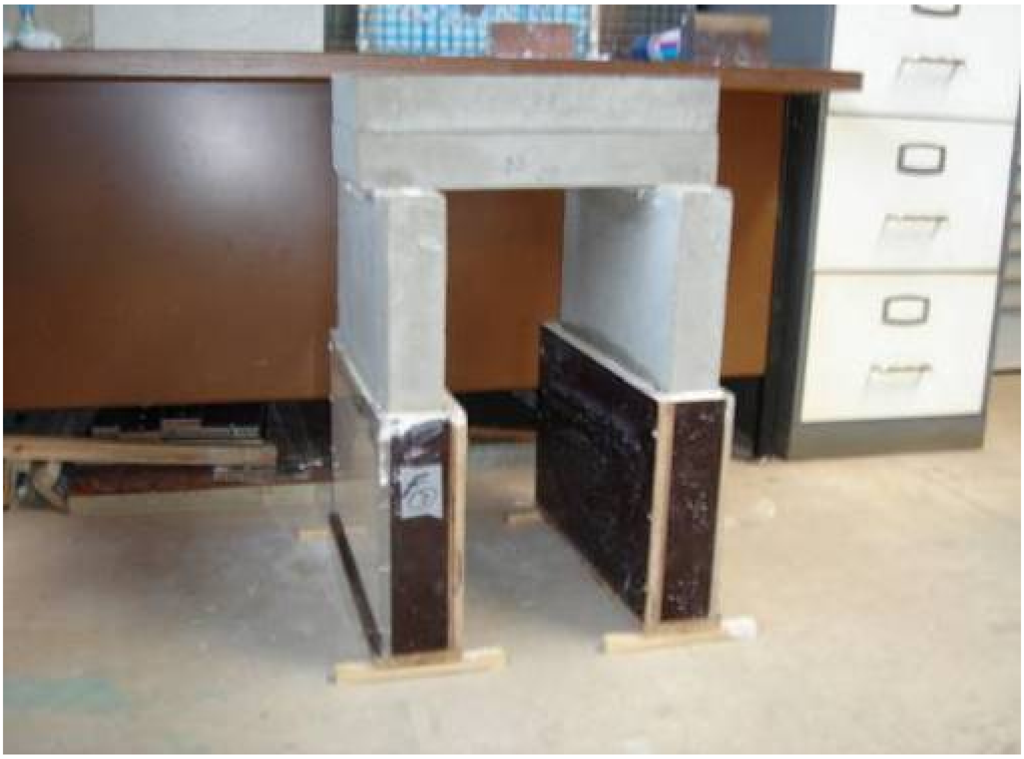

Figure 2.33: Applied the second concrete block.

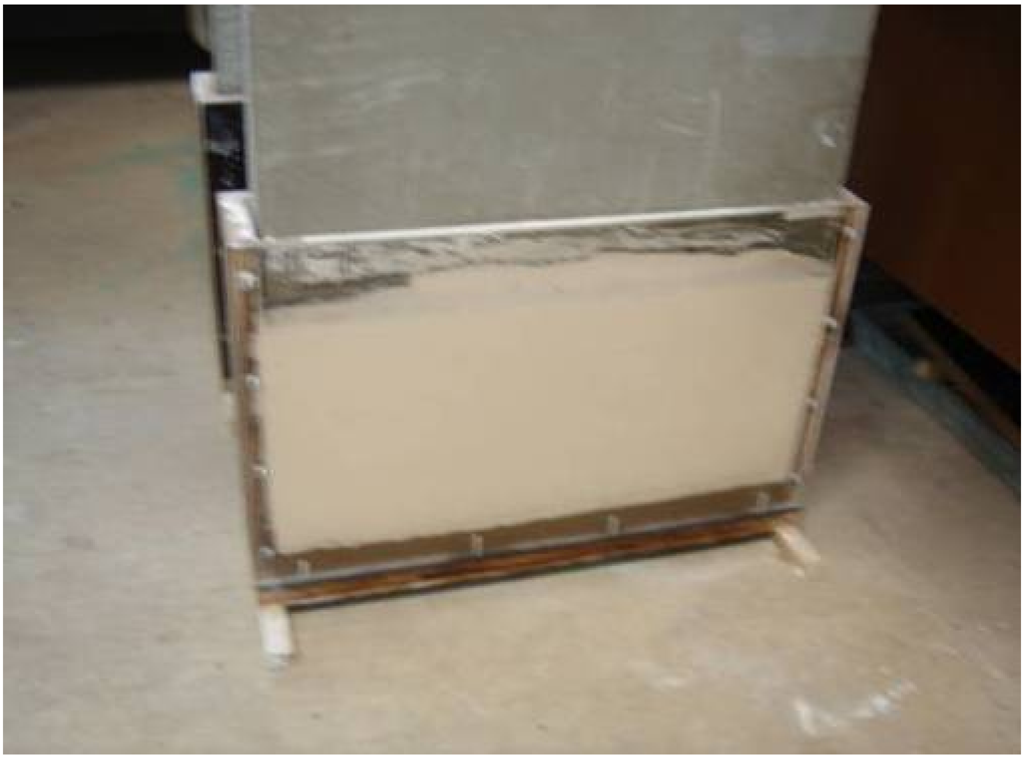

Figure 2.34: Settlement after applied the second concrete block.

The example of moisture content calculation is as follow:

Mixture of the two tanks,	Kaolin clay	= 18 *kg*
	Water	= 22 *kg*

Moisture content $= \dfrac{M_w}{M_s} = \dfrac{22}{18} = 122\%$

Initial volume of clay $= 0.258 \times 0.070 \times 0.450 = 0.008127\ m^3$

Volume of clay after one week $= 0.228 \times 0.070 \times 0.450 = 0.007182\ m^3$

Density of Kaolin clay, $\rho = 2300\ kg/m^3$

Mass of clay when wet $= \rho \times Volume = 2300 \times 0.008127 = 18\ kg$

Mass of clay after one week $= 2300 \times 0.007182 = 16.5\ kg$

After one week,

$\therefore$ Moisture content of one tank $= \dfrac{M_{w,\,after\,one\,week}}{M_s} = \dfrac{(16.5 - 9)}{9} = 83\%$

After two weeks,

Volume of clay $= 0.203 \times 0.070 \times 0.450 = 0.006394\ m^3$

Mass of clay $= 2300 \times 0.006394 = 14.7\ kg$

$\therefore$ Moisture content $= \dfrac{M_{w,\,after\,two\,weeks}}{M_s} = \dfrac{(14.7 - 9)}{9} = 63\%$

After three weeks,

Volume of clay $= 0.190 \times 0.070 \times 0.450 = 0.005985 \ m^3$

Mass of clay $= 2300 \times 0.005985 = 13.7 \ kg$

$$\therefore \text{ Moisture content } = \frac{M_{w, after\,three\,weeks}}{M_s} = \frac{(13.7 - 9)}{9} = 53\%$$

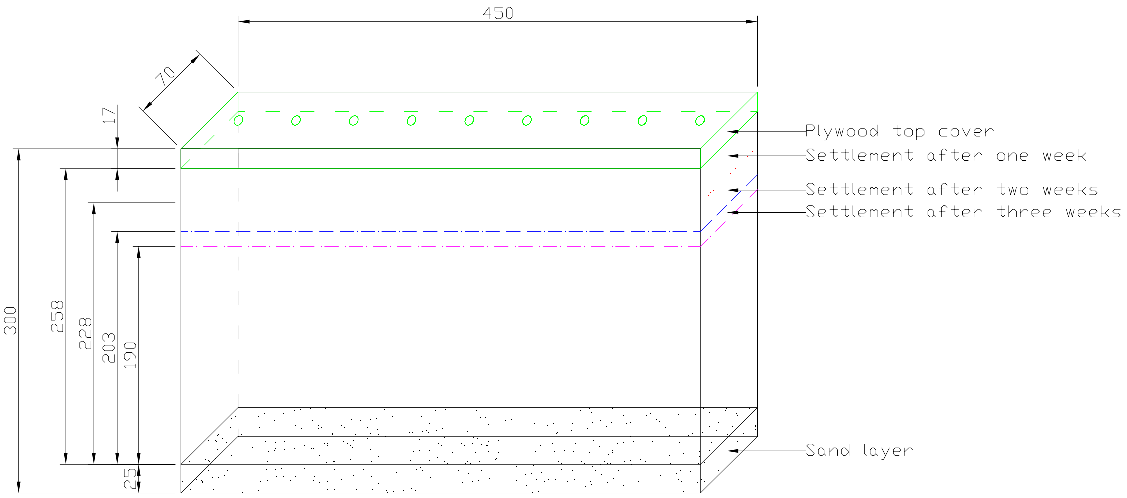
450
70
17
300
258
228
203
190
25
Plywood top cover
Settlement after one week
Settlement after two weeks
Settlement after three weeks
Sand layer

Figure 2.35: Diagram of clay model settlement.

2.7 Comparison of Results

Numerical Method

The ultimate bearing capacity, q_{ult} of the model can be calculated using:

$$q_{ult} = \frac{P_{\max}}{A} \tag{2.10}$$

where, P_{max} = Maximum load, kN

A = Area under footing, m^2

All the footings used in model testing are identical. So

$$A = 0.050 \times 0.070 = 0.0035\ m^2$$

One layer sand model

The maximum load of the one layer sand model is 1208 N.

The ultimate bearing capacity for this model is

$$q_{ult} = \frac{1.208}{0.0035} = 345\ kPa$$

Terzaghi's Method

The footing and soil parameters:

B = 0.05 *m* L = 0.07 *m* γ = 19.62 *kN/m*^{3}

c = 0 ϕ = 40°

P_{max} = 1.208 *kN* (model) q_{ult} = 345 *kPa* (model)

Since c = 0 and no surcharge load, any factors with subscript *c* and *q* do not need computing. Use 1.0 for s_γ factor. The equation reduced to

$$q_{ult} = 0.5\gamma B N_\gamma$$

When ϕ = 40°, the factor N_γ is 100.4 from Table 2.2.

The ultimate bearing capacity from Terzaghi equation is

$$q_{ult} = 0.5 \times 19.62 \times 0.05 \times 100.4 = 49.25\,kPa$$

The result is too far out because of the scale effects. Generally, models on sand do not produce reliable test results compared to full-scale prototypes. The model reaction involves only a statistically small quantity of soil grains compare with that involved with the full-scale elements. (*Bowls, 1996*)

For example, sand requires confinement to develop resistance. The confined zone beneath a 50 × 70 mm model is almost nil when compared with the confined zone beneath a small 1 × 2 m footing.

For the two layers sand model, the result cannot be compared with the theoretical result because the sample did not fail. Due to the air voids, the sample can carry more loads without failure.

Chapter 3

FLOW NET

3.1 Introduction

A cofferdam is a temporary structure to exclude water and to enable the construction in the dry of foundations, bridge piers, and the like, or a sheet-pile enclosure on land, on waterlogged earth, for the same purpose. The cofferdam method enables the permanent construction to be carried out in the open air, the alternatives being caissons, monoliths, or cylinders, the last possible conjunction with piles.

The essential difference between sheet pile walls and cofferdams is the drainage of the backfill with the former, to avoid the greater penetration and anchorage otherwise necessary. Cofferdams, on the other hand, invariably hold back the maximum hydrostatic head possible and consequently need greater support. Where open caissons can be used, these are often more economical for foundations of small plan area, but sometimes the advantage of the cofferdam method over caissons is the avoidance of compressed-air work. (*Lee, 1961*)

There are many types of cofferdam which have been evolved, from the primitive earth dam to the modern interlocking steel pile cofferdam. The principle is simple; the space to be occupied by the foundation is enclosed and the excess water is pumped out. Until steel sheet piling became available, the cofferdam was limited to very low heads and to positions where no sudden rise in water level was likely to occur. However, steel sheet piling can be driven to 18 m or more, although care still has to be taken to select suitable sites in order to avoid troubles due to leakage or underflow causing flooding.

Various types of cofferdam have been successfully used from earth and rock dams to timber and clay puddle dams and steel sheet piling. Bags half-filled with clay and sand, and built in an orderly fashion, with increasing thickness at the base to resist the increased water pressure is an exceeding useful and successful method.

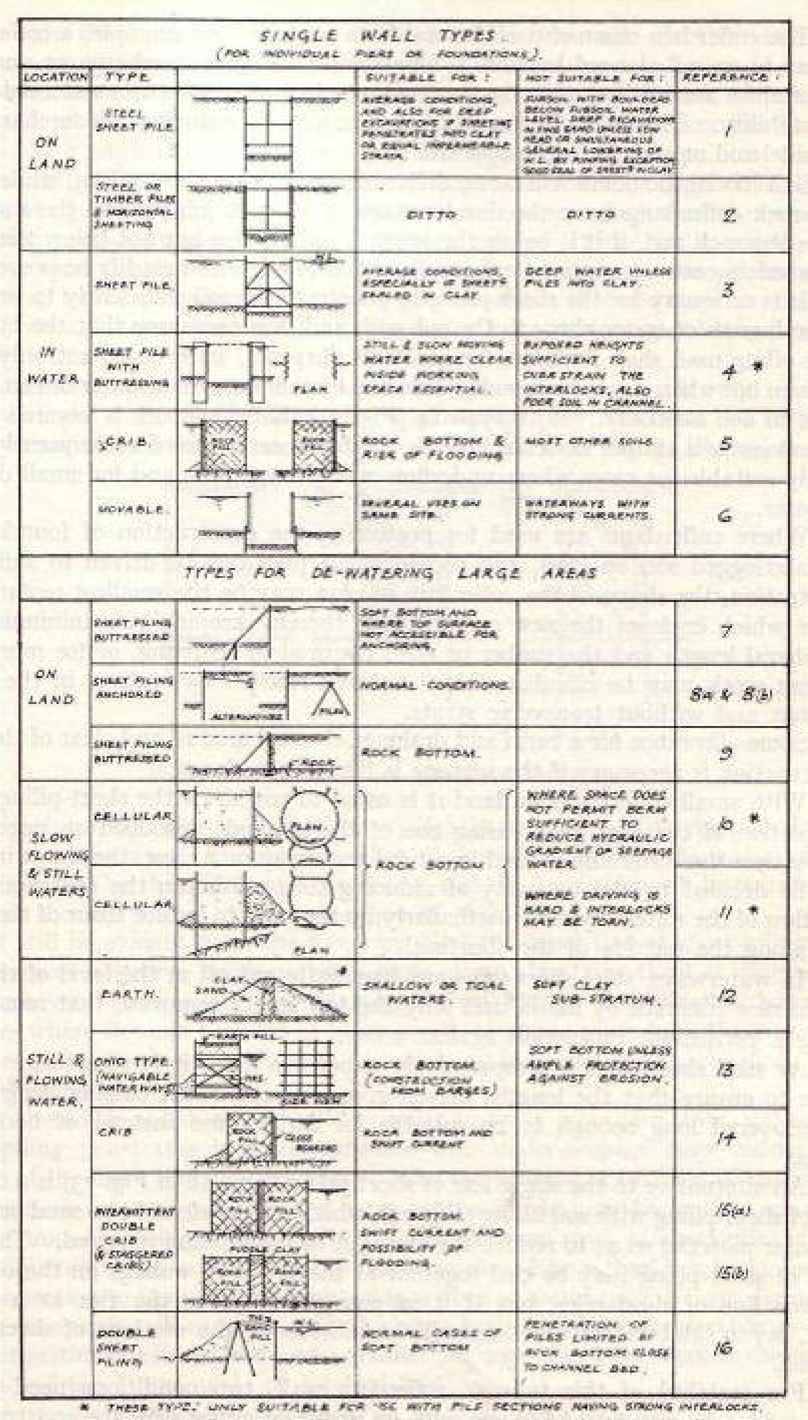
PLAN
ROCK FILL
CLAY
SAND
EARTH FILL
PUDDLE CLAY
CLOSE BOARDING
SIDE VIEW
ALTERNATIVE
W.L.

SINGLE WALL TYPES.
(FOR INDIVIDUAL PIERS OR FOUNDATIONS).

LOCATION	TYPE		SUITABLE FOR:	NOT SUITABLE FOR:	REFERENCE:
ON LAND	STEEL SHEET PILE		AVERAGE CONDITIONS, AND ALSO FOR DEEP EXCAVATIONS IF SHEETING PENETRATES INTO CLAY OR EQUAL IMPERMEABLE STRATA.	SUBSOIL WITH BOULDERS BELOW SUBSOIL WATER LEVEL. DEEP EXCAVATIONS IN THE SAME UNLESS LOW HEAD OR SIMULTANEOUS GENERAL LOWERING OF W.L. BY PUMPING EXCEPTION GOOD SEAL OF SHEETS IN CLAY	1
	STEEL OR TIMBER PILES & HORIZONTAL SHEETING		DITTO	DITTO	2
IN WATER	SHEET PILE.		AVERAGE CONDITIONS, ESPECIALLY IF SHEETS SEALED IN CLAY.	DEEP WATER UNLESS PILES INTO CLAY.	3
	SHEET PILE WITH BUTTRESSING		STILL & SLOW MOVING WATER WHERE CLEAR INSIDE WORKING SPACE ESSENTIAL.	EXPOSED HEIGHTS SUFFICIENT TO OVERSTRAIN THE INTERLOCKS, ALSO POOR SOIL IN CHANNEL.	4 *
	CRIB.		ROCK BOTTOM & RISK OF FLOODING	MOST OTHER SOILS.	5
	MOVABLE.		SEVERAL USES ON SAME SITE.	WATERWAYS WITH STRONG CURRENTS.	6
TYPES FOR DE-WATERING LARGE AREAS					
ON LAND	SHEET PILING BUTTRESSED		SOFT BOTTOM AND WHERE TOP SURFACE NOT ACCESSIBLE FOR ANCHORING.		7
	SHEET PILING ANCHORED		NORMAL CONDITIONS.		8a & 8(b)
	SHEET PILING BUTTRESSED		ROCK BOTTOM.		9
SLOW FLOWING & STILL WATERS.	CELLULAR.		ROCK BOTTOM	WHERE SPACE DOES NOT PERMIT BERM SUFFICIENT TO REDUCE HYDRAULIC GRADIENT OF SEEPAGE WATER.	10 *
	CELLULAR.			WHERE DRIVING IS HARD & INTERLOCKS MAY BE TORN.	11 *
STILL & FLOWING WATER.	EARTH.		SHALLOW OR TIDAL WATERS.	SOFT CLAY SUB-STRATUM.	12
	OHIO TYPE. (NAVIGABLE WATER WAYS)		ROCK BOTTOM. (CONSTRUCTION FROM BARGES)	SOFT BOTTOM UNLESS AMPLE PROTECTION AGAINST EROSION.	13
	CRIB		ROCK BOTTOM AND SWIFT CURRENT		14
	INTERMITTENT DOUBLE CRIB (& STAGGERED CRIBS)		ROCK BOTTOM. SWIFT CURRENT AND POSSIBILITY OF FLOODING.		15(a) 15(b)
	DOUBLE SHEET PILING		NORMAL CASES OF SOFT BOTTOM	PENETRATION OF PILES LIMITED BY ROCK BOTTOM CLOSE TO CHANNEL BED.	16

* THESE TYPES ONLY SUITABLE FOR USE WITH PILE SECTIONS HAVING STRONG INTERLOCKS.

Figure 3.1: Principal types of Cofferdam. (*Lee*, *1961*)

Water will enter the cofferdam in two ways: (*Lee, 1961*)

1. By leakage through the sheet piling.

   Practically all types of steel sheeting provide a reasonably watertight wall by reason of a practically continuous contact line in the interlocks of the piles when the wall defected by the lateral loading. Percolation through the interlocks is reduced by causing fine materials say, a mixture of ashes and sawdust, to pass into the leak from the water side, or alternatively the interlocks may be greased before driving so that fine material carried by seepage may lodge and seal the gap.

   More serious leaks may be reduced by a tarpaulin secured over the area concerned while the repair is effected, and stiffened so that it is not forced through any gap.

2. By under flow (Fig. 3.2).

   To prevent excessive underflow necessitates penetration sufficient, taking into account the permeability of the soil, to prevent the water coming in faster than it can conveniently be pumped.

   Where sheet piles have to be driven hard to obtain sufficient penetration to prevent excessive underflow, the ends of the sheet piles may become buckled and the interlock may be so damaged that the succeeding sheet will be forced out, with the result of considerable inflow of water being revealed when interior is being dewatered.

   With permanent piling, say along the bank of the river, penetration of the sheeting into clay or other impermeable strata is rather a disadvantage in preventing free drainage, and separate drainage should then be provided. In the case of cofferdams, however, to drive the sheeting through hard gravel to penetrate into an impermeable stratum will be most desirable in order to reducing pumping.

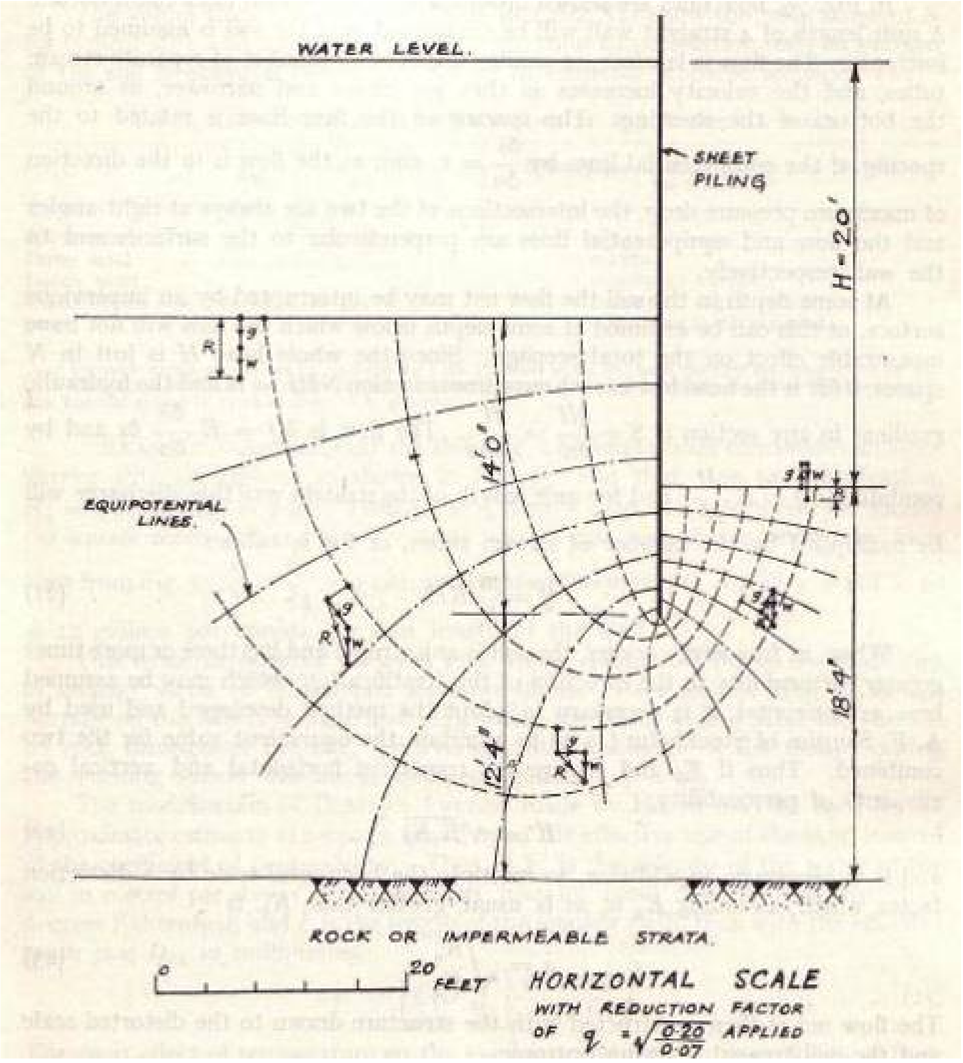
WATER LEVEL.
SHEET PILING
H=20'
R
g
w
14·0'
EQUIPOTENTIAL LINES.
12·4'
18·4'
ROCK OR IMPERMEABLE STRATA.
0
20 FEET
HORIZONTAL SCALE
WITH REDUCTION FACTOR OF q = √(0·20/0·07) APPLIED

Figure 3.2: Seepage by Underflow. (*Lee*, *1961*)

3.2 Seepage

It may be quite apparent that if one were pure water on a sandy or gravelly surface, the water would disappear into the ground. It may be equally apparent that one may not be successful in constructing an efficient dam from a sandy or gravelly soil; the water would *seep* out through the dam quite easily. On the other hand, the water flow through a fine-grain soil, such as silt or clay, would take place with more difficulty. In short, the quantity of flow, other conditions being equal (e.g. hydrostatic heads, stratum thickness, time, etc.), would be much greater in the granular soil than in the silty or clayey soil. The process of water flow through soil is commonly referred to as *seepage*.

Problems associated with the seepage phenomenon are likely to fall into one of the three groups dealing with:

1. Flow into pits or out of reservoirs.

2. Seepage pressures and related effects which they may have on the stability slopes, cuts, foundations, etc.

3. Drainage from fine grain soils subjected to load increase.

Like so many problems in soil mechanics, seepage analysis is frequently not much more than a reasonable estimate. The reason for this may very likely lie in the many assumptions that are made and which are most difficult to verify with any degree of accuracy.

3.2.1 Flow Net

When water flow through well-defined aquifers over long distances, the flow rate can be computed by using Darcy's law (Eq. (1.2)) if the individual terms in the equation can be evaluated. In case where the path of flow is irregular or if the water entering and leaving the permeable soil is over a short distance, flow boundary conditions may not be so well defined; an analytic solutions, such as the use of Eq. (1.2), become difficult. In such cases, flow may be evaluated by using *flow nets*. (*Liu & Evett, 1998*)

Figure 3.3 illustrated a flow net. In the figure, water *seeps* through the permeable stratum beneath the wall from the upstream side (left) to the downstream side (right). The solid lines below the wall are known as *flow lines*. Each flow line represents the path along which given water particle travels in moving from the upstream side through the permeable stratum to the downstream side. The dashed lines in Fig. 3.3 represent *equipotential lines*. They connect points on different flow lines having equal total energy heads. A collection of flow lines intersecting equipotential lines, as shown in Fig. 3.3, constitutes a flow net; and as demonstrated subsequently, it is a useful tool in evaluating seepage through permeable soil.

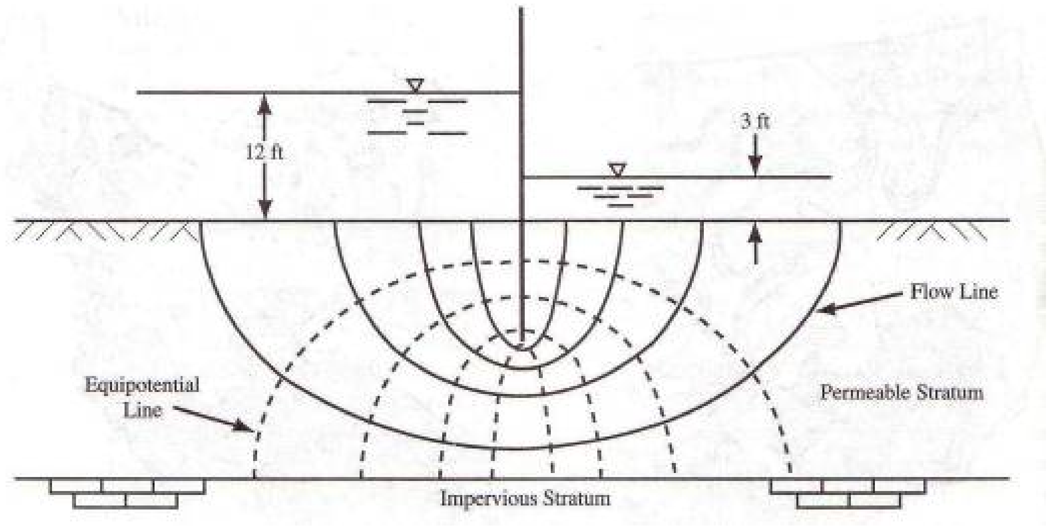

Figure 3.3: Flow net. (*Liu & Evett, 1998*)

Flow net can be of several types, depending on the configuration and the number of zones of soil or rock through which seepage is taking place. a primary subdivision can be made that depends on the following conditions:

1. Flow is *confined* within known saturation boundaries and the phreatic line is therefore known.

2. Flow is *unconfined* and the upper level of saturation (the phreatic line) is *not* known.

A second subdivision can be made that depends on whether (a) the cross section can be drawn as one zone or unit of a single permeability or (b) the cross section contains two or more zones or units of different permeabilities. That latter is described as a *composite section*.

These criteria give four possible combinations of flow conditions:

1a. Confined flow in single permeability sections.

1b. Confined flow in composite sections (those having two or more permeability abilities).

2a. Unconfined flow in single permeability sections.

2b. Unconfined flow in composite sections.

This paper will discuss the confined flow in both single and composite permeability abilities.

3.2.2 Construction of Flow Net

If all the boundaries to the flow regime are known at the outset, the flow net is described as confined. The construction of a confined flow net is illustrated below. (*Powrie, 1997*)

Figure 3.4 shows cross section through a long excavation in Norwich Crag, a fine sand mean permeability $k = 1.5 \times 10^{-4}$ m/s. The sides of the excavation are supported by steel sheet piles, a structure known as a cofferdam. the purpose of the excavation is to enable the construction of a cooling water outfall pipe for a coastal power station. The excavation is therefore to be made across a beach, so that the ground surface outside the sheet pile cofferdam must be assumed to be flooded with seawater to a depth of 2 m at high tide.

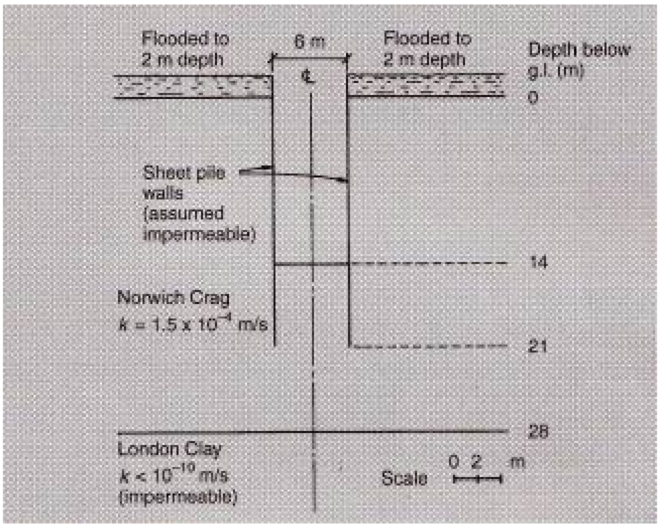
Flooded to 2 m depth
6 m
℄
Flooded to 2 m depth
Depth below g.l. (m)
0
Sheet pile walls (assumed impermeable)
14
Norwich Crag
$k = 1.5 \times 10^{-4}$ m/s
21
28
London Clay
$k < 10^{-10}$ m/s
(impermeable)
Scale
0 2 m

Figure 3.4: Geometry for example flow net construction: excavation for cooling water outfall pipe. (*Powrie, 1997*)

Newcomers to flow net sketching are often nervous about making a start, in case they make a mistake. It is at this stage that you must bear in mind that flow net sketching is an iterative process: it is only by making mistake, which are then corrected, that a satisfactory solution is approached. The flow net should be constructed methodically, and the following procedure should enable the newcomers to make a reasonable start. Remember also that the person who never made a mistake, never made anything: do not be afraid to try.

1. Is the problem geometry symmetrical about the centerline? If so - as in this case - it is only necessary to sketch one half of the flow net. Remember, however, that if only half the flow net is sketched, the number of flow tubes must be multiplied by two in order to calculated the flow rate per metre length.

2. Identify where the water is going to - the sink. Sketch in the bottom equipotential (i.e. the one with the smallest value of total head h) - in this case, the excavation floor, which we shall assume remains just covered in a shallow depth of water. Make this (or some other convenient point) the datum level from which the total head or potential is measured (Fig. 3.5a).

3. Identify where the water is coming from - the source. Sketch in the top equipotential (i.e. the one with the greatest value of the total head h) - in this case, the flooded beach on either side of the excavation (Fig. 3.5a: only the left-hand side is shown in the diagram).

   In Figure 3.4, the top equipotential has a value of 16 m relative to the floor of the excavation, even though the beach 1s only 14 m above the floor of the excavation. This is because the beach is flooded to a depth of 2 m. (Imagine a standpipe piezometer placed with its tip at the retained soil surface. Water will rise in the standpipe to the level of the free water surface, which is 2 m above the piezometer tip and 16 m above the floor of the excavation.)

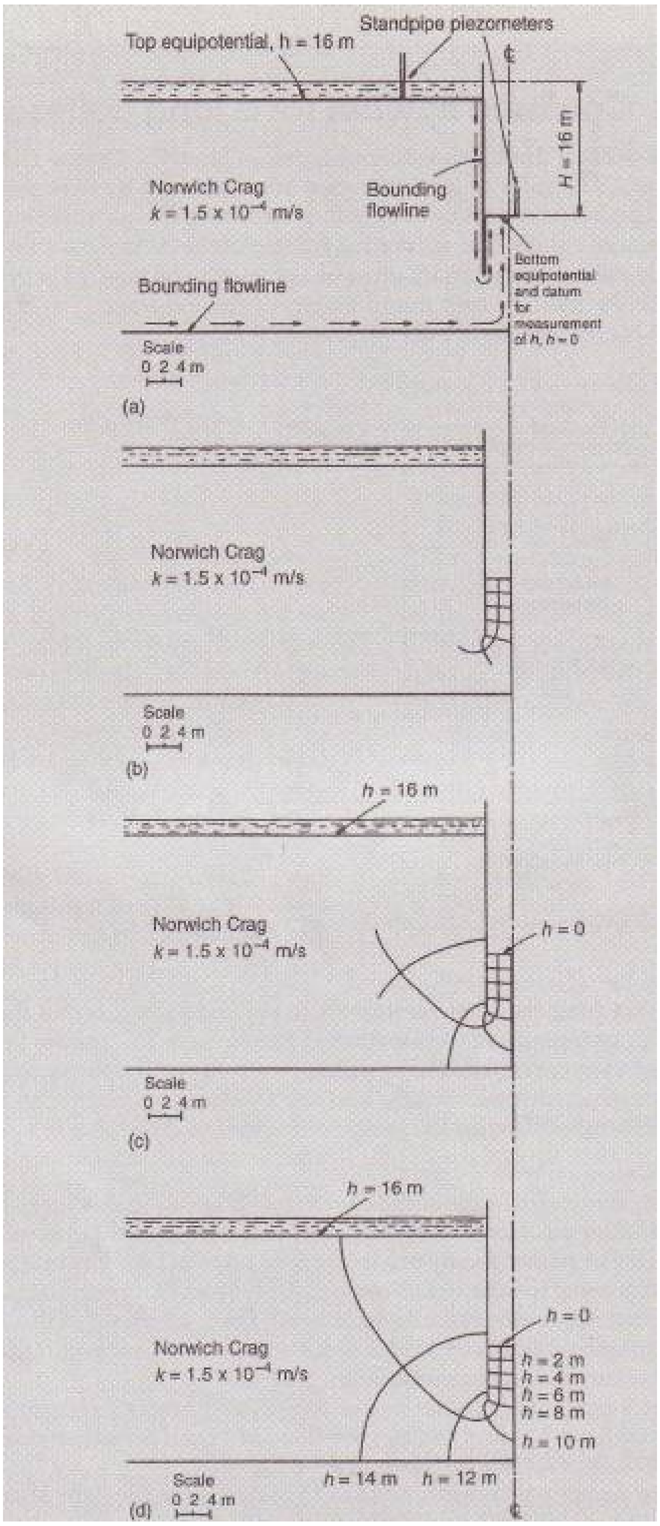
Standpipe piezometers
Top equipotential, h = 16 m
℄
H = 16 m
Norwich Crag
k = 1.5 x 10⁻⁴ m/s
Bounding flowline
Bottom equipotential and datum for measurement of h, h = 0
Bounding flowline
Scale
0 2 4 m
(a)
Norwich Crag
k = 1.5 x 10⁻⁴ m/s
Scale
0 2 4 m
(b)
h = 16 m
Norwich Crag
k = 1.5 x 10⁻⁴ m/s
h = 0
Scale
0 2 4 m
(c)
h = 16 m
h = 0
Norwich Crag
k = 1.5 x 10⁻⁴ m/s
h = 2 m
h = 4 m
h = 6 m
h = 8 m
h = 10 m
Scale
0 2 4 m
h = 14 m
h = 12 m
(d)
℄

Figure 3.5: Construction of flow net for cooling water outfall pipe excavation: (a) identify the sink, the source and the bounding flow lines; (b), (c) start sketch in intermediate flow lines and equipotentials, but keep it simple; (d) the finished flow net. (*Powrie, 1997*)

4. Identify the bounding flow lines. In this case, one flow line runs from the beach down the back of each of the sheet pile walls, round the bottom of the wall and into the excavation. The underlying London Clay has a permeability of perhaps 10-11 m/s, and in comparison with the Norwich Crag, is effectively impermeable. Bounding flow lines therefore follow the interface between the Norwich Crag and the London Clay, coming in from the left (and right) and turning through 90° to follow the centreline up to the floor of the excavation (Fig. 3.5a: only the left-hand side is shown).

5. Starting with zones where the flow pattern is reasonably well-defined (in this case between the sheet pile walls of the cofferdam), begin to sketch in equipotentials and flow lines within the boundaries you have now defined (Fig. 3.5b and 3.5c). Keep it simple: in this case, one intermediate flow line is sufficient, at least for a start. You can always go back and subdivide large slow elements by sketching in further flow lines and equipotentials as a check, but if you start off by being too ambitious, you will get into a hopeless mess.

6. If some flow lines and equipotentials do not cross at right angles, or if some flow elements are not 'square', rub out the offending lines and redraw them so that the significant errors are gradually eliminated. The flow net does not have to be perfect. You will soon reach a stage where further improvements make very little practical difference.

7. When you are satisfied with the flow net (Fig. 3.5d), count up the number of flow tubes N_f (i.e. the spaces between the flow lines themselves) and the number of head drops N_d (again, the spaces between the equipotentials, not the equipotentials themselves). The head on each equipotential is calculated using the fact that the head drop between adjacent equipotentials is H/N_d, where H is the overall head drop.

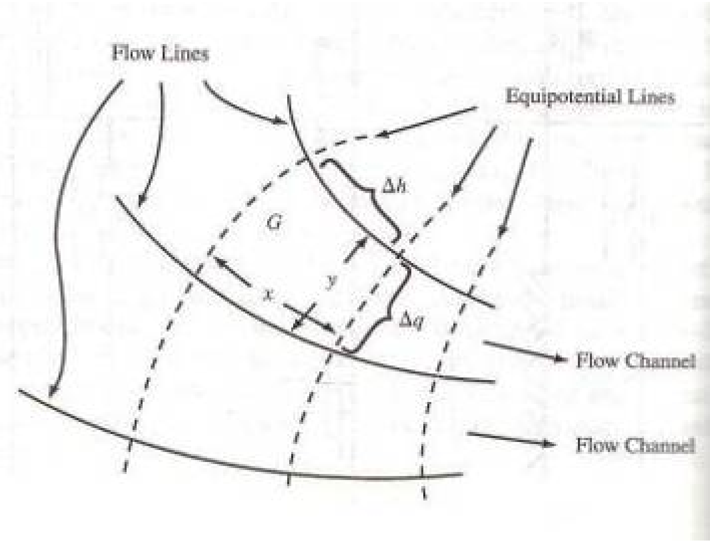

Figure 3.6: Flow channel and equipotential drops. (*Liu & Evett, 1998*)

Once a suitable flow net has been prepared as described above, seepage flow can be determined by modifying Darcy's law, as follows.

$$q = kiA$$

Consider one square in a flow net - for example, the one labeled "*G*" in Fig. 3.6. Let Δq and Δh denote the flow rate and drop in head (energy), respectively, for this square. Since each square is *x* units wide and *y* units long and has a unit width perpendicular to the figure, term *i* in the Darcy's law is given by $\Delta h/x$ and term *A* is equal to *y*. Hence,

$$\Delta q = k \frac{\Delta h}{x} y \tag{3.1}$$

However, since the figure is square, y/x is unity and

$$\Delta q = k \, \Delta h \tag{3.2}$$

If N_d represents the number of equipotential increments (space between equipotential lines), then Δh equals h/N_d and

$$\Delta q = \frac{k\,h}{N_d} \tag{3.3}$$

If N_f denotes the number of flow paths (space between flow lines), then Δq equals q/N_f (where q is the total flow rate per unit width) and

$$\frac{q}{N_f} = \frac{k\,h}{N_d} \tag{3.4}$$

or

$$q = \frac{k\,h\,N_f}{N_d} \tag{3.5}$$

From Figure 3.4, the required flow rate is given by

$$q = \frac{k\,h\,N_f}{N_d}$$

with k = 1.4×10^{-4} m/s
H = 16 m
N_f = 2, × 2 for symmetry = 4
N_d = 8

$$\therefore \qquad q = \frac{1.4\times10^{-4} \times 16 \times 4}{8} = 1.2\times10^{-3}\, m^3/s\; per meter length$$

In the foregoing discussion of flow net, it was assumed that soil was isotropic - that is, equal soil permeability in all directions. In actuality, natural soils are not isotropic, but often soil permeabilities in vertical and horizontal directions are similar enough that the assumption of isotropic soil is acceptable for finding flow without appreciable error. In stratified soil deposits, however, where horizontal permeability is much greater than vertical permeability, the flow net must be modified and Eq. (3.5) altered to compute flow.

For the situation where k_y and k_x (representing average vertical and horizontal coefficients of permeability, respectively) differ appreciably, the method for constructing the flow net can be modified by use of a *transformed section* to account for the different permeabilities, The modification is done when the scale drawing of the cross section of the flow path is prepared. vertical lengths are plotted in the usual manner to fit the scale selected for the sketch, but horizontal dimensions are first altered by multiplying all horizontal lengths by the factor $\sqrt{k_y / k_x}$ and plotting the results to scale.

The resulting drawing will appear somewhat distorted, with apparently shortened horizontal dimensions. The conventional flow net is then sketched on the transformed section in the manner described previously. In analyzing the resulting flow net to compute seepage flow, one must replace the k term in Eq. (3.5) with the factor $\sqrt{k_y / k_x}$ which was used in plotting the drawing. Thus, for flow through stratified, nonisotropic soil, the seepage equation becomes

$$q = \sqrt{\frac{k_y}{k_x}} \frac{h N_f}{N_d} \tag{3.6}$$

3.2.3 Calculation of Pore Water Pressures using Flow Net

The pore water pressure at any point may be calculated from flow net by interpolation between equipotentials. The example below shows the calculation of pore water pressure from flow net. (*Powrie, 1997*)

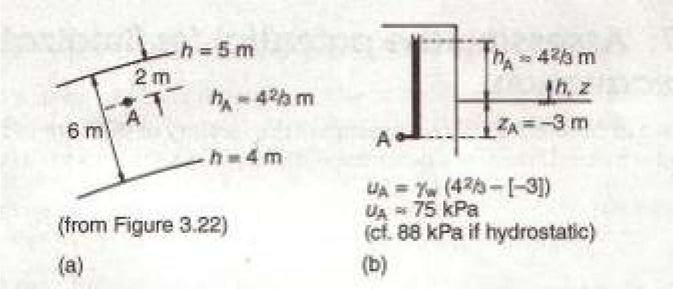

Figure 3.7: Calculating pore water pressure form flow net. (a) Determining the total head h_A; (b) relationship between total head and pore water pressure. (*Powrie, 1997*)

The first step is to calculate the total head h at the point A, by linear interpolation between the equipotential line on the flow net. The point A is approximately 2 m from the 5 m equipotential (h = 5 m), in a region where 5 m and 4 m equipotentials are separated by a distance of about 6 m (Fig. 3.7a).

The potential at A is therefore given by

$$h_A = 5\,m - \left[\left(\frac{2}{6}\right) \times 1\,m\right] = 4.67\,m$$

This must now be converted to a pore head u_A / γ_w, by subtracting the elevation of the point A above the datum for the measurement of *h*:

$$u_A = \gamma_w \left(h_A - z_A\right) \tag{3.7}$$

Figure 3.7b: u_A is the gauge pore water pressure at A, h_A is the total head at A and z_A is the elevation of A above the datum used for the calculation of total head.

In this case, the point A is approximately 3 m below the datum of h, so z_A is negative: z_A = -3 m.

Hence

$$u_A = \gamma_w \left(h_A - z_A\right) = 9.81 kN/m^3 \times \left[4.67m - \left(-3m\right)\right]$$

$\therefore$ Gauge pore water pressure, $u_A \approx 75\ kPa$

In hydrostatic conditions, the pore water pressure at a depth of 9 m below the water table would be approximately 88 *kPa*. This example illustrates the effect of downward seepage in reducing pore water pressures, compared with hydrostatic conditions. Conversely, upward seepage will increase pore water pressures, perhaps to such an extent that the soil '*fluidizes*' or '*boils*'. This will discuss in the next section.

3.2.4 Mechanics of Piping due to Heave

The mechanics of failure by piping due to heave are illustrated by Fig. 3.8*a* which represents a vertical section through one side of a single sheet pile wall cofferdam. To a depth h1 below the water level, the soil outside the cofferdam consists of coarse gravel, whereas the gravel within the cofferdam has been removed by dredging. The gravel rests on a bed of uniform sand. The loss of head in the gravel is so small that it can be disregarded. We wish to compute the factor of safety *F* with respect to piping, after the water level on the inside has been pumped down to the surface of the sand. (*Terzaghi, 1922*)

Before making this computation, we shall consider the hydrostatic conditions at the instant of failure. As soon as the water level within the cofferdam is lowered by pumping, water begins to flow downward through the sand on the left side of the sheet piles and upward on the right. The excess hydrostatic pressure on a horizontal section such as *Ox* (Fig. 3.8*b*) reduces the effective pressure on that section. As soon as the average effective pressure on and above a portion of *Ox* near the sheet piles becomes equal to zero, the water that flows through the sand can straighten and widen the flow channels without meeting any resistance.

This process greatly increases the permeability of the sand adjoining the sheet piles and it diverts an additional part of the seepage toward this zone. The surface of the sand then rises (see Fig. 3.8a). Finally, the sand starts to boil and a mixture of water and sand rushes from the upstream side of the sheet piles, through the space below the lower edge of the sheet piles, and toward the zone where the boiling started.

By model tests (Terzaghi, 1922) it has been found that the rise of the sand occurs within a distance of about *D/2* from the sheet piles. The failure, therefore, starts within a prism of sand having a depth *D* and a width *D/2*. At the instant of failure the effective vertical pressure on any horizontal section through the prism is approximately equal to zero. At the same time the effective lateral pressure on the sides of the prism is also approximately zero. Therefore, piping occurs as soon as the excess hydrostatic pressure on the base of the prism becomes equal to the effective weight of the overlying sand.

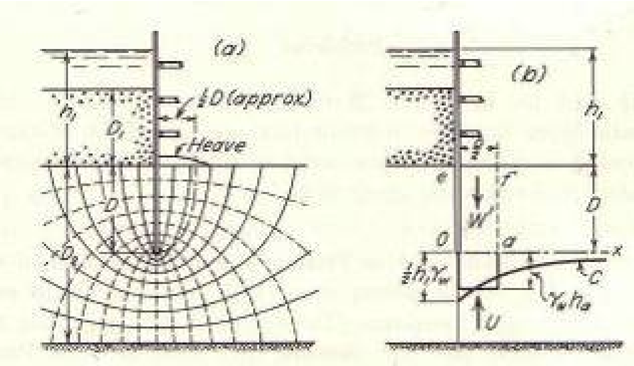

Figure 3.8: Use of flow net to determine factor of safety of row of sheet piles in sand with respect to piping. (*a*) Flow net. (*b*) Forces acting on sand within zone of potential heave. (*Terzaghi, 1922*)

In order to compute the excess hydrostatic pressure a flow net must be constructed. After this has been done (Fig. 3.8*a*) the intensity of this pressure can be determined readily at every point on the base of the prism at depth *D* by means of the procedure as previously described.

In Fig. 3.8a prism of sand are represented by the ordinates of curve *C* with reference to a horizontal axis through *O*. Within the distance *D/2* from the sheet piles the average excess hydrostatic pressure on the base of the prism has the value $\gamma_w h_a$, and the total excess hydrostatic pressure on the base is $U = \frac{1}{2} D \gamma_w h_a$. Failure by piping occurs as soon as *U* becomes equal to the effective weight of the sand which, in turn, is equal to the submerged weight $W' = \frac{1}{2} D^2 \gamma'$. Therefore, the factor of safety with respect to piping is

$$F = \frac{W'}{U} = \frac{D\gamma'}{h_a \gamma_w} \tag{3.8}$$

In a similar manner, we may compute the factor of safety for a dam with a sheet pile cutoff. If the factor of safety against failure by piping is too small, it may be increased by establishing on top of the prism *Oafe* (Fig. 3.8*b*) an inverted filter which has a weight W. The pressure of the filter does not alter the excess hydrostatic pressure *U*, but i increase the effective weight of the prism from *W'* to *W'* + *W*. Hence, it increases the factor of safety with respect to piping from *F* (Eq. (3.8)) to

$$F' = \frac{W + W'}{U} \tag{3.9}$$

In the case of a cofferdam the depth of penetration of the piles could be increased, or a layer of coarse filter material could be laid on the downstream side before pumping down to the final level.

In the case of dams, both an increase in the factor of safety against piping and a reduction in the quantity of seepage can be obtained by increasing the length of the flow path. This may be done by driving a row of sheet piles, preferably at or near the upstream face, or by laying an apron of impermeable paving in front of the upstream face. A layer of coarse filter material laid on the downstream side is another possibility (see Fig. 3.9). (*Whitlow, 1996*)

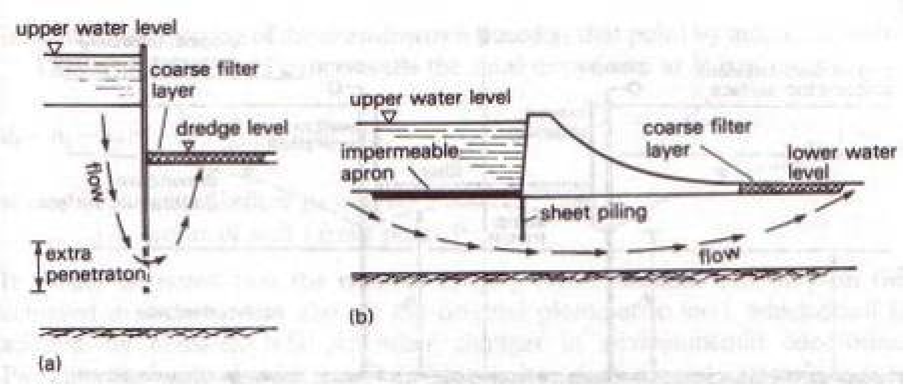
upper water level
coarse filter layer
dredge level
flow
extra penetraton
(a)
upper water level
impermeable apron
sheet piling
coarse filter layer
lower water level
flow
(b)

Figure 3.9: Methods of improving seepage conditions. (a) Cofferdam. (b) Concrete or masonry dam. (*Whitlow, 1996*)

3.3 Analysis of the Physical Models

This physical model is an imitation of the two-dimensional section of theoretical calculation for seepage quantities through cofferdam. The section was scaled down and developed for the analysis. The models will be constructed and tested to view flow patterns.

3.3.1 Preparation

Similar to the first part of this project, the designs were documents for this model. The drawings were achieved using AutoCAD 2005. However, the Perspex tank has been built by previous year project student. Some modifications were required to construct the model. The location of the sheet pile wall and expected flow lines were sketched on the tank. The complete drawings are shows in Appendix X.

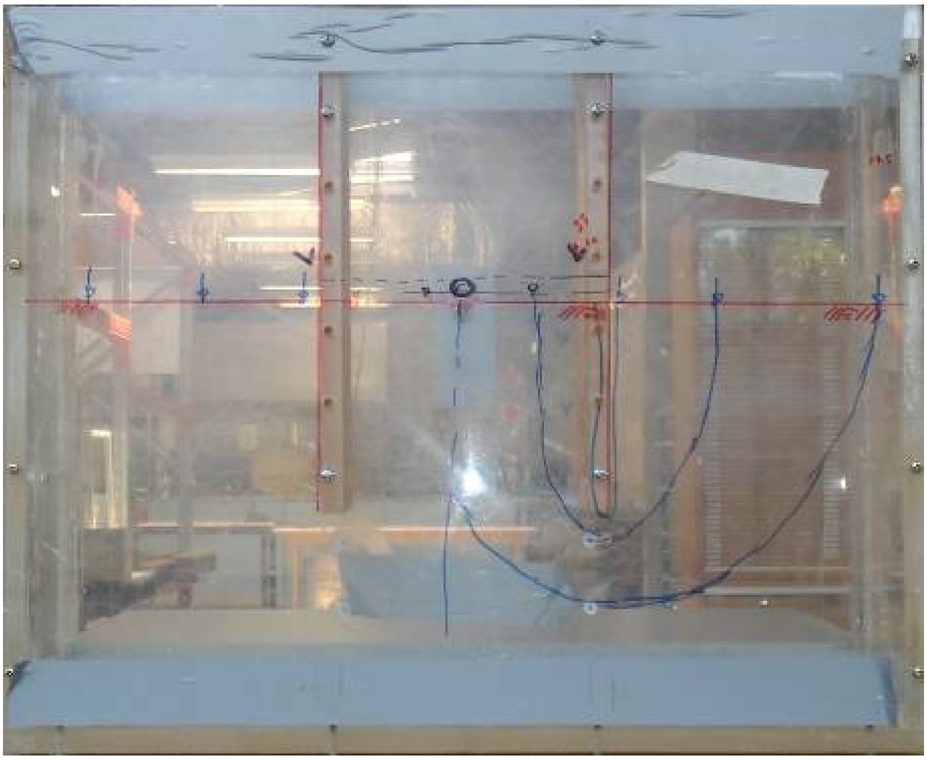

Figure 3.10: Expect flow lines.

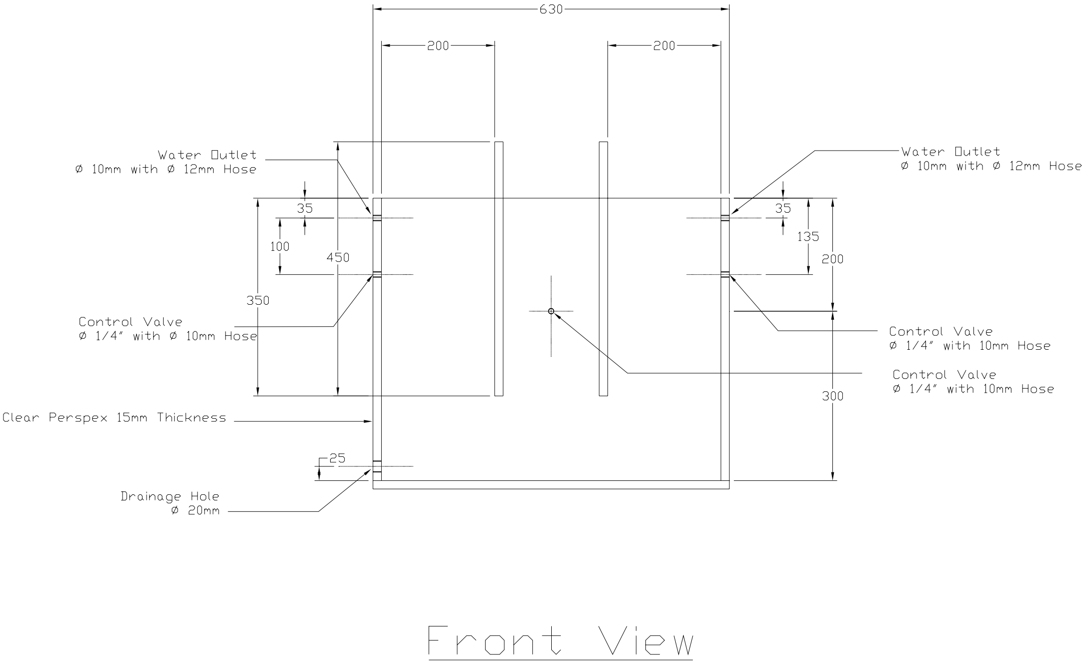
630
200
200
Water Outlet
ø 10mm with ø 12mm Hose
Water Outlet
ø 10mm with ø 12mm Hose
35
100
450
350
35
135
200
Control Valve
ø 1/4" with ø 10mm Hose
Control Valve
ø 1/4" with 10mm Hose
Control Valve
ø 1/4" with 10mm Hose
300
Clear Perspex 15mm Thickness
25
Drainage Hole
ø 20mm
Front View

Figure 3.11: Front view drawing of the physical model.

3.3.2 Construction

The materials required to construct this physical model are:

- Clear Perspex
- Fine and coarse sand
- Hose and valves
- Pump

Firstly, the tank must be cleaned. The sheet pile wall and the valves locations were then marked. The drill was used to drill the hole, the hole sizes are as indicated in the drawing. The tank was cleaned again after finished drilling. Insert the sheet pile wall to its location, use screws to hold the wall into it position. It is then sealed along the edge using water-resist silicon adhesive; silicone required a minimum of 24 hours before gain maximum works ability. The valves were then installed as indicated in Fig. 3.11.

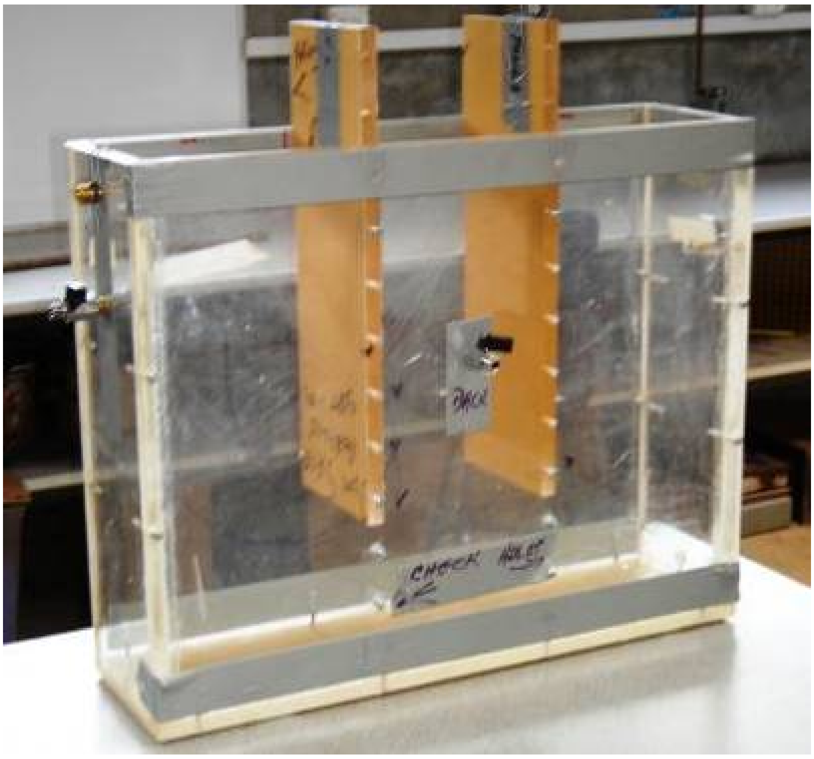

Figure 3.12: Physical model under construction.

Before filling the tank with sand, it must be tested for any leakage by filling it up with water. With no leakage, the sand is placed in layer and compact well. Then, the tank is filled with water and the sand left to saturate for one night.

The syringe was then placed as shows in Fig. 3.15 for shooting the dye to visualize the flow lines.

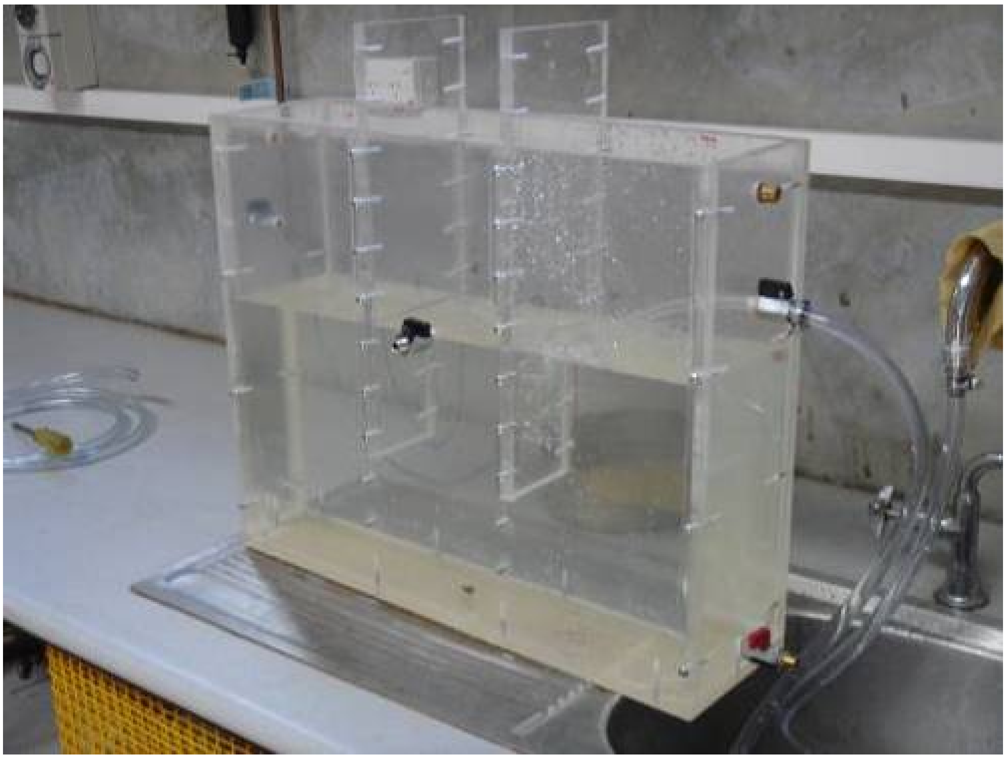

Figure 3.13: Testing the tank for leakage after construction.

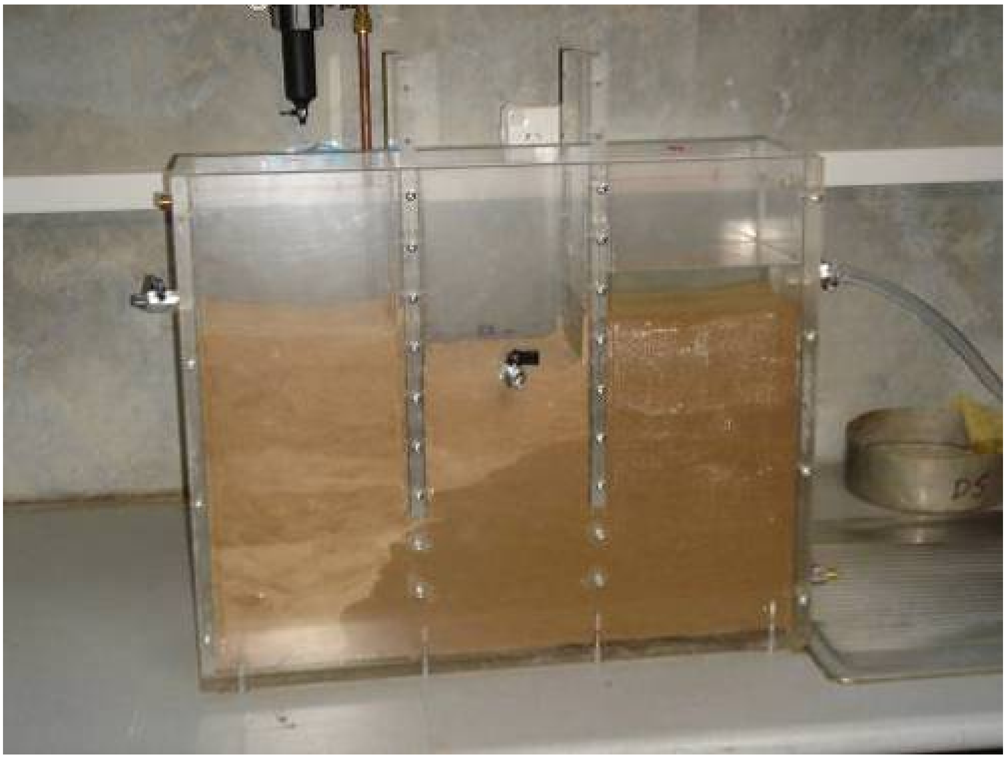

Figure 3.14: Fill up the water and saturated the sand sample.

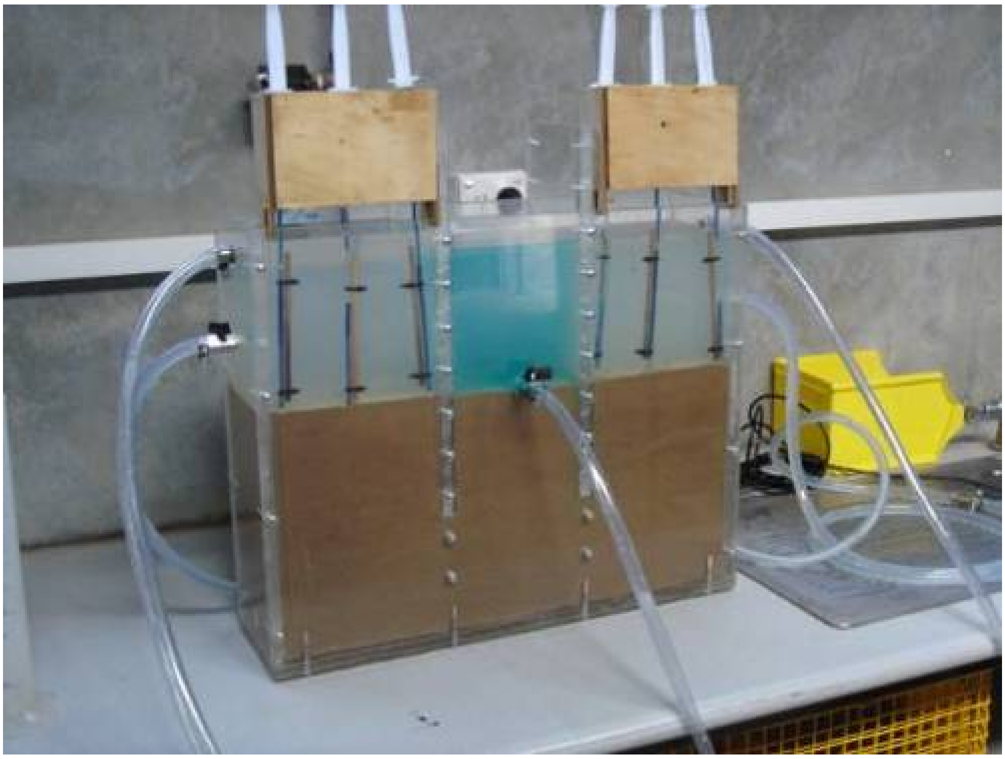

Figure 3.15: Finished cofferdam model.

3.3.3 Results and Discussions

The objective of this analysis is to determine the seepage quantities under a cofferdam. From Fig. 3.15 the inlet valve on the left and right hand side is acting as the water inlet which being pump from the sink. The control valve at the middle of the cofferdam is acting as a dewatering pump (to control the water level inside the cofferdam). Two outlets are provided on both sides to maintain the surface water level.

The process involved in analyzing the physical model is outlined below.

1. Initially, all the valves are closed and the surface water level is at outfall.

2. Start the process by turn on the inlet valve on both side and switch on the inlet pump.

3. Dewatering the cofferdam by turn on the control valve.

4. Wait until the water level inside the cofferdam reduced to the bed of the excavation.

5. Measure the amount of water that flow out from the cofferdam in 10 second and record.

6. Injecting the dye with syringe to visualized the flow lines.

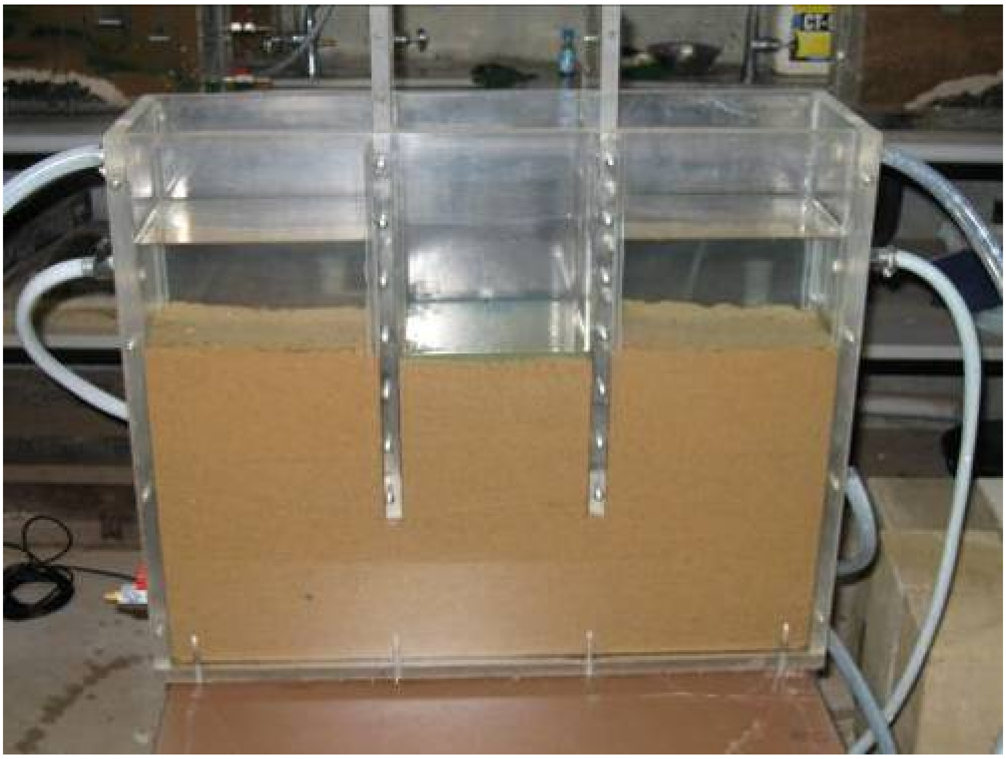

Figure 3.16: Dewatering the cofferdam.

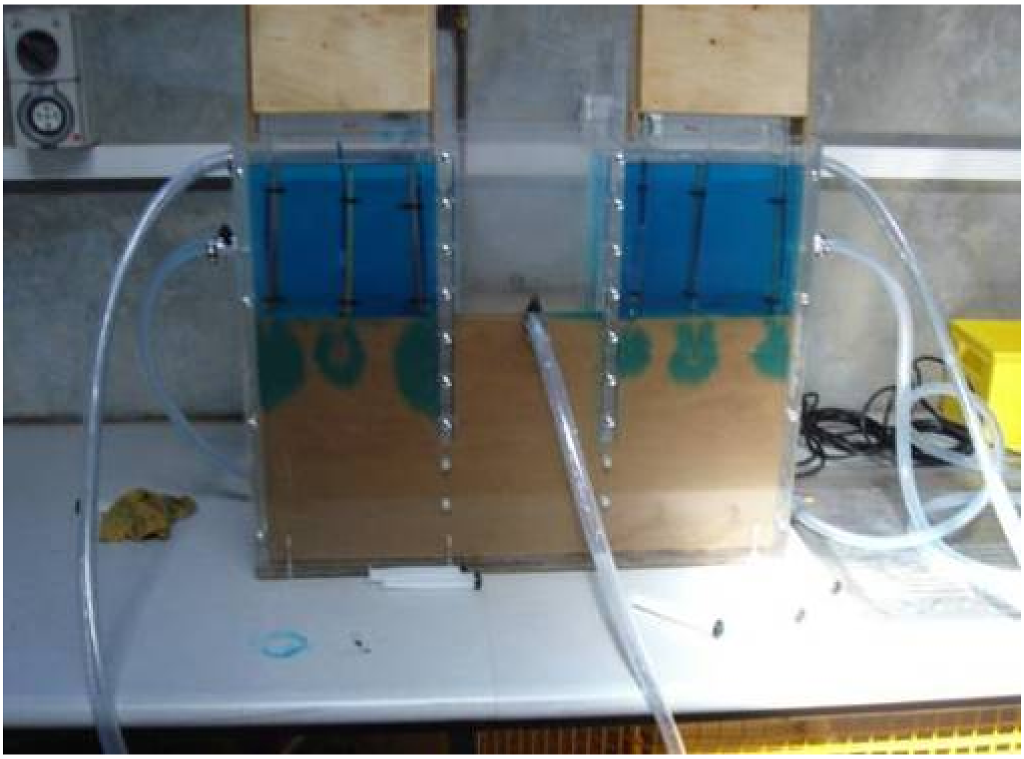

Figure 3.17: Injecting the dye.

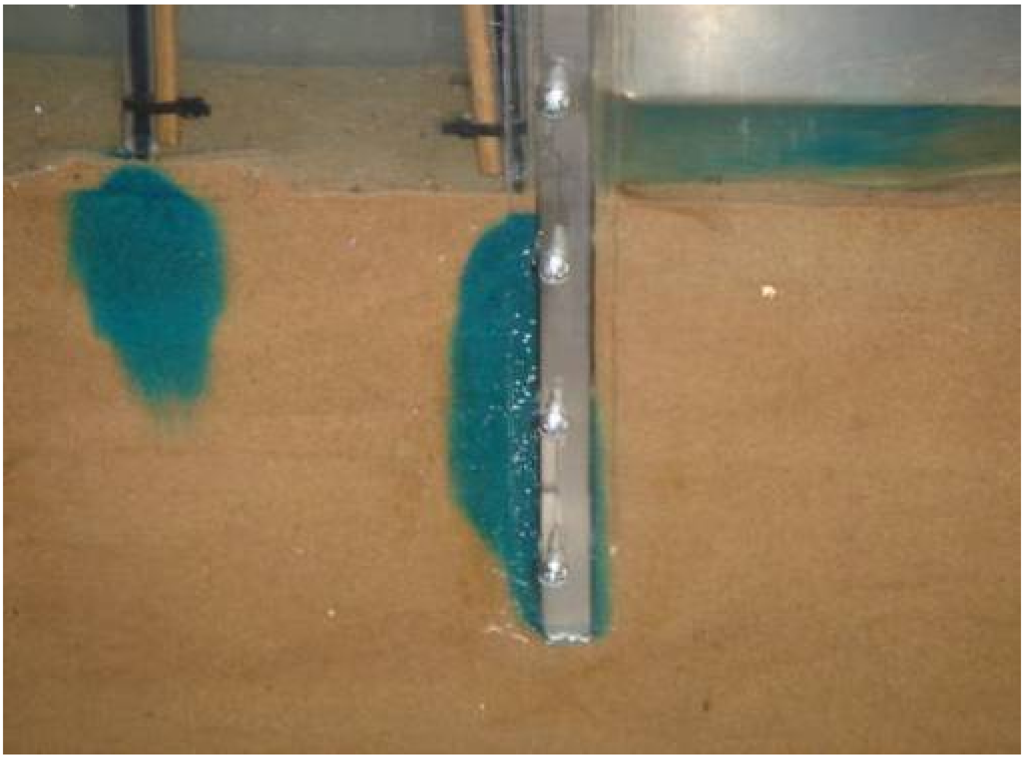

Figure 3.18: Shortest flow path.

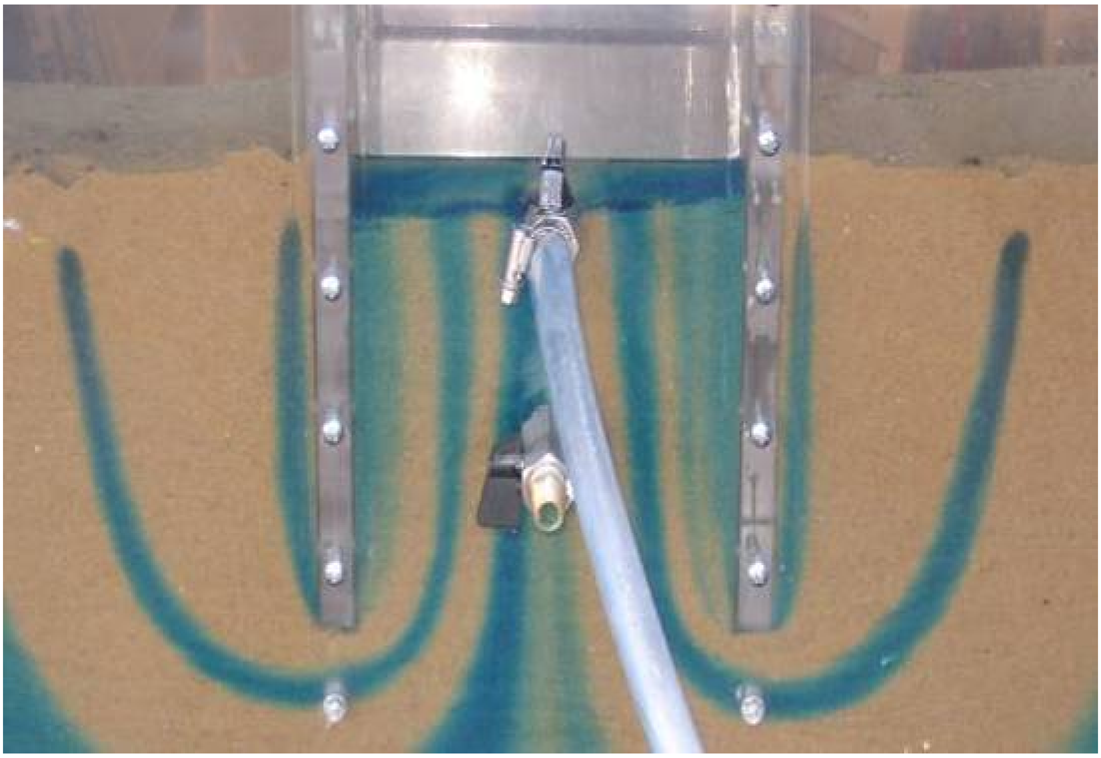

Figure 3.19: Flow lines.

In order to study the piping effect from this model, the depth of the sheet pile wall must be reduced. Since the sheet pile wall have been sealed with silicone, changing the location of the wall is difficult. So, the second control valve was installed at 70 mm below the first control valve.

Similar to the above process except that the two control valve are opened in order. Turn on the second valve after the water level inside the coffer dam is reduced to the first control valve. The following figure shows the piping effects from the model.

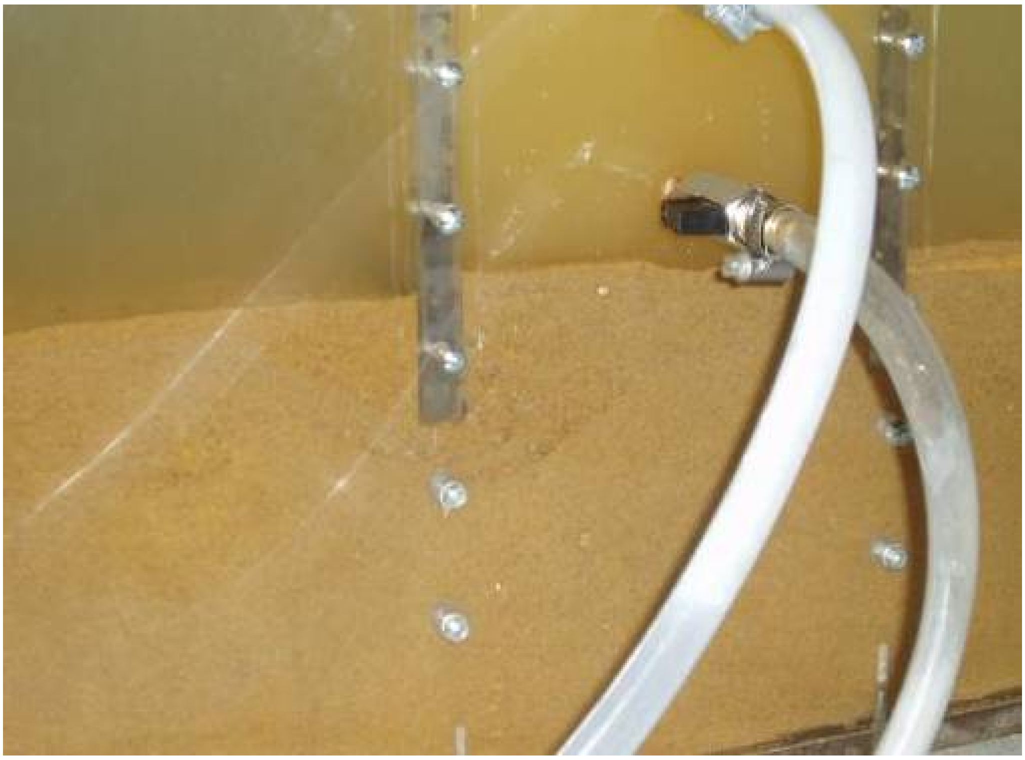

Figure 3.20: Heave and boiling.

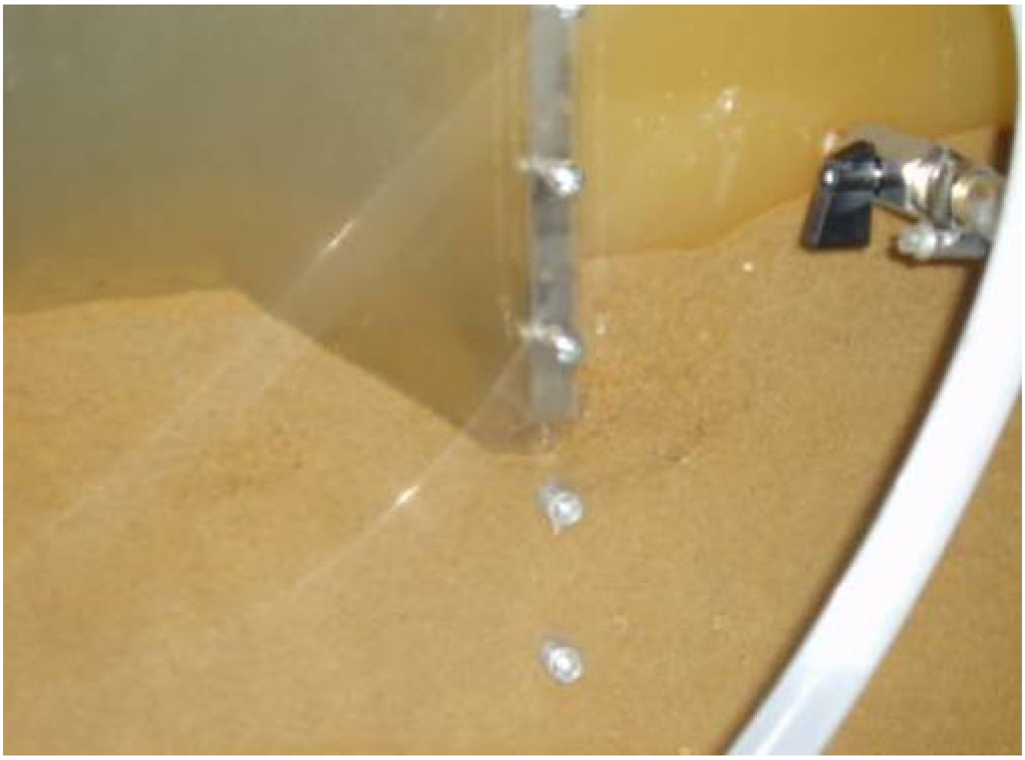

Figure 3.21: Collapse.

3.4 Comparison of results

The theoretical solution is performed to determine the flow rate using the flow net concepts. In the physical model experimentation, the flow rate is measured directly from the control valve.

Experimental Result:

Volume of water @ 10 sec. = 0.02 *l*

Flow rate, $Q = \frac{0.02}{10} = 0.002\ l/s = 2 \times 10^{-5}\ m^3/s$

Theoretical Result:

The flow rate can be calculated using equation 3.5.

$$q = \frac{k\,h\,N_f}{N_d}$$

with $k = 1.2 \times 10^{-4}\ m/s$

$h = 0.20\ m$

$N_f =$ 3.1 (one side only)

$N_d =$ 7 (one side only)

$$\therefore \quad q = 1.2 \times 10^{-4} \times 0.20 \times \left(\frac{3.1}{7}\right) \times 2$$

$$= 2.125 \times 10^{-5}\ m^3/s$$

Chapter 4

OPEN DAY DEMONSTRATION

4.1 Introduction

The finished physical models were demonstrated at the Open Day of the University of Southern Queensland. They were used in the geotechnical demonstration models area. For bearing capacity models, participants were asked to sketch the failure patterns of the one layer sand model and the 90° slope model. In cofferdam model, participants were asked to sketch the flow lines.

4.2 Preparation

Two sets of poster were used, one for bearing capacity models and another one for cofferdam model. The poster is a useful aid in communicate with the participants, which includes background, theory, and application of the physical models.

ULTIMATE BEARING CAPACITY
BACKGROUND
BEARING CAPACITY
FAILURE MODE
FAILURE MECHANISMS AND DERIVATION OF EQUATIONS
SEMI-CIRCULAR SLIP
CIRCULAR ARC SLIP

Figure 4.1: Poster for the bearing capacity model.

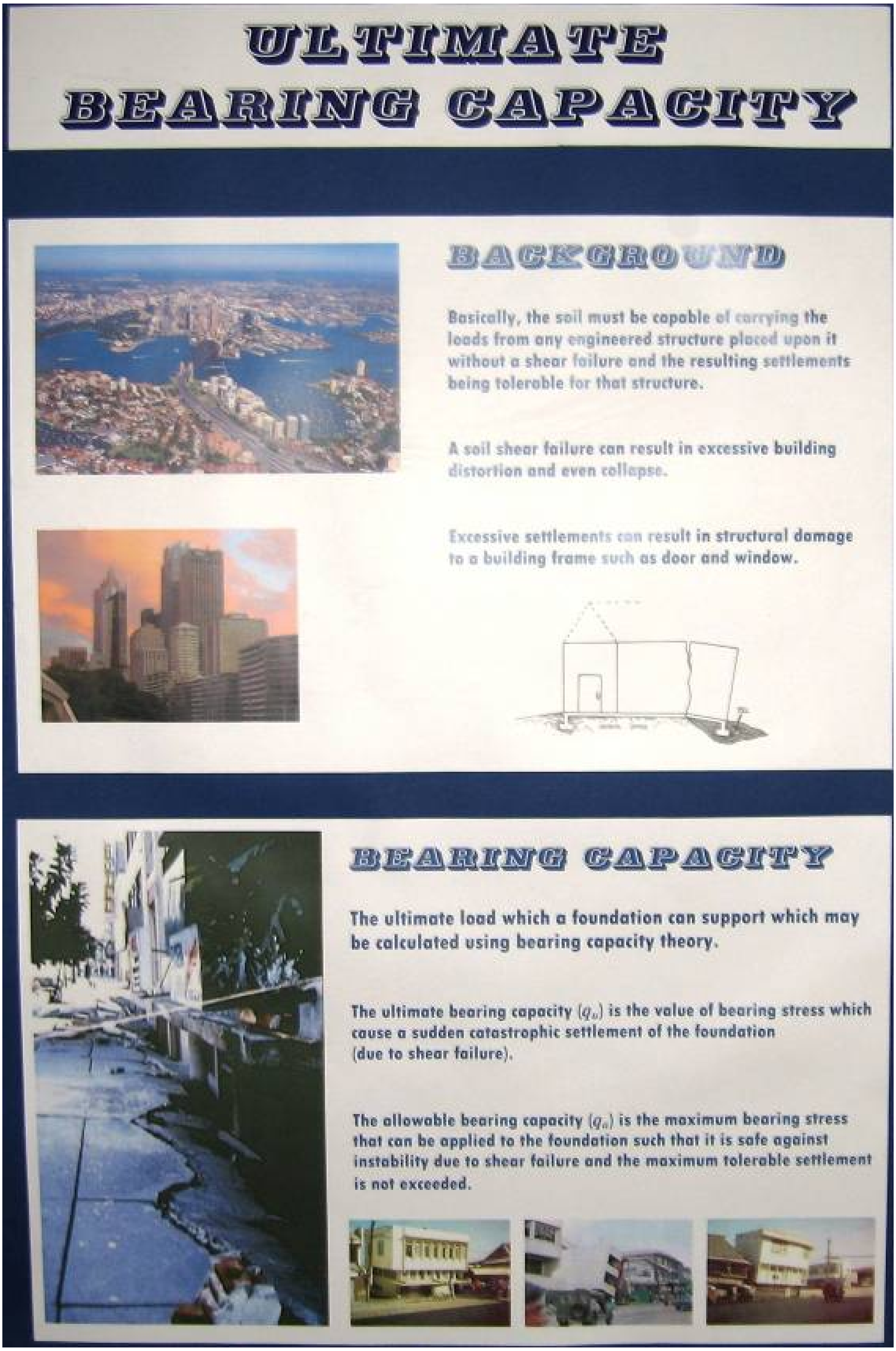

ULTIMATE
BEARING CAPACITY

BACKGROUND

Basically, the soil must be capable of carrying the loads from any engineered structure placed upon it without a shear failure and the resulting settlements being tolerable for that structure.

A soil shear failure can result in excessive building distortion and even collapse.

Excessive settlements can result in structural damage to a building frame such as door and window.

BEARING CAPACITY

The ultimate load which a foundation can support which may be calculated using bearing capacity theory.

The ultimate bearing capacity (q_u) is the value of bearing stress which cause a sudden catastrophic settlement of the foundation (due to shear failure).

The allowable bearing capacity (q_a) is the maximum bearing stress that can be applied to the foundation such that it is safe against instability due to shear failure and the maximum tolerable settlement is not exceeded.

Figure 4.2: Bearing capacity background and applications.

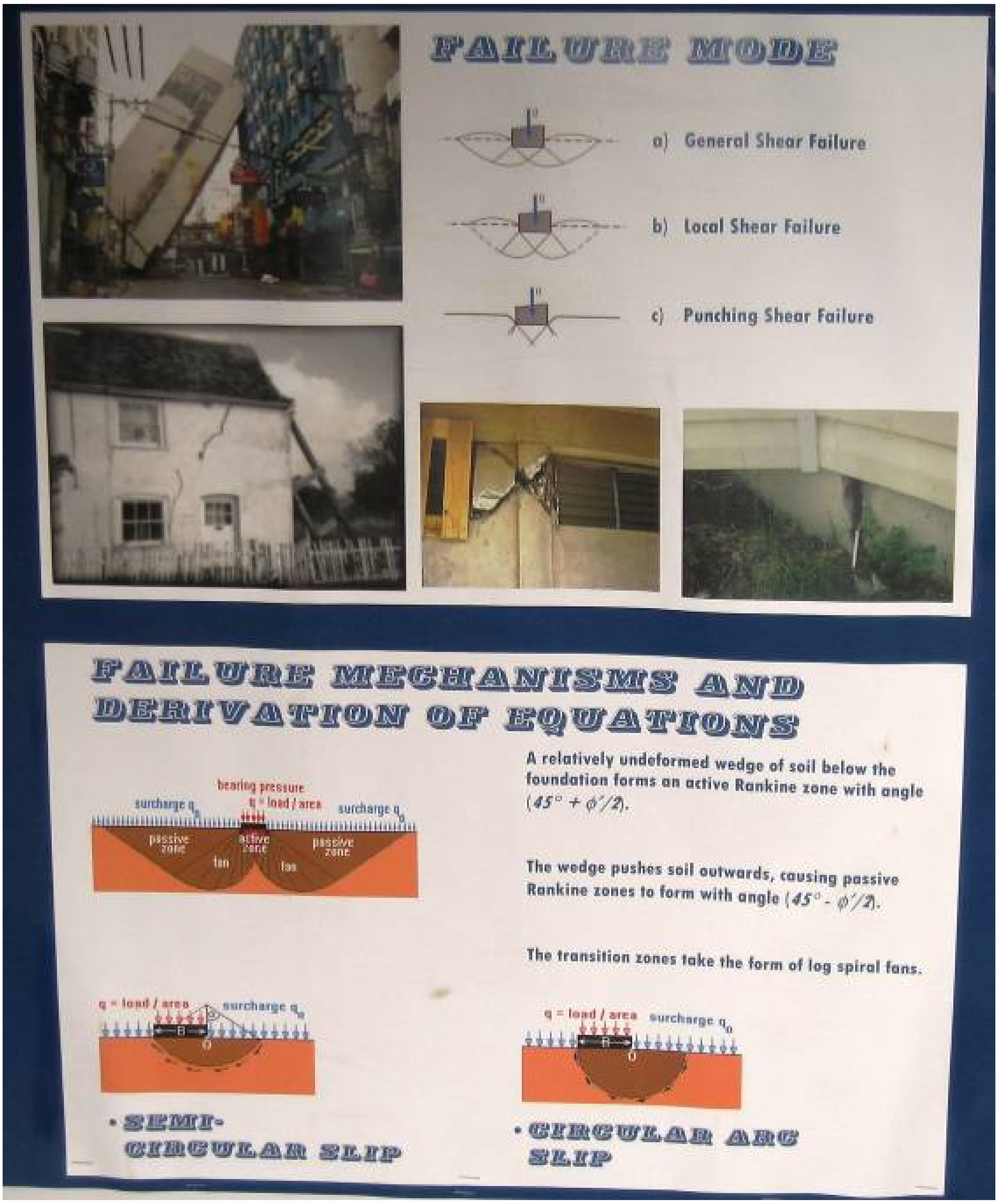

FAILURE MODE

a) General Shear Failure

b) Local Shear Failure

c) Punching Shear Failure

FAILURE MECHANISMS AND DERIVATION OF EQUATIONS

A relatively undeformed wedge of soil below the foundation forms an active Rankine zone with angle ($45° + \phi'/2$).

The wedge pushes soil outwards, causing passive Rankine zones to form with angle ($45° - \phi'/2$).

The transition zones take the form of log spiral fans.

- SEMI-CIRCULAR SLIP
- CIRCULAR ARC SLIP

bearing pressure
q = load / area
surcharge q_o
surcharge q_o
passive zone
active zone
passive zone
fan
fan
q = load / area
surcharge q_o
B
O
q = load / area
surcharge q_o
B
O

Figure 4.3: Failure mode and derivation of equations.

COFFERDAM
BACKGROUND
SEEPAGE AND FLOW
TYPICAL FLOW NETS AS USED FOR COFFERDAM
FINITE ELEMENT
SHEETED TYPES:
DOUBLE SKIN TYPES:
GRAVITY AND CRIB TYPES:
PORTADAM®
M1721

Figure 4.4: Poster for the cofferdam model.

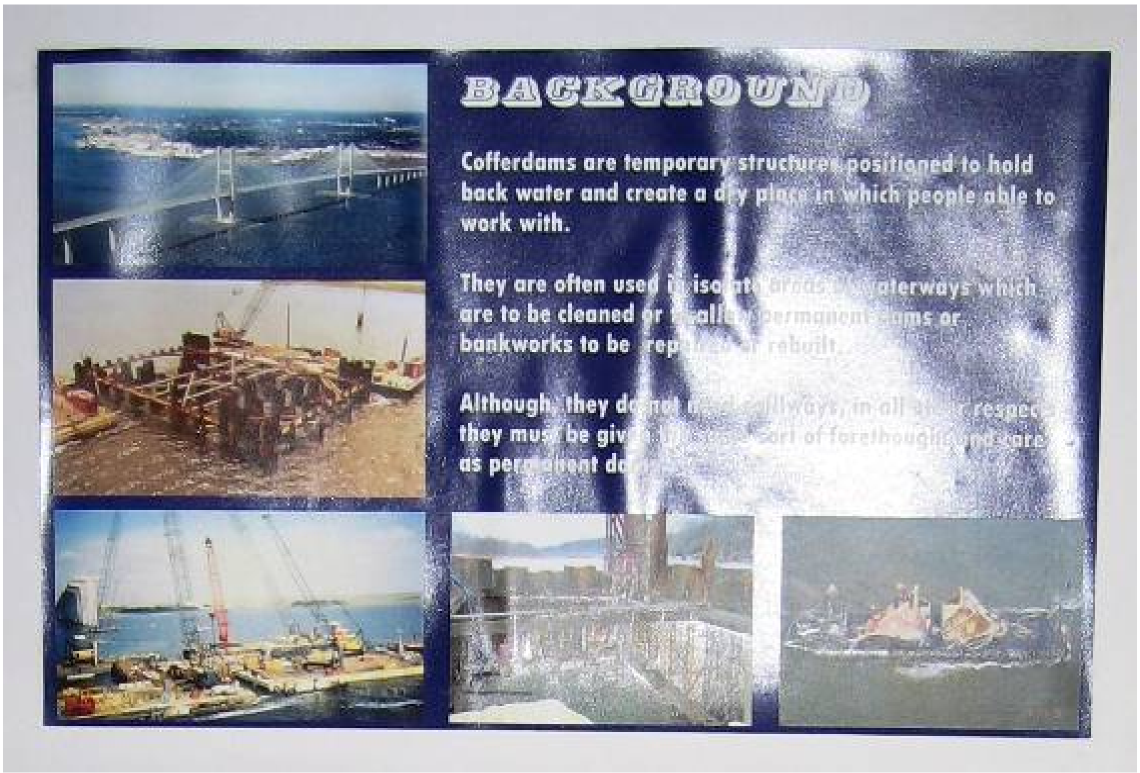

BACKGROUND

Cofferdams are temporary structures positioned to hold back water and create a dry place in which people able to work with.

They are often used [illegible] isolate areas [illegible] waterways which are to be cleaned or [illegible] allow permanent dams or bankworks to be repaired or rebuilt.

Although, they do not need spillways, in all other respects they must be given [illegible] sort of forethought and care as permanent dams.

Figure 4.5: Cofferdam background and applications.

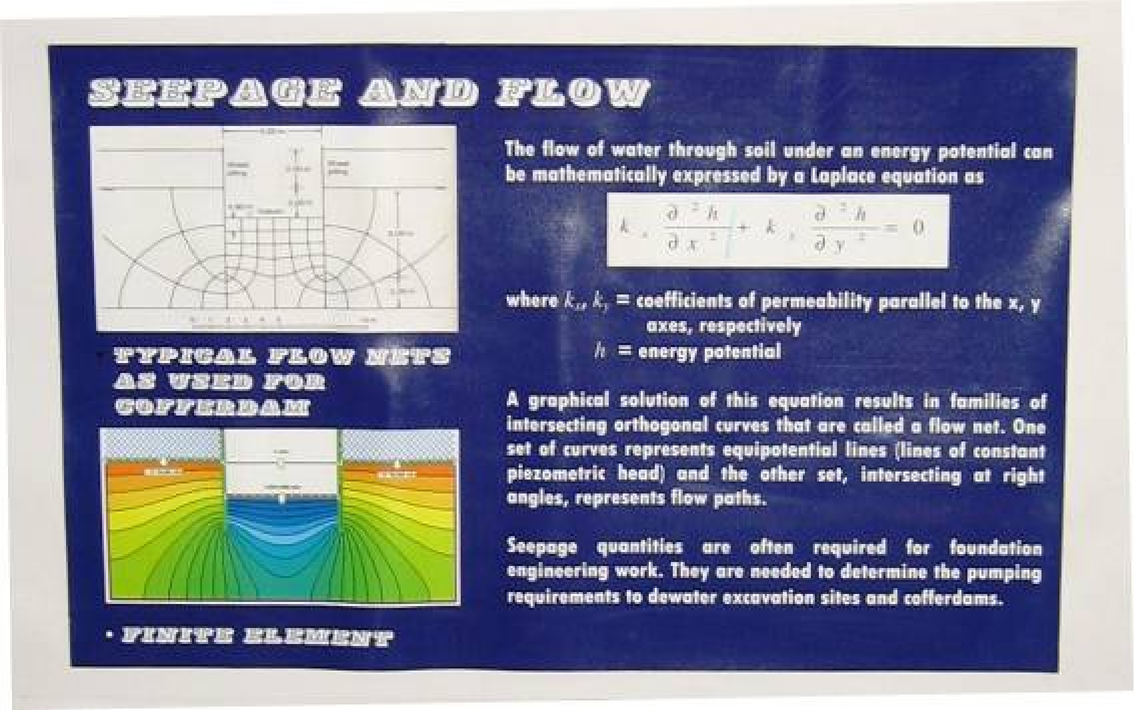

SEEPAGE AND FLOW

The flow of water through soil under an energy potential can be mathematically expressed by a Laplace equation as

$$k_x \frac{\partial^2 h}{\partial x^2} + k_y \frac{\partial^2 h}{\partial y^2} = 0$$

where k_x, k_y = coefficients of permeability parallel to the x, y axes, respectively

h = energy potential

A graphical solution of this equation results in families of intersecting orthogonal curves that are called a flow net. One set of curves represents equipotential lines (lines of constant piezometric head) and the other set, intersecting at right angles, represents flow paths.

Seepage quantities are often required for foundation engineering work. They are needed to determine the pumping requirements to dewater excavation sites and cofferdams.

Figure 4.6: Seepage and flow net.

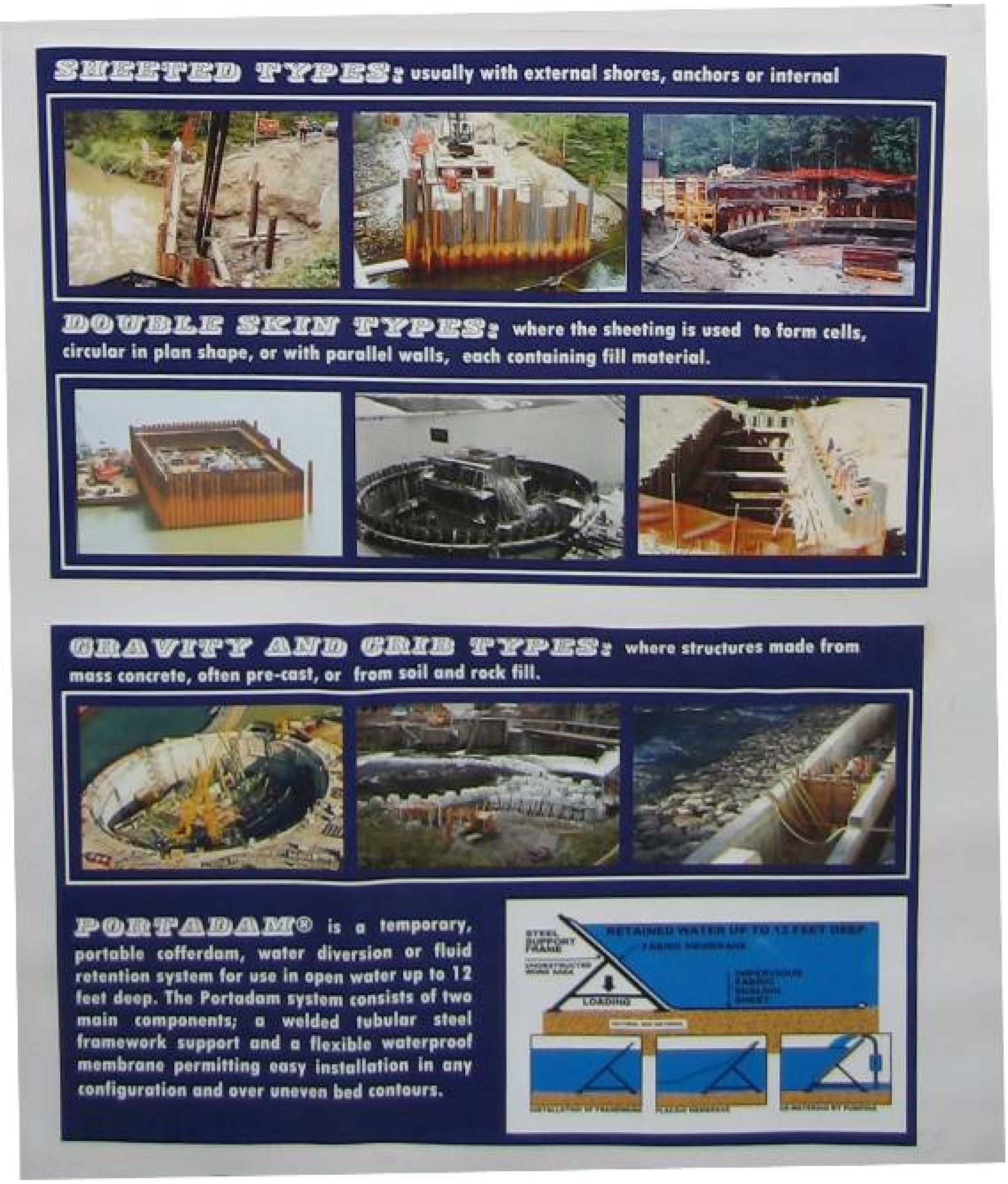

SHEETED TYPES: usually with external shores, anchors or internal

DOUBLE SKIN TYPES: where the sheeting is used to form cells, circular in plan shape, or with parallel walls, each containing fill material.

GRAVITY AND CRIB TYPES: where structures made from mass concrete, often pre-cast, or from soil and rock fill.

PORTADAM® is a temporary, portable cofferdam, water diversion or fluid retention system for use in open water up to 12 feet deep. The Portadam system consists of two main components; a welded tubular steel framework support and a flexible waterproof membrane permitting easy installation in any configuration and over uneven bed contours.

STEEL SUPPORT FRAME
RETAINED WATER UP TO 12 FEET DEEP
FABRIC MEMBRANE
UNOBSTRUCTED WORK AREA
IMPERVIOUS FABRIC SEALING SHEET
LOADING

Figure 4.7: Types of cofferdam.

4.3 Procedure

4.3.1 Bearing Capacity Models

1. Initially the models are covered to hide the failure pattern.

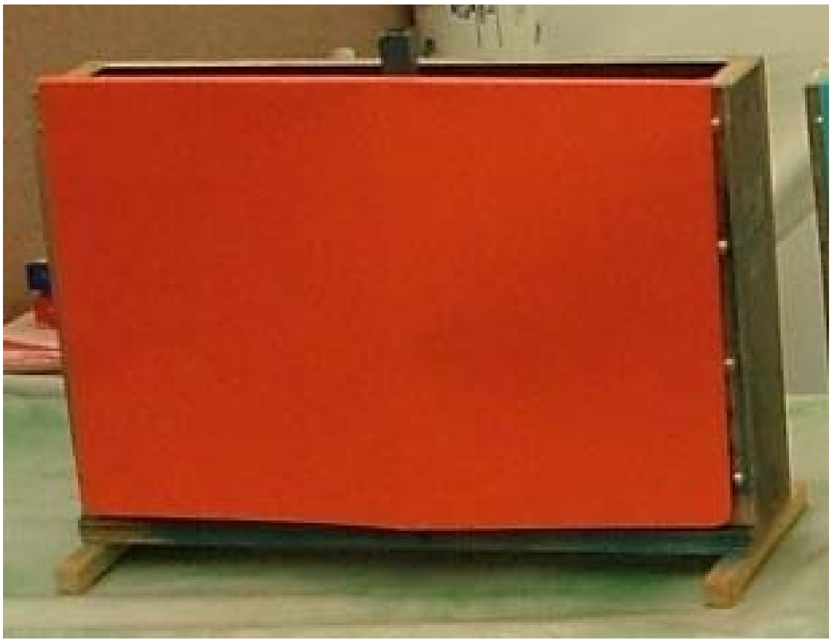

Figure 4.8: Covered physical model.

2. Participants are then given some background on previous real situations involving the failure due to the ultimate bearing capacity.

3. Participants are handed an A4 size paper of the diagram of the model, and asked to sketch the failure patterns for the two models.

4. After they sketch, the model is then uncovered to reveal the actual slip failure from the model.

Figure 4.9: Participants listening to the background information.

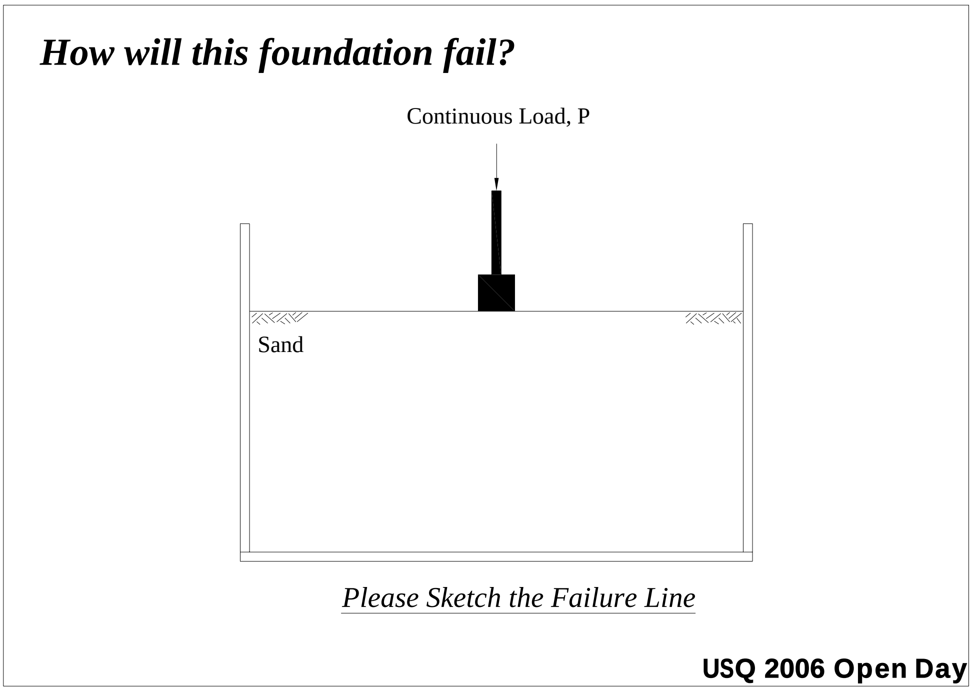
How will this foundation fail?
Continuous Load, P
Sand
Please Sketch the Failure Line
USQ 2006 Open Day

Figure 4.10: Drawing for sketching the failure patterns.

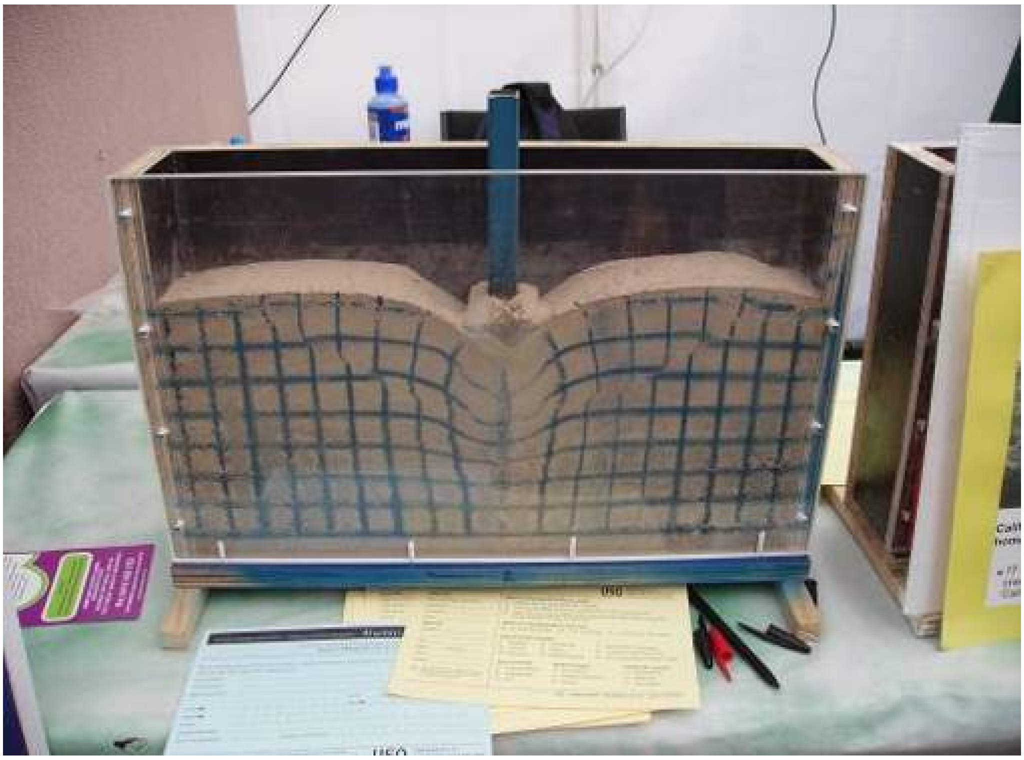

Figure 4.11: Revealed failure patterns.

4.3.2 Cofferdam Model

1. This model required a minimum of one hour to set up and injecting the dye.

2. The injection point is on the back of the model in order to hide the flow lines.

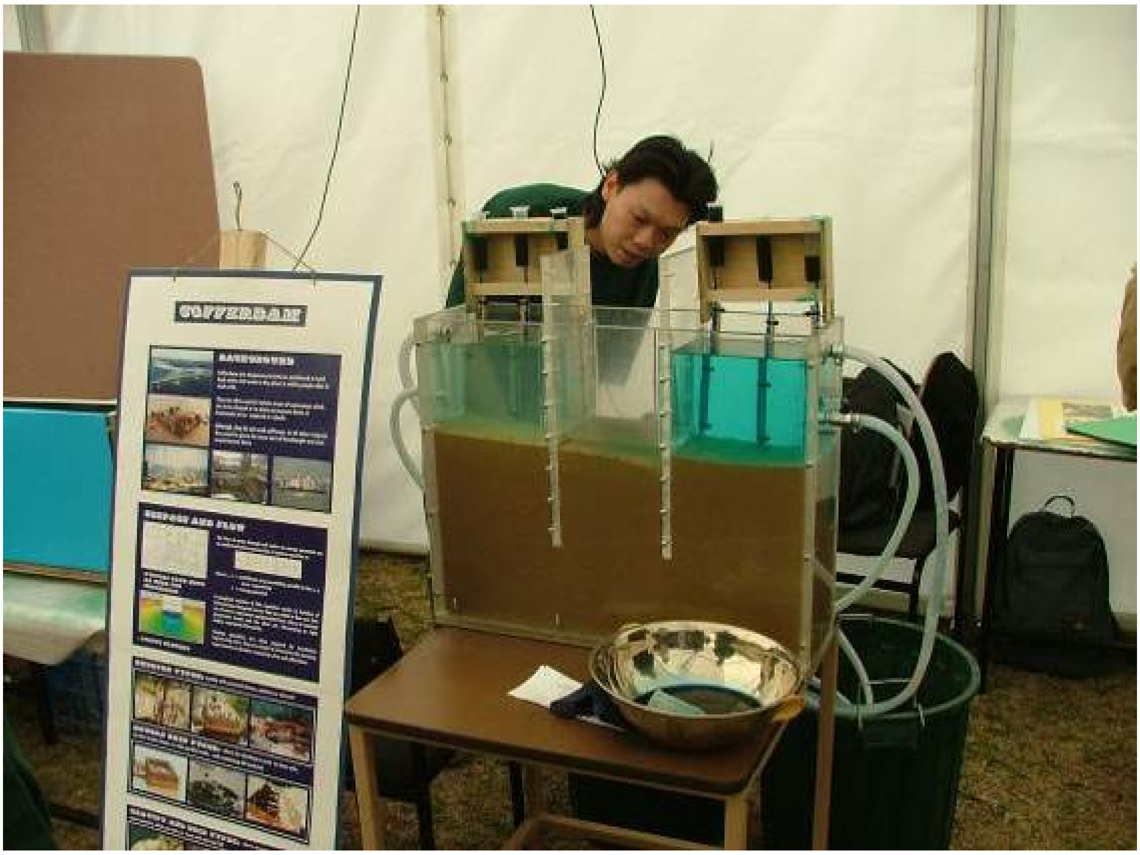

Figure 4.12: Setting the cofferdam model.

3. Similar to the above procedure, participants are given some background on the concepts and applications of cofferdam and flow net.

4. Participants are handed an A4 size paper of the diagram of the model, and asked to sketch the flow lines.

5. After they sketch, participants then walk around the back and check the results.

Emerald
City
Workers

Figure 4.13: Participants listening to the concepts and application.

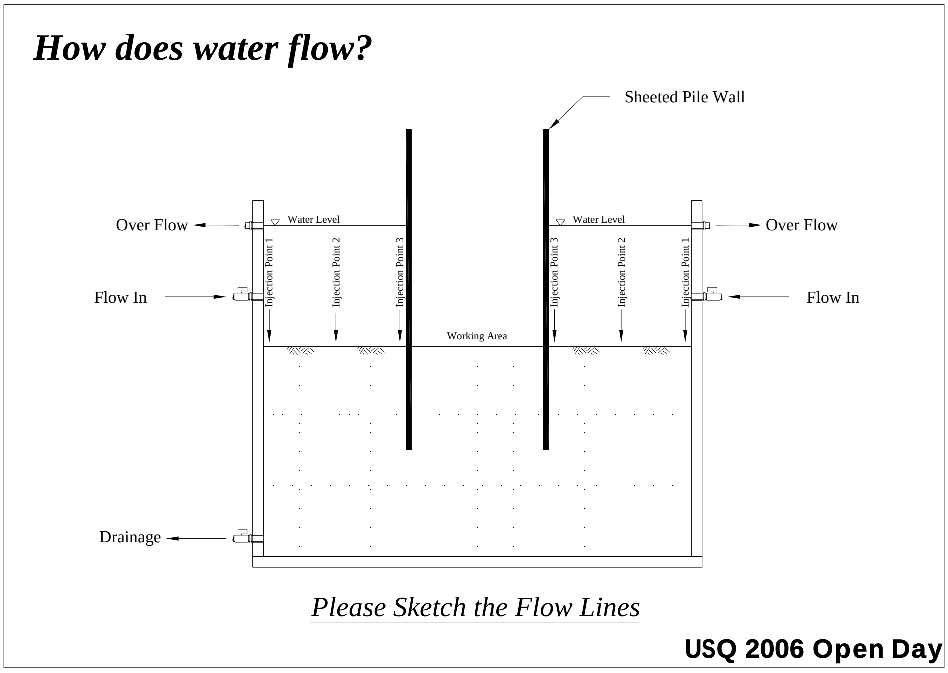
How does water flow?
Sheeted Pile Wall
Over Flow
Over Flow
Water Level
Water Level
Flow In
Flow In
Injection Point 1
Injection Point 2
Injection Point 3
Injection Point 3
Injection Point 2
Injection Point 1
Working Area
Drainage
Please Sketch the Flow Lines
USQ 2006 Open Day

Figure 4.14: Drawing for sketching the flow lines.

Figure 4.15: Participants checking the results.

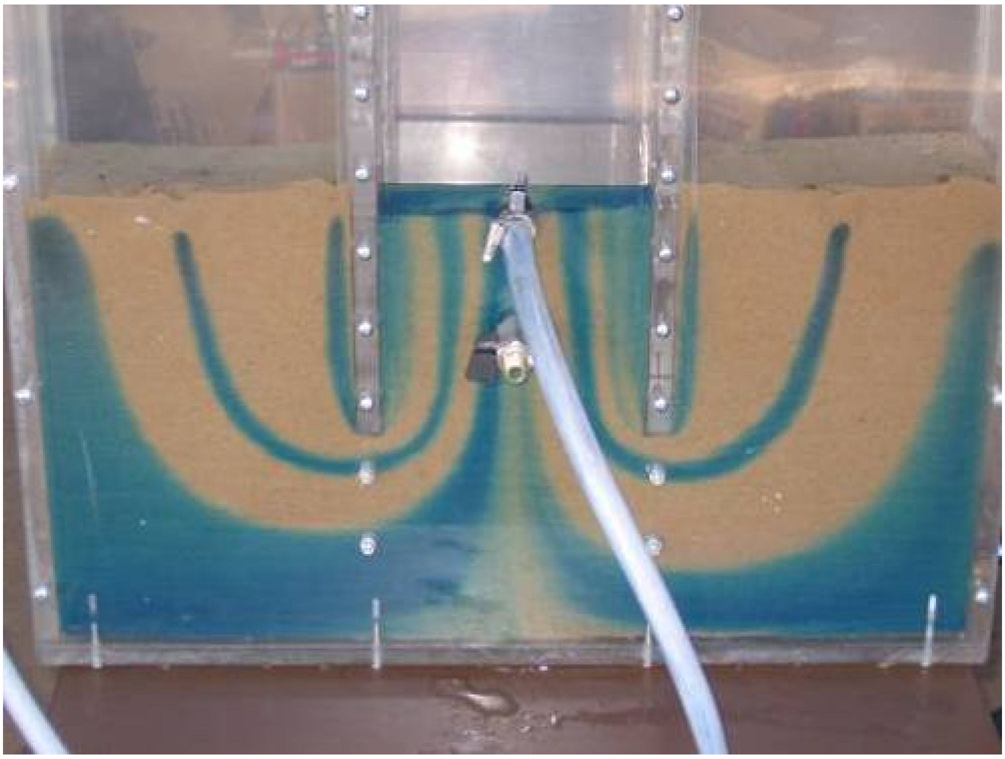

Figure 4.16: Revealed flow lines.

Chapter 5

PROJECT CONCLUSIONS

5.1 Project Achievements

The achievements of this project are as follows:

- The physical models for both bearing capacity and cofferdam were successfully constructed.

- The bearing capacity models were used to clearly explain the failure mechanisms at ultimate load.

- The process in preparing Kaolin clay materials were well developed and effectively reduced the moisture content without leaving any air voids.

- The cofferdam model was used to clearly explain the seepage and flow net concepts. The model was also successfully used to study the piping mechanics due to heave and boiling.

- During the USQ Open Day demonstration, the participants have shown interest and understanding of the geotechnical engineering works.

5.2 Conclusions

The development of the small scaled physical models has lead to some interesting conclusions. It has showed that the physical models are an important tool in expanding geotechnical theory and putting it into practice.

The bearing capacity models showed clearly the result of the ultimate load failure due to the continuously applied loads. The models demonstrate clearly of what happens when the soils under footing subjected to carry loads. The results obtained from these models after testing were compared with theoretical results using Terzaghi's method. The ultimate bearing capacity for the one layer sand model after failure was found to be 345 *kPa* and the theoretical value obtained using Terzaghi's method was 25.1 *kPa*. The result was about ten times difference due to the scale effects of the footing as mentioned in Section 2.7.

The process in preparing the Kaolin clay was successfully developed. From last year, the process involved putting the Kaolin clay sample into the oven at 50° *C*. The water content inside the clay sample was evaporate, however, this will replace by the air voids. The air voids can be spotted when preparing the slope. The air voids also reduced the soil bearing capacity. Another disadvantage in using the oven is that the clay sample around the tank boundary was dry but the clay sample around the middle of the tank still wet. One-dimensional consolidation process was then introduced into this project; a compression machine was the first choice, however, the applied load rate was too fast and pushing the clay sample out of the tank. A 200 *N* concrete block was then used to consolidate the clay sample and double the weight every week. This process enabling in removing the air voids and makes the soil sample homogeneous.

It was found that the cofferdam model is effectively illustrated the seepage theory. The model clearly demonstrates the flow patterns under a cofferdam. The results obtained from the model after testing were compared with theoretical results using flow net. The flow rate that measured from the cofferdam model was found to be $2 \times 10^{-5}\ m^3/s$. This compared well with the theoretical value obtained using flow net, the flow rate obtained from flow net was found to be $2.125 \times 10^{-5}\ m^3/s$.

After developing and testing, both models were successfully demonstrated at the USQ Open Day' 2006 where participants were required to sketch the failure patterns and the flow lines. About fifty participants showed a great interest by listening to the background information and sketching the failure patterns and the flow lines for both models. The demonstration of the small scaled physical models was a very good promotion of the geotechnical engineering field. Overall the development of these physical models will assist in the teaching and research in geotechnical engineering.

5.3 Recommendations for Further Study

Some further investigations are highly recommended for continuous development of small scaled physical models. Several recommendations are outlined below:

- More models for bearing capacity should be built to study the scale effect of sand materials. Difference cross section of the footing should also be considered.

- The use of materials from the fields should be considered to investigate real project situations.

- More laboratory tests on Kaolin clay should be carried out to get some more properties of the soil (c_u for different moisture content).

- A better compression machine should be used in order to produce a more accurateness results.

- Different analysis techniques must be consider in analyzing the failure pattern (digital image correlation, DIC)

- The finite element method analysis should also be considered, to try and get more accurate results. Including the finite element analysis can lead to quite a lot of interesting results from the models. This will minimize an erroneous work from the results.

- Using computer to record the data will eliminate the time spent at the laboratory and avoid losing any necessary data.

- Excess pore water pressure reading should be build and install to measure the excess pore water pressure from the cofferdam.

- The needle that used for injecting the dye must be identical in order to produce a neat flow lines.

REFERENCES

References

Bowles, J.E., 1996, "*Foundation Analysis and Design*", 6th edn, McGRAW-HILL, New York, USA.

Cedergren, H.R., "*Seepage, Drainage, and Flow Nets*", 3rd edn., Wiley, New York.

Cernica, J.N., 1982, "*Geotechnical Engineering*", CBS College Publishing, New York, USA.

Craig, R.F., 1974, "*Soil Mechanics*", 5th rdn, Chapman & Hall, London, British.

Das, B.M., 1979, "*Introduction to Soil Mechanics*", U.M.I., Michigan, USA.

Das, B.M., 1999, "*Shallow Foundations - Bearing Capacity and Settlement*", CRC Press LLC., Florida, USA.

Donaghe, R.T., Chaney, R.C. & Silver, M.L., 1988, "*Advanced Triaxial Testing of Soil and Rock*", ASTM, Philadephia, USA.

Fletcher, G.A. & Smooths, V.A., "*Construction Guide for Soils and Foundations*", John Wiley & Sons, New York, USA.

Guler, M., Edil, T.B. & Bosscher, P.J., 1999, "*Measurement of Particle Movement in Granular Soils using Image Analysis*", Journal of Computing in Civil Engineering, Volume 13, No. 2, ASCE.

Hansen, J.B. 1961, "*A General Formula for Bearing Capacity*", Ingenioren.

Lee, D.H., 1961, "*Deep Foundations and Sheet-Pilling*", Concrete Publications Ltd., London.

Liu, C. & Evett, J.B., 1998, "*Soild and Foundations*", 4th edn., Prentice Hall, New Jersey, USA.

Liu, J., 2004, "*Adaptive Cross Correlation for Imaging Displacements in Soils*", Journal of Computing in Civil Engineering, Volume 18, No. 1, ASCE.

McCarthy, D.F., 1998, "*Essentials of Soil Mechanics and Foundations - Basic Geotechnics*", 5th edn, Prentice Hall, Upper Saddle River, New Jersey.

Meyerhof, G.G., 1951, "*The Ultimate Bearing Capacity of Foundations*", Danish Geot Inst.

Newson, T. & White, D., 2005, "Modeling Geotechnical Problems in Soft Clays using the Mini-Centrifuge", The University of Western Ontario,

Parry, R.H.G., 1995, "*Mohr circles, Stress Paths and Geotechnics*", E & FN SPON, London, British.

Powrie, W., 1997, "*Soil Mechanics - Concepts and Applications*", E & FN SPON, London, British.

Puller, M., 1996, "*Deep Excavations - A practical manual*", Thomas Telford, Londeo

Reynolds, H.R., 1960, "*Practical Problems in Foundations*", Crosby Lockwood & Son Ltd., London.

Sadek, S., Iskander, M.G. & Liu, J., 2003, "*Accuracy of Digital Image Correlation for Measuring Deformations in Transparent Media*", Journal of Computing in Civil Engineering, Volume 17, No. 2, ASCE.

Scott, C.R., 1980, "*An Introduction to Soil Mechanics and Foundations*", 3rd edn., Applied Science Publishers Ltd., London.

Shiau, J.S., Lyamin, A.V. & Sloan S.W., 2003, "*Bearing Capacity of a Sand Layer on Clay by Finite Element Limit Analysis*", Volume 40, Number 5, National Research Council, Canada.

Szechy, C., 1961, "*Foundation Failures*", Concrete Publications Limited, London.

Terzaghi, K. & Peck, R.P. 1948, "*Soil Mechanics in Engineering Practice*", John Wiley & Sons, Inc., New York, USA.

Whitlow, R., 1996, "*Basic Soil Mechanics*", 3rd edn., Longman, Malaysia.

Williams, A.E., 1994, "*Bearing Capacity of Soils*", Technical engineering and design guides as adopted from the US Army Corps of Engineers, No. 7, American Society of Civil Engineers.

APPENDICES

Appendix A

PROJECT SPECIFICATION

University of Southern Queensland
Faculty of Engineering and Surveying

ENG 4111/4112 Research Project
PROJECT SPECIFICATION

FOR:	**MANOP JIANKULPRASERT**
TOPIC:	Experimental study of ultimate bearing capacity on two layer soils and flow nets under a cofferdams
SUPERVISOR:	Dr. Jim Shiau
ENROLMENT:	ENG 4111 – S1, D, 2006 ENG 4112 – S2, D, 2006
SPONSOR:	Faculty of Engineering and Surveying, USQ
PROJECT AIM:	The project aims to build small scale physical models for geotechnical application. It is expected that such model testing will provide a better understanding of ultimate bearing capacity on two different soil types and flow nets under a cofferdam.
PROGRAMME:	**Issue A, 19th March 2006**

1. Research the background information relating to ultimate bearing capacity of footings on single layer soil and two layer soils.
2. Research the background information of flow nets and seepage force under a cofferdam.
3. Design and construct a small scale physical model to demonstrate and study the failure mechanisms of soils under footing.
4. Design and construct a small scale physical model to demonstrate and study the behaviour of underground water flow under a cofferdam.
5. Perform simple laboratory testing of soil sample, which include strength parameters, gravimetric-volumetric data, and permeability.
6. Design practical methods on preparing Kaolin Clay for testing purposes.
7. Analyse ultimate bearing capacity of footing on sand, clay, and sand on clay.
8. Analyse flow nets and effect of seepage force on fine sand and coarse sand.
9. Demonstrate the models at 2006 USQ Open Day.

As time permits

10. Testing of ultimate bearing capacity on different soil properties with different moisture contents.
11. Adjust the depth of the cofferdam model to study seepage force that cause quick or boiling sand.

AGREED: ____________________ (Student) ___________________ (Supervisor)
____/____/____ ____/____/____

Appendix B

PROJECT WORKING SCHEDULE

Objectives	**Jan**	**Feb**	**Mar**	**Apr**	**May**	**Jun**	**Jul**	**Aug**	**Sep**	**Oct**	**Nov**	**Dec**
Part A: Cofferdams										▦	▦	▦
1. Literature review	█	█	█	█	█	█	█	█	█	▦	▦	▦
2. Design and construc the physical model	▓	▓								▦	▦	▦
3. Experimental study with the model			▒	▒	▒					▦	▦	▦
4. Analysis and compare the results						░	░			▦	▦	▦
5. Demonstrate on 2006 Open Day, USQ										▦	▦	▦
6. Project Conference									▥	▦	▦	▦
7. Project Dissertation									▤	▦	▦	▦
Part B: Ultimate Bearing Capacity of Layer Soils										▦	▦	▦
1. Literature review	█	█	█	█	█	█	█	█	█	▦	▦	▦
2. Design and construc the physical model		▓	▓							▦	▦	▦
3. Experimental study with the model			▒	▒	▒					▦	▦	▦
4. Analysis and compare the results					░	░	░			▦	▦	▦
5. Demonstrate on 2006 Open Day, USQ										▦	▦	▦
6. Project Conference									▥	▦	▦	▦
7. Project Dissertation									▤	▦	▦	▦

Appendix C

QUOTATION FOR PHYSICAL MODEL DEVELOPMENT

ENG 4111 Research Project Part I & II

Project Title: Experimental study of a cofferdams and the ultimate bearing capacity of two layer soil

Materials list for the project

Item	Description	Unit Price	Quantity	Total
1	Prespex plastic 20mm thick	$ 200.00	1	$ 200.00
2	Prespex plastic 15mm thick	$ 135.00	2	$ 270.00
3	Plywood 10mm thick (1200x2400)	$ 55.70	2	$ 111.40
4	Steelplate 25mm thick (75x150)	$ 10.00	4	$ 40.00
5	Aluminium angle 20x20mm (3m length)	$ 11.08	4	$ 44.32
6	Comercial sand (m^3)	$ 15.00	1 m^3	$ 15.00
7	Comercial clay (m^3)	$ 30.00	1 m^3	$ 30.00
8	Silicone sealent (for prospex joint)	$ 10.00	4	$ 40.00
9	Hard plastic scrapper	$ 5.00	1	$ 5.00
10	Pipette or Syringe	$ 30.00	3	$ 90.00
11	Food colour (blue, green, red)	$ 5.00	3	$ 15.00
12	Flexible hose ∅ 5mm	$ 1.40	5 m	$ 7.00
13	Tubing clear ∅ 10 mm	$ 1.30	10 m	$ 13.00
14	Tubing clear ∅ 12 mm	$ 1.10	10 m	$ 11.00
15	Hollow glass rod ID. 2mm	$ 1.10	5	$ 5.50
16	Cable tier (2.5x500mm white)	$ 10.98	1	$ 10.98
17	Bostik	$ 5.00	1	$ 5.00
18	Wire ∅ 4mm	$ 5.00	2 m	$ 10.00
19	Ruler 150mm	$ 3.00	2	$ 6.00
20	Screw ∅ 5mm x 500mm	$ 0.80	50	$ 40.00
21	Silicon glue remover	$ 11.00	1	$ 11.00
22	Pump	$ 150.00	1	$ 150.00
	Pipe and hose connection			
22	Valve ∅ 1/4˝	$ 7.50	3	$ 22.50
23	Brass connector ø1/4"	$ 3.04	3	$ 9.12
24	Brass connector ø10 mm	$ 1.35	3	$ 4.05
25	Brass connector ø20 mm	$ 2.40	1	$ 2.40
26	Brass cap ø20 mm	$ 2.85	1	$ 2.85
27	Brass T - connection ø1/4"	$ 4.19	1	$ 4.19
28	Clamp hose 8-12 mm	$ 1.05	10	$ 10.50
29	Clamp hose 12-16 mm	$ 1.45	10	$ 14.50
		Total		**$ 1,200.31**

Appendix D

BEARING CAPACITY MODELS CONSTRUCTION PLAN

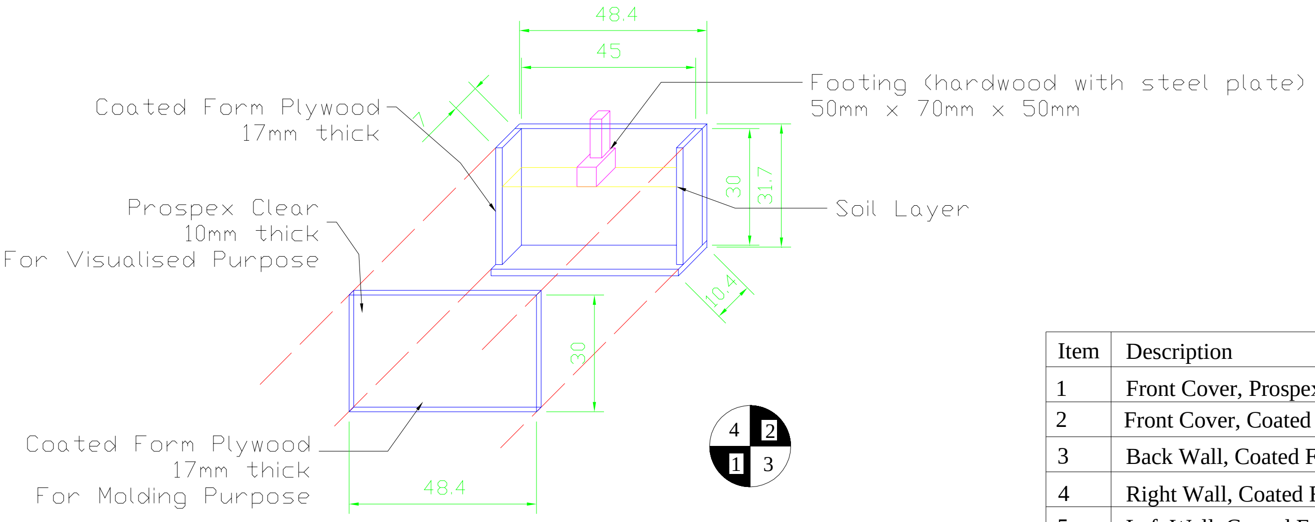
48.4
45
Coated Form Plywood
17mm thick
Footing (hardwood with steel plate)
50mm x 70mm x 50mm
7
Prospex Clear
10mm thick
For Visualised Purpose
30
31.7
Soil Layer
10.4
30
Coated Form Plywood
17mm thick
For Molding Purpose
48.4
4
2
1
3

ISOMETRIC VIEW

Item	Description	Quantity
1	Front Cover, Prospex	4
2	Front Cover, Coated Form ply	4
3	Back Wall, Coated Form Ply	4
4	Right Wall, Coated Form Ply	4
5	Left Wall, Coated Form Ply	4
6	Bottom Plate, Coated Form Ply	4
7	Top Cover, Coated Form Ply	4
8	Steel Column, 20x20x150 mm	1
9	Steel Plate, 50x70x25 mm	1
10	Wood Plate, 50x70x25 mm	5
11	Visualised Plate	1

ULTIMATE BEARING CAPACITY

SPONSOR: University of Southern Queensland		
COURSE: ENG 4111 / 4112 Research Project		
TITLE: Developing a geotechnical physical models	SCALE:	
SUPERVISOR: Dr. Jim Shiau	DATE: 13 March 2005	DRAFT: Mr. Manop Jiankulprasert

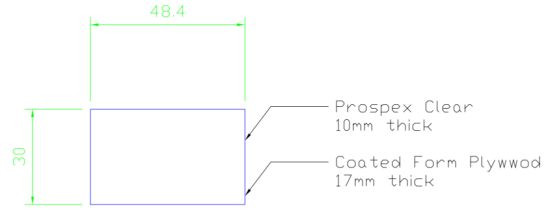
48.4
30
Prospex Clear
10mm thick
Coated Form Plywwod
17mm thick

SECTION 1

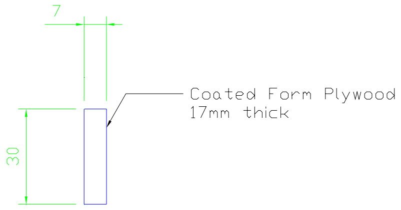
7
30
Coated Form Plywood
17mm thick

SECTION 3 and 4

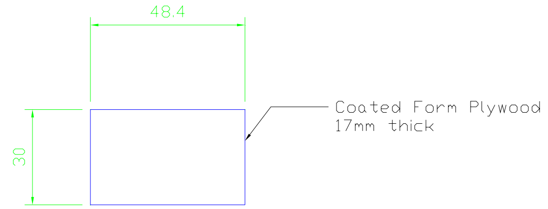
48.4
30
Coated Form Plywood
17mm thick

SECTION 2

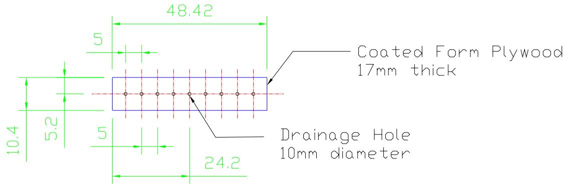
48.42
5
Coated Form Plywood
17mm thick
10.4
5.2
5
Drainage Hole
10mm diameter
24.2

SECTION 5

ULTIMATE BEARING CAPACITY

SPONSOR: University of Southern Queensland		
COURSE: ENG 4111 / 4112 Research Project		
TITLE: Developing a geotechnical physical models	SCALE:	
SUPERVISOR: Dr. Jim Shiau	DATE: 2 December 2005	DRAFT: Mr. Manop Jiankulprasert

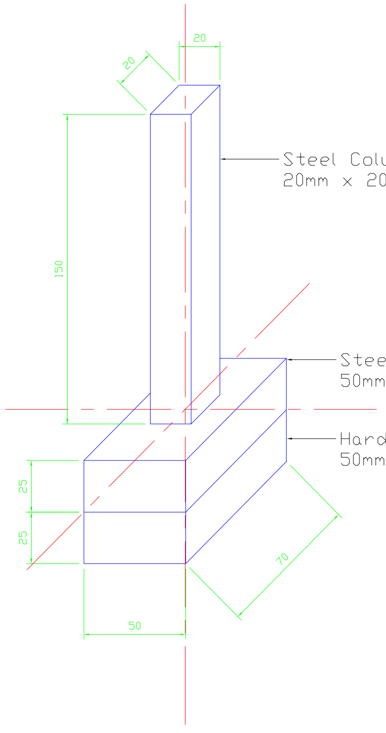
20
20
150
Steel Column
20mm x 20mm x 150mm
Steel Plate
50mm x 70mm x 25mm
Hardwood
50mm x 70mm x 25mm
25
25
70
50

FOOTING

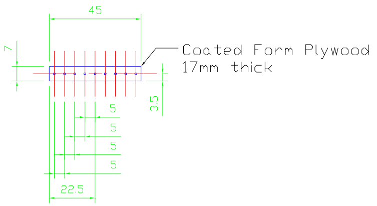
45
7
Coated Form Plywood
17mm thick
3.5
5
5
5
5
22.5

COVER PLATE

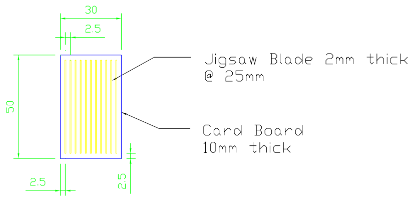
30
2.5
Jigsaw Blade 2mm thick
@ 25mm
50
Card Board
10mm thick
2.5
2.5

VISUALISED PLATE

ULTIMATE BEARING CAPACITY

SPONSOR: University of Southern Queensland		
COURSE: ENG 4111 / 4112 Research Project		
TITLE: Developing a geotechnical physical models	SCALE:	
SUPERVISOR: Dr. Jim Shiau	DATE: 2 December 2005	DRAFT: Mr. Manop Jiankulprasert

Appendix E

COFFERDAM MODEL CONSTRUCTION PLAN

External Items	Quantity	Length
? 10mm Pressure Connection		
? 10mm Clear Tube		10 m
? 10mm Globe Valve	3 Items	
? 10mm Extension Pipe	2 Pipes	10 cm
? 10mm Pipe Cap	2 Caps	
? 20mm Extension Pipe	1 Pipes	10 cm
? 20mm Pipe Cap	1 Cap	
? 20mm Screens	1 Pieces	

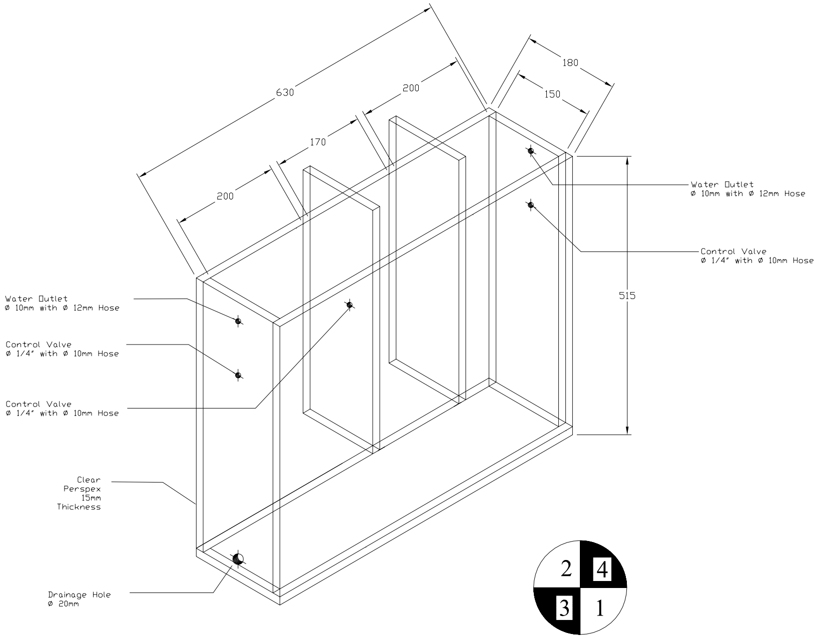
630
200
170
200
180
150
515
Water Outlet
Ø 10mm with Ø 12mm Hose
Control Valve
Ø 1/4" with Ø 10mm Hose
Water Outlet
Ø 10mm with Ø 12mm Hose
Control Valve
Ø 1/4" with Ø 10mm Hose
Control Valve
Ø 1/4" with Ø 10mm Hose
Clear
Perspex
15mm
Thickness
Drainage Hole
Ø 20mm
2
4
3
1

Isometric View

PHYSICAL MODEL OF COFFERDAMS

SPONSOR: University of Southern Queensland		
COURSE: ENG 4111 / 4112 Research Project		
TITLE: Developing a physical model of a cofferdams	SCALE: 1:150	
SUPERVISOR: Dr. Jim Shiau	DATE: 2 December 2005	DRAFT: Mr. Manop Jiankulprasert

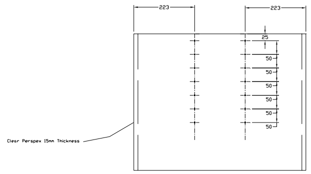
223
223
25
50
50
50
50
50
50
Clear Perspex 15mm Thickness

Section 1

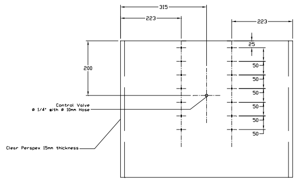
315
223
223
25
200
50
50
50
50
50
50
Control Valve
ø 1/4" with ø 10mm Hose
Clear Perspex 15mm thickness

Section 2

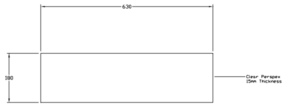
630
180
Clear Perspex
15mm Thickness

Section 5

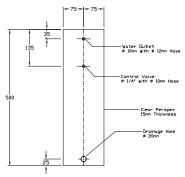
75
75
35
135
500
25
Water Outlet
ø 10mm with ø 12mm Hose
Control Valve
ø 1/4" with ø 10mm Hose
Clear Perspex
15mm Thickness
Drainage Hole
ø 20mm

Section 3

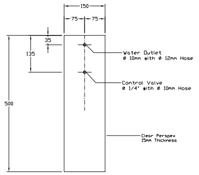
150
75
75
35
135
500
Water Outlet
ø 10mm with ø 12mm Hose
Control Valve
ø 1/4" with ø 10mm Hose
Clear Perspex
15mm Thickness

Section 4

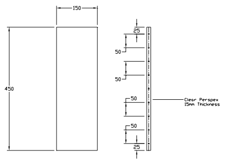
150
450
25
50
50
50
50
25
Clear Perspex
15mm Thickness

Section 6 and 7

PHYSICAL MODEL OF A COFFERDAMS

SPONSOR: University of Southern Queensland		
COURSE: ENG 4111 / 4112 Research Project		
TITLE: Developing a physical model of a cofferdams	SCALE: 1:75	
SUPERVISOR: Dr. Jim Shiau	DATE: 2 December 2005	DRAFT: Mr. Manop Jiankulprasert